SYNTHESIS AND CHARACTERIZATION OF HYDROXYAPATITE (HA) FROM COW BONE AND ITS COMPOSITE WITH POLY(LACTIC ACID) FOR BONE REPLACEMENT

RDU1603139

Project Leader:
Professor Dr. Mohammad Dalour Hossen Beg

Members:
Dr. Suriati Binti Ghazali
Dr. Mohd Saiful Zaidi Bin Mat Desa
Dr. Mohd Bijarimi Bin Mat Piah

ABSTRACT

The wide application of hydroxyapatite (HA) for medical applications such as bone tissue replacement sometimes constitutes environmental challenges as the conventional HA synthesis routes require the use of organic solvents. On the other hand, the current trend of research is to incorporate biomaterials such as HA into polymer matrices for some medical applications such as bone replacements. However, this often produces composites with inferior properties. This is due to poor HA dispersion within the composites as well as compatibility issues. In this study, natural HA was produced from cow bone through ultrasound and calcination processes at various temperatures. Composites then were produced from poly (lactic acid) (PLA) and hydroxyapatite (HA) through extrusion and injection molding. In order to foster good interaction between PLA and HA, and to impart antimicrobial properties onto the HA, surface of the HA was modified. On the other hand, impact properties of the PLA-HA composite was improved through the incorporation of impact modifier. Characterization of the produced HA was carried out through thermogravimetric (TGA) and field emission scanning electron microscope (FESEM) analysis. Spectrum obtained for the HA through Fourier Transform Infrared Spectroscopy was also compared with standard HA. Likewise, X-ray diffraction analysis of the HA in comparison with International Centre for Diffraction Data (ICDD) index for standard HA was conducted. On the other hand, Ca/P ratio of the produced HA was verified through Energy Dispersive X-ray analysis for elemental analysis. Likewise, different characterization techniques were used to characterize the composite produced. These include Fourier transforms infrared spectroscopy (FTIR), thermogravimetric analysis (TGA), Differential Scanning Calorimetry (DSC), Dynamic Mechanical Analysis (DMA), tensile, flexural and impact analysis. Also microbial properties of the produced HA and its composite with PLA were assessed. In addition, in vitro biocompatibility study was used to assess the cell attachment and cell proliferation properties of the composites. Results showed that modification of HA led to increased HA dispersion within the PLA matrix, which resulted into significantly higher mechanical, thermal and dynamic mechanical properties of the resulting composite. Similarly, impact properties of the PLA-HA composite was remarkably improved after incorporation of biostrong impact modifier. In addition, in vitro study revealed that the PLA-HA composite exhibits good biocompatibility properties. In general, the results from this study shows that combination of the salient properties of HA with the good mechanical properties of PLA holds great potential for production of bone replacement composite materials with good load bearing ability. The composite produced herein can help to overcome the secondary operation procedures often associated with the conventional bone replacement procedures.

TABLE OF CONTENT

CHAPTER 1

INTRODUCTION

1.1 Introduction

The population of patients living with bone diseases such as bone tumour, bone damage and bone degradation is growing at a disturbing rate. Research is on-going to reduce this number, since most of the traditional surgical procedures such as allograft and autografts are often accompanied by peculiar limitations (Hickey et al., 2015; Narayanan et al., 2016). Due to the problems associated with autograft and allografts, metallic materials are the commonly used internal fixation materials especially due to their highly desirable mechanical properties. However, it has been shown in previous studies that metal based materials most often has limitations such as poor adhesion, creep, stress shielding, non-degradability, metallic ion release, and problems of biocompatibility with host tissues (Liuyun et al., 2012). Attention is therefore being focused on the development of biomaterials which would be suitable for bone replacement and other internal fixations (Liuyun et al., 2012; Meng et al., 2012).

Inorganic biomaterials namely calcium orthophosphates are currently being investigated for potential medical applications in different areas which include bone replacements and other internal fixations (Dorozhkin, 2015b). These materials are being investigated based on their salient properties such as low density, chemical stability, biocompatibility, and their compositional resemblance to the mineral phase of natural bones (Ficai et al., 2010; Ilie et al., 2011). Hydroxyapatite (HA) being the main phase of calcium phosphate present in bone, have drawn large research interest. Report from previous research shows that HA exhibit the desired properties such as bioactivity, nontoxic, biocompatible, nonimunogenic, noninflammatory, osteoconductive and good osteointegration properties (Cucuruz et al., 2016; Dorozhkin, 2015b; Fu et al., 2016). However, the brittle, fragile, and inherent hardness of HA makes it difficult to be

processed into the form suitable for bone replacement and implantations. In addition, the poor strength of HA often limits its use for loadbearing applications. In order to take advantage of HA properties and also to overcome its associated limitations, HA is being combined with different polymers to produce biomaterials suitable for orthopaedic and other related applications (Sun et al., 2011).

Poly(lactic acid) (PLA) is one of the mostly investigated polymers for potential applications in bone tissue engineering. The wide interest in PLA is based on its bioresorbability, biodegradability, biocompatibility, and versatility (Gupta et al., 2007; Hickey et al., 2015). PLA and PLA-based biomaterials are easily processed by any of the methods such as extrusion, injection molding, film casting, fiber spinning, stretch blow molding, thermoforming, electrospinning, foaming and so on. This has further increased the widespread acceptance of PLA-based materials for wide variety of applications (Lim et al., 2008). Based on these, a synergistic bioresorbable, bioactive, biodegradable, biocompatible, and osteoconductive biomaterial can be fabricated by taking advantage of the individual salient properties of HA and PLA to produce PLA-HA biocomposite. The main benefit of these degradable materials is their property tunability to meet different application. Also, using these materials can help to reduce the need for secondary surgical procedures often associated with non-degradable material based implants (Cheng et al., 2009; Yu et al., 2012).

Among the available techniques for PLA processing, extrusion process is by far the most desirable technique for melt processing of PLA to suit different applications. In fact, most of the other techniques often take advantage of the important features of the extrusion process (Lim et al., 2008). Specifically, extrusion and injection molding processes are often used to carry out routine evaluation of new materials for their potentiality to be used in clinical applications. Utilising extrusion method to produce dense solid materials could outrightly substitute the presently used medical biomaterials in no distant time (Narayanan et al., 2016). Hence fabrication of polymer based medical biomaterials via extrusion/injection molding techniques is difficult to be replaced by other methods especially based on the great balance between cost, technical feasibility and material properties. Moreover, this approach is a well-established industrial processing method making it suitable to close the gap between demand and production

of orthopaedic materials. In addition, since no organic solvents are required for this technique, it is environmentally benign (Ferri et al., 2016; Ojijo et al., 2013).

However, challenges often envisaged for PLA-HA composite includes the high possibility for agglomeration of HA in the PLA matrix, and possible poor adhesion between the hydrophobic PLA and hydrophilic HA. This may lead to undesirable failure at the PLA-HA interface and invariably poor mechanical properties of the PLA-HA composite. To overcome these challenges, modification of the HA in order to enhance its dispersion and compatibility with the polymer matrix is needful. Although there have been several reports on this subject (Borum-Nicholas et al., 2003; Dong et al., 2001; Liuyun et al., 2012; Wang et al., 2002), there is room for improvement. Increasing the electrophoretic mobility of HA in the PLA matrix can be a way of improving its dispersion and improve the interfacial interaction of the PLA-HA composite.

1.2 Problem Statement

Recently, there has been huge demand for regeneration of bone due to the many health challenges arising from traumatic effects of bone loss, bone tumours and other bone infections. The structure of hydroxyapatite is compatible and seems suitable for this application. However, most of the common methods for preparing HA are either very complicated or not environment friendly due to the use of organic solvents. The use of organic solvents also increases the production cost of HA which makes it necessary to explore new approach and investigations. Interestingly, hydroxyapatite can be extracted from some natural sources such as bio wastes. In this study, HA was produced from natural sources through an entire chemical free route. Specifically, ultrasound technique in an ordinary water medium is being used for the preparation of the raw cow bone. Then calcination process was used to extract HA from the cleaned raw cow bone. This would help to protect the integrity of the environment on one hand as well as offer economic value to materials which otherwise might have be considered a. In addition, it would help to reduce the production cost of HA as no chemical are used.

The compatibility and biological suitability of natural HA favours its preferential acceptance in tissue and bone engineering but the widespread application of hydroxyapatite is very low at the moment due to its brittle nature and powdery form

(Cucuruz et al., 2016). Therefore, HA is being combined with polymeric materials to produce composites herein. The poor dispersion and low compatibility between HA and polymer is often a challenge which is envisaged for the development of HA-polymer bone replacement composites (Liuyun et al., 2012). In this study, chemical modification was used to enhance the dispersion of HA within the polymer as well as to increase the compatibility.

Most of the conventional orthopaedic treatments involve multiple surgical procedures. Interestingly, biodegradable polyester polymers and their copolymers are presently being investigated and used for bone engineering, orthopaedic fixation devices, dental repair and other biomedical applications. Particularly, poly (lactic acid) (PLA) is presently being considered a valuable biopolymer which can suit short term and long term applications (Hickey et al., 2015). However, PLA often suffers from certain shortcomings such as inherent brittle nature and long degradation times (Bouzouita et al., 2017; Liuyun et al., 2013) . These shortcomings are addressed in this study through the use of impact modifier to reduce the inherent PLA brittleness. This also helps to facilitate the degradation of PLA. Dense composites are produced unlike the films being produced in previous studies. This would make it easier to produce bone substitutes for any kind of patient. More importantly, it will help to overcome the multiple surgical procedures associated with conventional orthopaedic treatments.

1.3 Objective

The objective of this study is to fabricate and characterize HA-PLA composites from bio waste and biodegradable polymer (PLA). In order to achieve this objective, the aims of the study are as follows:

1. To synthesize hydroxyapatite (HA) from biowaste, namely cow bone through ultrasound and calcination techniques and to investigate the effect of calcination temperature.

2. To modify the HA surface and to investigate the effect of modification on its elemental and antimicrobial properties.

3. To produce and characterize PLA-HA composite using different (0-20 wt% HA) content, and to incorporate modified HA and biostrong impact modifier (0-15 wt%) into the optimum composite.

4. To investigate the effect of HA modification and impact modifier on the composite and to perform in-vitro test on PLA and selected categories of the PLA-HA composite.

1.4 Scope of Study

1.4.1 Scope for first objective

i. Bone preparation after collection from local sources.

ii. Ultrasound treatment of the bone at different temperature (60-150 min) and time (1-3 h).

iii. Calcination of bone powder at different temperature (650-950 ^{o}C) and for different period of time (1-3 h).

iv. Characterization of obtained apatite and comparison with standard hydroxyapatite.

1.4.2 Scope for second objective

i. Modification of HA surface through the use of phosphate based modifier.

ii. Elemental analysis of produced HA.

iii. Antimicrobial analysis of produced HA.

1.4.3 Scope for third objective

i. Production of composite from PLA and obtained apatite at different HA wt% content (0-20 wt%).

ii. Characterization of the composite through morphological, spectroscopic, thermal, mechanical and dynamic mechanical testing.

iii. Incorporation of biostrong impact modifier (0-15 wt%) into the optimum PLA-HA composite.

iv. Characterization of composite with respect to HA content, HA modification and incorporation of impact modifier.

1.4.4 Scope for fourth objective

i. In-vitro testing of PLA and selected categories of PLA-HA composite using human osteoblast cells.

ii. Controlled degradation of PLA and selected categories of PLA-HA composite.

ii. Characterization of PLA and the selected composite categories for biological performance such as cytotoxicity, biocompatibility and antibacterial properties.

1.5 Significance of Study

There is an increasing demand for hydroxyapatite (HA) in several medical applications. Specifically, HA is highly needed for treatment of bone diseases and infections. The conventional method for production of (HA) is through synthetic routes which require the use of organic solvents. These solvents often pollute the environment which shifted attention to production of HA from natural sources. Most of the conventional methods for the extraction of HA from natural sources often sacrifice the biological performance of the HA due to elimination of carbonates and other important components from the HA. This study explores the potential of ultrasound in combination with calcination process for the production of HA from natural source. This approach is environment friendly and economically feasible. Moreover, it can facilitate large scale production of HA. Results indicated that carbonate group was retained in the produced HA and about 11 other beneficial elements are present.

In order to use HA for bone replacement purposes, there is need to process the HA into a desired form which can only be possible when it is combined with other materials such as polymers. Most of the available polymers for bone replacement applications are not biodegradable. In this study, composites have been prepared from PLA (which is biodegradable) and HA. The material produced has the potential to be used for bone replacement applications. The main benefit of this material is that it

would help to overcome the several surgical procedures associated with conventional bone replacement methods.

Production of polymer based HA composites is often faced with the challenge of poor dispersion and low compatibility between HA and the polymer. Dispersion of HA in PLA matrix was successfully achieved in this study through the use of phosphate based modifier. Moreover, the possibility to use PLA-HA composite for load bearing applications was investigated and the inherent brittle nature of the composite was reduced through the use of impact modifier. Interestingly, the produced PLA-HA composite does not elicit observable cytotoxicity tendencies towards osteoblast cells. This indicates that it has great potential to be used for load bearing bone replacement applications.

CHAPTER 2

LITERATURE REVIEW

2.1 Research Background

Medical treatments directly related to orthopaedics was responsible for about 225 million patients with an overall cost of over 215 billion dollars in just 2 years from 2009 to 2011 (Narayanan et al., 2016). Among these, about 1 million cases required overall knee and hip replacement. Worst still, there is at least an annual 100,000 request for ligament reconstruction which gulps up to about 25 billion dollars every year (Agarwal et al., 2015; Lee et al., 2008). Medical treatments administered to orthopaedic patients mainly involve artificial grafts. This could be in form of allografts, autografts or plastic and metal implants. Metal implants have been on for a long period of time due to their unique mechanical strength (Bos, 2005). It has however been reported that metal implants are often accompanied by certain shortcomings. One of these is non-uniformity in mechanical strength of the native bone and the metallic materials due to poor interfacial adhesion. Others include inflammation of local tissues due to discharge of metallic ions and most commonly biocompatibility issues between metal implant and native tissues (Liuyun et al., 2012; Narayanan et al., 2016).

Similarly, allografts are notable for inherent drawbacks such as donor scarcity, immunogenicity as well as the risk of possible disease transfer from donor to receptors (Malinin et al., 2002). Autografts would have been a suitable alternative but it is also being faced with challenges of donor shortage and donor-site morbidity (Shelton et al., 1997). Therefore, there is progressing research for suitable solution to these challenges through development of biocompatible materials for use especially as internal fixation materials. At the moment, the number of synthetic biomaterials with potential bone grafting applications is very large. These include demineralized porous bovine bones,

bioactive glasses, demineralized human bone matrix, glass-ceramics, coral, coral derivatives and calcium phosphates ($CaPO_4$) (Dorozhkin, 2015a; Panchbhavi, 2010).

Among the available biomaterials, inorganic calcium phosphate ($CaPO_4$) biomaterials have been perceived to possess broad range of applicability in the field of medicine including bone replacements. Biomaterials from $CaPO_4$ are prominent mainly due to their excellent biocompatibility features and good bonding properties to living tissues. In fact, whereas other artificial implants are often been encapsulated by fibrous tissues within the body, $CaPO_4$ are not being encapsulated (Dorozhkin, 2015a). The main calcium phosphate phase in bone is hydroxyapatite (HA) (Dorozhkin, 2015b; Gokcekaya et al., 2015; He et al., 2008). Calcium orthophosphates are being used as bone substitutes mainly because of their chemical stability, low density, and biocompatibility. They also possess close resemblance to the natural bone mineral phase especially in terms of composition (Ficai et al., 2010; Ilie et al., 2011). HA has been particularly reported to possess highly desirable biocompatible, nontoxic, osteoconductive, noninflammatory, bioactive as well as nonimunogenic properties. These properties make it a suitable candidate for proper osteointegration (Cucuruz et al., 2016; Dorozhkin, 2015b; Fu et al., 2016). It is however very important to ensure compliance with environmental regulations even while attempting to proffer solution to other problems.

There has been series of report on the synthesis of HA both from synthetic and natural sources. Synthetic HA may be obtained by means of either dry or wet methods (Sadat-Shojai et al., 2013). Some of the methods which have been used to synthesize HA includes hydrolysis (Shih et al., 2004), emulsion liquid membrane (Jarudilokkul et al., 2007), chemical precipitation (Pang et al., 2003), microemulsion (Guo et al., 2005), microwave mediated methathesis (Parhi et al., 2004), and expeditious microwave irradiation (Sarig et al., 2002). Mechanochemistry approach have also been used to synthesize HA with the help of different reactants such as $Ca(NO_3)_2$ and $(NH_4)_3PO_4$ (Barakat et al., 2009), $Ca(NO_3)_2$ and $C_6H_{15}O_3P$ (Liu et al., 2001), CaO and $CaHPO_4$ (Yeong et al., 2001), and $Ca(OH)_2$ and H_3PO_4 (Isobe et al., 2002). It was found however that most of these synthetic methods are either biologically unsafe or somewhat complicated and time consuming. This often lead to safety issues due to the chemical solvents involved, which also often lead to high cost of HA obtained through

these methods (Barakat et al., 2009; Lü et al., 2007). In addition, most of these techniques are restricted to small scale synthesis (Ruksudjarit et al., 2008).

A suitable solution to this problem is the extraction of HA from natural sources. Some of the benefits of this approach includes but not limited to possible large scale production, economic feasibility and environmental friendliness (Wu et al., 2015). Indeed, HA have been reportedly extracted from biowastes such as bovine bones, fish bones and also bones and teeth of pig (Joschek et al., 2000; Lü et al., 2007; Quan et al., 2015). However, it was reported that the carbonate groups in the produced HA was eliminated during production which often affect the biological performance of the obtained HA (Antonakos et al., 2007). Nevertheless, extraction of HA from these sources can offer high economic and environmental benefits. The commonly used extraction method of HA from biowastes is through ordinary calcination. Progress in research however gave birth to other methods such as alkaline hydrothermal and subcritical extraction processes (Barakat et al., 2009).

In a particular research, the three main methods (thermal decomposition, subcritical extraction and alkali hydrothermal technique) were compared for the extraction of HA from bovine bones. It was reported that the thermal decomposition method produced HA nanorod rather than nanoparticles which was obtained from the other techniques (Barakat et al., 2009). However, alkali hydrothermal and subcritical processes were said to produce smaller particle sized HA as observed from SEM and FESEM results. Generally from their research, it was reported that the three methods offers the advantage of being simple and cheap, thereby deserving large scale applications (Barakat et al., 2009).

In a similar research, chemical and thermal processes were combined for HA extraction from cortical portions of bovine bones. Result showed that the produced HA has much resemblance with calcified tissues of human. It was suggested that nanoporous structure, chemical constituents and resorbable nature of the HA would be of immense benefit if exploited for bone engineering application (Murugan et al., 2006). Notwithstanding, most of these researches incorporated some chemicals for defleshing/cleaning the waste materials or for the purpose of fat removal from the materials prior to extraction. This therefore further contributes to the overall amount of chemical circulation in the environment. Reports also showed that unlike natural bones,

carbonate groups were eliminated from the obtained HA thereby affecting the biological characteristics of the apatite produced (Barakat et al., 2009). This may be associated with resultant effect of the chemicals used for defleshing and general cleaning of the biowastes. Due to these shortcomings, there is need for alternative methods of HA production from biowastes.

There is progressing effort from researchers around the world to overcome this challenge, leading to the very many reports on synthesis of HA (Sadat-Shojai et al., 2013), which date back to over 4 decades (Champion, 2013). However, so far the potential of ultrasound technique for defleshing and general cleaning of the raw biowastes prior to HA extraction has not been exploited. Interestingly, ultrasound technique has been perceived as a suitable technique for safe and convenient treatment of biowaste in preparation for extracting HA from them. Ultrasound can offer a more technically feasible, easy and environmental friendly approach for biowaste treatment. It has the potential to remove fat, bone marrow, pieces of meat and other adhering particles from the cortical bone without the use of any chemical. In fact, it may be used to clean both freshly obtained bones and bones that have been left as waste piles over a period of time. The use of ultrasound technique has been largely accepted in separation technology but was recently observed to possess certain advantages for biowaste treatment (Akindoyo et al., 2015; Akindoyo et al., 2015b).

Some of the noticeable benefits include better purification at little or no alkali concentrations, faster rate of reaction, economic feasibility and property enhancement (Akindoyo et al., 2015b). This technique works via the unusual set up of extreme chemical environment inside a solution due to creation of several expanding and imploding cavities. During this phenomenon, movement of ultrasound waves through the solution helps to agitate the biowaste, thereby generating strict forces on the fleshy part and other adhering materials on the biowaste. This process which also produces large quantum of heat carries significant potential for proper treatment of biowaste. Combination of ultrasound treatment and calcination process can therefore offer great economic and environmental values for bone regeneration, bone replacement and other related medical application.

On the other hand, in the area of environmental sustaining products and processes, poly(lactic acid) (PLA) is one of the best polymeric substitutes for most

petroleum based polymers (Raquez et al., 2013). Specifically, PLA based materials have been reported to exhibit good bioresorbability when it is used for applications such as in bone plates and regeneration of broken or damaged bones. Despite the many advantages of PLA, elastic modulus of PLA (2-7 GPa), is relatively lower compared with natural cortical bone (3-30 GPa) and the requirements of modulus is about 5 GPa. Interestingly, due to its higher modulus, HA has the potential to effectively improve the modulus of PLA based products when it is incorporated (Kasuga et al., 2000). However, in order to overcome dispersion issues in the PLA-HA composite, surface modification of the HA is often needed.

The most abundant functional groups on the surface of HA are the P-OH groups. Chemical modifications could therefore by carried out on the HA surface by increasing the number of, or substituting the P-OH groups as much as possible (Choi et al., 2006). Increasing the number of surface P-OH groups is important not only for its ability to act as ionic surface charges that could favour protein adsorption. It would also increase the electrophoretic mobility as well as increased solubility in aqueous phase. Similarly, due to the inherently sparing solubility of HA, there is need to reduce the Ca/P ratio in order to make it more acidic thereby increasing the solubility (Wang et al., 2008).

2.2 Requirements of Orthopaedic Biomaterials

Frequent remodelling processes often take place in the bone tissues. However factors such as trauma, hormonal imbalance, genetic defects, and bone tumors can cause a compromise of these processes. Complications associated with the conventional treatment methods necessitate the development of biomaterial based substitutes for regeneration of bone tissues (Deng et al., 2011; Laurencin et al., 2006). Complex and sensitive biomechanical processes are often associated with bone, an ideal scaffold intended to be used for bone tissue regeneration should therefore meet certain requirements. These requirements are generally manifold and can be highly challenging.

One of the main requirements for an orthopaedic scaffold is biocompatibility. This signifies the ability of material to support the normal activities of living cells including molecular signalling processes, without causing any observable systemic or local toxicity to the host tissues (Williams, 2008). The scaffold must not elicit immunogenicity, cytotoxicity, or cause any unresolved inflammation of the host tissue.

It should be bio-functional, biocompatible, biodegradable, and should offer non-toxic features.

Also, an ideal orthopaedic scaffold should be osteoconductive which means that the material should permit the adherence and proliferation of bone cells, as well as act as extracellular matrix on its pores and general surface. Sometimes, it is also necessary that the scaffold should be capable of inducing the formation of new bone (osteoinduction) via biomolecular signalling and efficient mobilization of progenitor cells (Bose et al., 2012). But it is always expected that the material should exhibit surface epitopes suitable for cell adherence and proliferation (osteoconductive properties).

In another vein, an ideal orthopaedic scaffold should exhibit sufficient mechanical properties, without any premature failure either during handling or after implant. The mechanical properties should be in close match with the mechanical properties of the host bone, alongside very good load transfer efficiency. As such, during the design of orthopaedic scaffold, the wide variability in geometry, and mechanical properties of bone should be put in consideration (Olszta et al., 2007). In short, chemical and physical properties of the material should be similar to that of native tissue in terms of the organic/inorganic bone composite structure.

Another very important requirement of orthopaedic scaffold intended to be applied for bone tissue regeneration is bioresorbability (Williams, 2008). This means that the material should in addition to possessing similar mechanical properties to the host bone, also undergo in vivo degradation with time, in order to create space for the newly formed bone tissue to grow. The rate of degradation should match the rate of tissue regeneration.

Based on these requirements, one major challenge of orthopaedic biomaterials is the ability to naturally design and manufacture scaffolds with the ideal composition, mechanical properties and excellent bioresobability (Lichte et al., 2011; Olszta et al., 2007). The requirements for ideal orthopaedic scaffold are actually numerous and in a bid to meet as many as are possible among these requirements, synergistic composite systems are being investigated. These composites combine the salient advantages of

polymers with the biological features of inorganic calcium phosphates, notably HA to produce biocomposites for bone tissue engineering (Rezwan et al., 2006).

Several biomaterials meet most of these requirements especially in terms of chemical, mechanical, as well as cell-material relationships. For instance, collagen being a constituent of the organic phase of bone tissues (Keogh et al., 2010), is a great choice of biomaterial for bone tissue regeneration. Likewise, ceramics which constitute the inorganic phase of bone tissue (López-Álvarez et al., 2013), could be another good option. However, brittleness and poor processability often limits the use of ceramics whereas collagen fibers are generally known for their poor mechanical strength (Narayanan et al., 2016).

Therefore, there is extensive investigation on polymeric biomaterials such as poly lactic acid for bone tissue regeneration and other orthopaedic applications. PLA based materials exhibit excellent mechanical properties, biocompatibility, suitable degradation rates, and do not manifest observable inflammatory responses. Nevertheless, the major limitation to PLA based materials is the lack of sufficient surface epitopes which could facilitate the process of cell adhesion and proliferation. In order to overcome these challenges, different approaches have been attempted such as plasma treatment, hydrophilic molecules immobilization, protein adsorption, and surface modification through incorporation of bioactive epitopes. These approaches can help to make the material more conducive for the process of bone regeneration (Nakagawa et al., 2006; Woo et al., 2007).

2.3 Evolution of Poly(lactic acid)/Hydroxyapatite Biomaterials

In the last years, use of devices such as fasteners, stitches, screws, anchor e.t.c for bone tissue reconstruction and regeneration has gained interest. Over time, biocompatible materials obtained from polymeric matrices had slowly replaced the conventional insoluble ceramics and high strength biostable and biocompatible metallic alloys (Ferri et al., 2016). These days, it is common to find vast majority of materials with potential biomedical applications. Efforts in the past to develop ceramics, metallic, polymeric and other composite materials indicate the dire need for these materials in medical applications (Jeon et al., 2011; Witte et al., 2007). Regarding metallic materials, alloys of titanium have been widely used (Geetha et al., 2009; Kangping et

al., 2012; Li et al., 2014). Other alloys including CoCr (Friedman et al., 1995), CoCrMo (Webster et al., 2004), and stainless steel (Bordjih et al., 1996) have also been used. Although these metal alloys are biocompatible, they do not support bone tissue regeneration which necessitates the need for surface modification (Choy et al., 2014; Metikoš-Huković et al., 2003; Wang et al., 2004).

On the other hand, HA and other calcium phosphate ceramic materials are highly desirable for their osteoconductive properties. HA biocrystal in combination with collagen can be found in human bones (Ferri et al., 2016). Thus HA may be regarded as biomimetic material which does not exhibit any rejection phenomenon when it comes in contact with connective tissues (Ferri et al., 2016). However, there are some concerns on the use of $CaPO_4$ biomaterials which include the poor tensile strength, brittle nature, low elasticity, low fracture toughness and poor mechanical reliability. Moreover, it is difficult to shape them into forms desired for implantation (Dorozhkin, 2013). Specifically, due to its ceramic nature, HA is inherently brittle which makes the medical sector to demand good balance in mechanical performance, cost and density. Nevertheless, biodegradation and bioresorption of fixation devices in physiological media is always an added advantage. This is because it permits and enhances the growth of bone tissues at the interface of fixation devices (osteointegration), which makes HA highly desirable.

Biodegradable polymeric materials are interesting choices for this requirement based on their ease of processing and suitable degradation in physiological media (Hutmacher et al., 2001; Wahit et al., 2012). The ideal approach for bone tissue engineering is "the best bone substitute is the regenerated bone itself" (Ferri et al., 2016). With polymeric materials, there is this possibility as the material can slowly degrade in a progressive manner during which it is resorbed and concurrently substituted by new soft tissue and other specialized connective tissues. This further increase the chance of polymeric materials to substitute conventional ceramic and metallic materials especially since no secondary surgical procedures would be required to eliminate the materials after bone regeneration. Biodegradable polymers such as poly(lactic acid) PLA, poly(glycolic acid), PGA, poly(caprolactone), PCL, poly(ester amides), PEA, poly(butylene succinate), PBS, and their copolymers are increasingly being exploited for biomedical applications (J. Liuyun et al., 2013b; Tayton et al., 2014;

Vila et al., 2013). For optimum recovery, resorption time of these polymers can be tailored based on their different biodegradation rates.

Necessarily, formulation of resorbable, biocompatible osteoconductive devices should comprise two main components such as a polymer matrix which is biodegradable and osteoconductive fillers such as HA whose composition is similar to that of natural bones (Chae et al., 2014). As particles of HA solubilize, it will enhance mineralization through controlled supply of calcium and phosphate to the bone fixation interface such that new connective tissues can be formed and osteointegration can take place (Yanoso-Scholl et al., 2010). Osteointegration would therefore enhance optimum growth and healing of bones such that the fractured site can be stabilized (Böstman et al., 2000). Fabrication of a suitable polymeric biocomposite requires that individual properties of the polymer and the filler be combined to form a synergy. The most commonly combined properties of the organic and inorganic phases in polymeric biocomposites are summarized in Table 2.1.

Table 2.1 Commonly combined properties of organic and inorganic phases in polymeric biocomposites

Bioorganic	**Inorganic**
Elasticity, plasticity	Hardness, brittleness
Low density	High density
Permeability	Thermal stability
Hydrophobicity	Hydrophilicity
Selective complexation	High refractive index
Chemical reactivity	Mixed valence slate (red-ox)
bioactivity	Strength

There is a growing interest in biocomposites produced from poly(lactic acid) (PLA) and hydroxyapatite (HA) for biomedical applications, as confirmed through the series of research activities on these materials (Armentano et al., 2010; Ignjatovic et al., 2004; Ignjatović et al., 1999; Li et al., 2008; Rakmae et al., 2012; Shen et al., 2009; Thanh et al., 2015). These materials combine the biocompatibility and osteoconductivity of HA with the good absorbability and easy processability of PLA and its copolymers (Murariu et al., 2016). In a particular study, the effect of different parameter such as filler loading, copolymer type, and silane surface modification on microstructural and mechanical properties of PLA-HA composites was investigated (Gültekin et al., 2004). It was reported that the best mechanical performance were

obtained for PLLA composites reinforced with 1 wt% aminofunctional silane treated HA, and PDLA composites reinforced with 0.5 wt% mercaptopropyltrimethoxy silane (Gültekin et al., 2004). Similarly, in another study, HA was surface modified using silane derivatives and it was reported that there was improved adhesion at the PLA-HA interface after HA modification which resulted into enhancement in the ultimate mechanical properties (Zhang et al., 2005). However, the poor dispersion of HA in PLA matrix is often a major limitation to the use of PLA-HA composites for load bearing applications.

In general, several other researchers have focused on modifying the HA surface through different approaches using a variety of surface modifiers such as poly acids, different coupling agents, polyethylene glycol, dodecyl alcohol, isocyanates and zirconyl salts (Borum-Nicholas et al., 2003; Borum et al., 2003; Dong et al., 2001; Misra, 1985; Wang et al., 2002). Report however, showed that most of these techniques are not environment friendly (Liuyun et al., 2012). In addition, there are very few reports on improvement of bending strength of the resulting HA-polymer composite. However, sufficient bending strength is a very important feature required of internal fixation materials.

In order to enhance the bending strength and other mechanical properties of HA-polymer composites, a particular research was conducted which used three different HA surface modification methods (Liuyun et al., 2012). In their study, stearic acid, grafted l-lactide and combination of stearic acid and surface grafted l-lactide were adopted. Series of HA-PLGA composites were prepared through solution mixing, and the composite properties were investigated accordingly. It was reported that the three approaches were able to successfully modify the HA surface and combination of stearic acid with surface grafted l-lactide produced the best dispersion. This resulted in increased bending strength of the HA-PLGA composite compared with other methods (Liuyun et al., 2012). However, this study incorporated only 3 wt% HA into the composite which might not be sufficient to really investigate the composite properties. Moreover, PLGA is a fast degrading polymer which can result into accumulation of degradation product at implant sites, which makes PLA more desirable.

Different in vivo investigation of PLA-HA composite materials revealed remarkable mesenchymal stem cells (MSCs) proliferation bringing about further

differentiation of adipose derived stem cells (ASCs). In fact, the rejection rate of PLA-HA system is highly negligible (Ferri et al., 2016). This is associated with the low degradation rate of PLA as well as its formation of buffer solution with dissolved HA particles which helps to keep the pH constant due to presence of alkaline salts such as phosphates (PO_4^{3-}) (Agrawal et al., 1997).

CHAPTER 3

METHODOLOGY

3.1 Materials

The Poly(lactic acid) (PLA) used for this research is NatureWorks Biopolymer 3052D injection molding grade, with density of 1.25 g/cm^3 and a melt flow index of 30–40 g/10 min (190 °C/2.16 kg). The PLA has a melting temperature of 160–170 °C. The chemicals used such as ethanol (95%) and ethyl acetate (99.8%) were procured from Roth, Germany. These reagents are of analytical grade and were used without further purification. Phosphate based modifier, marketed as Fabulase$^{(R)}$ 361 was obtained from Chemische Fabrik, Budenheim KG, Germany. This surface modifier contains both phosphate and functional hydroxyl moieties. The impact modifier Biomax® Strong 120, (BS) was kindly supplied by Dupont, Switzerland. The BS is a commercially available ethylene-acrylate copolymer which contains epoxy moieties particularly designed for modifying the impact properties of PLA. Details of the chemical used are presented in Table 3.1.

Table 3.1 List of chemicals used for the study

Chemical Name	Purity/Grade	Supplier
PLA	3052D	Roth, Germany
Ethanol	95%	Roth, Germany
Dicopper hydroxide phosphate	Fabulase® 361	Chemische Fabrik, Budenheim KG, Germany
Ethyl acetate	99.8%	Roth, Germany
Ethyl Alcohol	99.7%	R & M, Essex, UK
Biostrong	Biomax® Strong 120	Dupont, Switzerland

3.2 Methods

The flow chart for the method followed in this study is shown in Figure 3.1 and Figure 3.2.

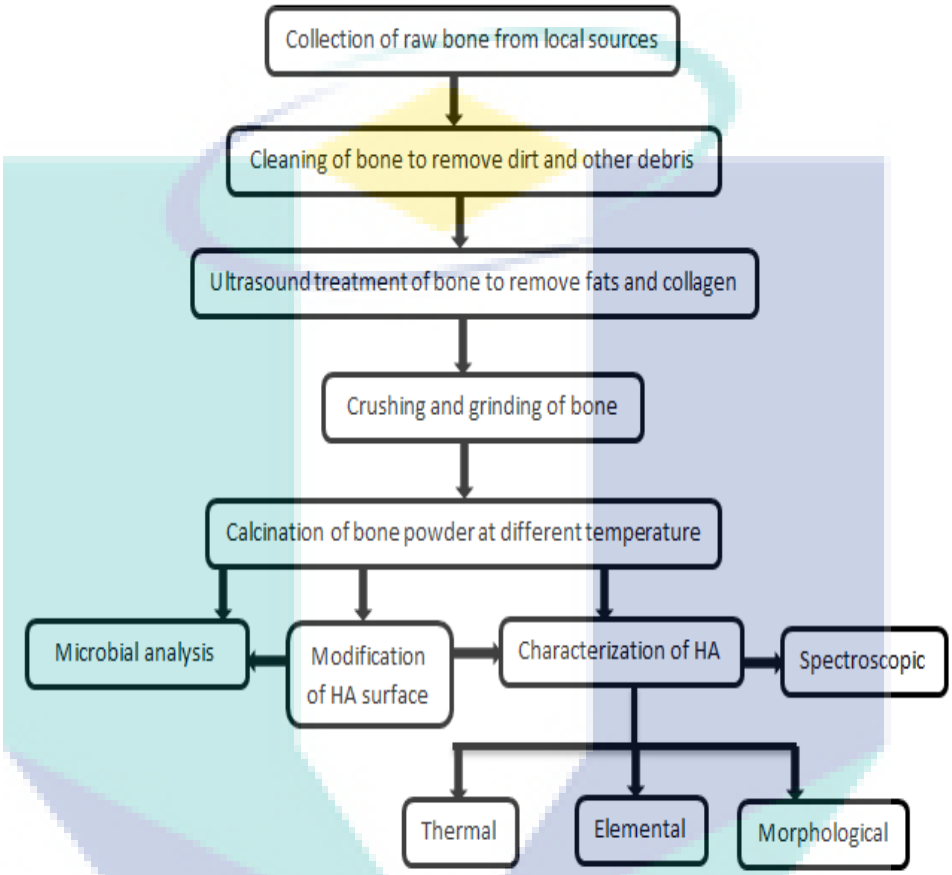

Figure 3.1 Flow chart of methodology for production, modification and characterization of HA

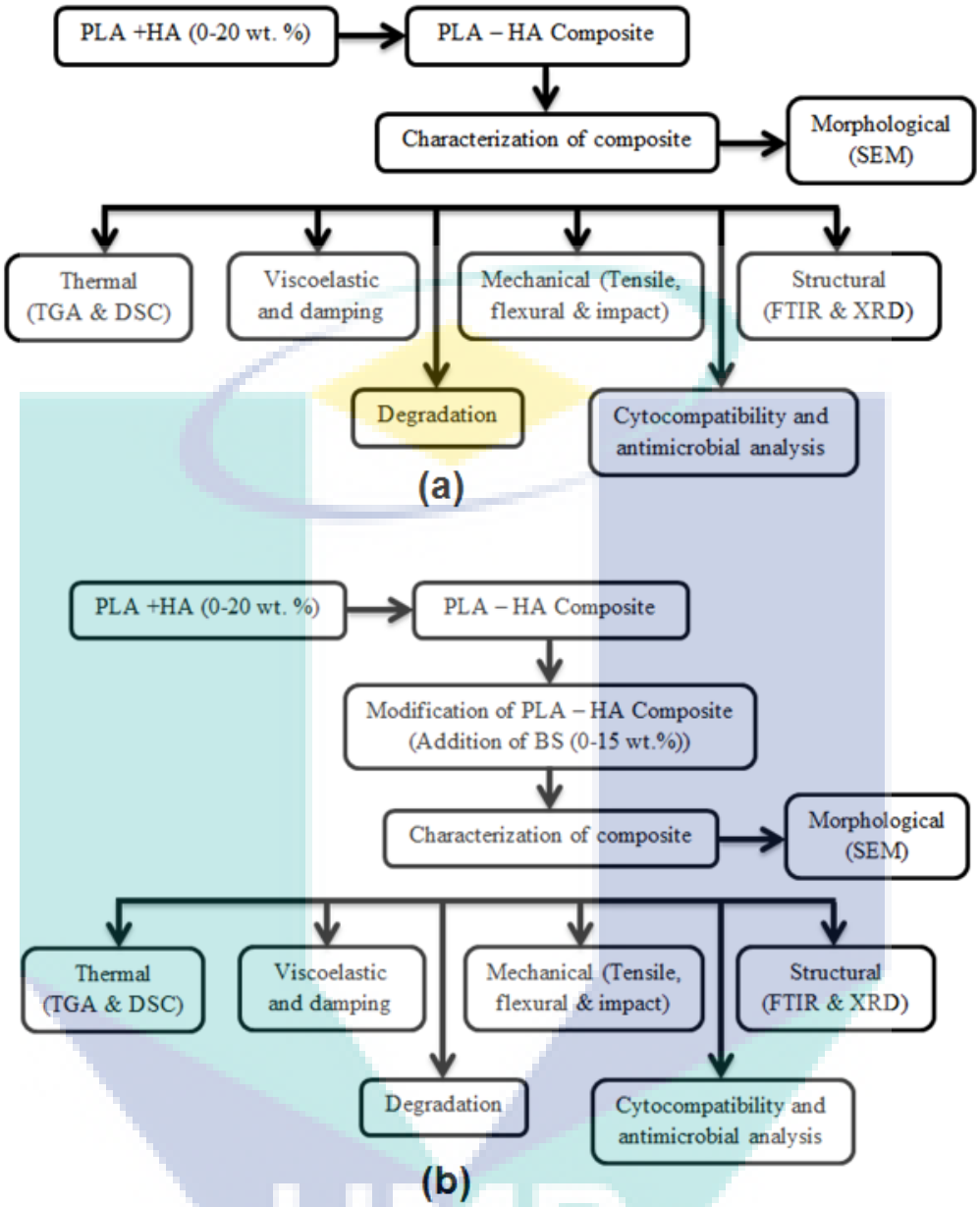

Figure 3.2 Flow diagram of methodology for (a) production and characterization and (b) modification and characterization of PLA-HA composite

3.2.1 Bone preparation and ultrasound treatment

The femur of adult cow (~3 years old) was obtained from Jaya Gading, Kuantan, Malaysia. Treatment of the bone prior to HA extraction, was carried out through ultrasound. Treatment was carried out using a laboratory scale Crest ultrasonics Daihan ultrasound bath operated at 9 W for 2 h at 85 ^{o}C and the ratio of bone to water was kept at 1:50. Selection of ultrasound treatment parameters was made based on preliminary studies (J. Akindoyo et al., 2017b). After ultrasound treatment, the bones were wiped in distilled water using an aluminium sponge at 40 ^{o}C, and then left to dry normally for 24 h after which it was oven dried at 105 ^{o}C for 8 h. Grinding of the dried bones was

performed using an ultra-centrifugal mill (Germany Retsch, ZM 200), and the bone powder was sieved using a laboratory mechanical sieve shaker. The final size of the powder was approximately 450 µm.

3.2.2 Production of hydroxyapatite

The natural HA was produced through thermal processing of the bone powder *via* calcination process at different temperature such as 650 ^{o}C, 750 ^{o}C, 850 ^{o}C and 950 ^{o}C. For the purpose of comparison, an untreated bone powder sample referred to as RAW was used as control and its properties were compared with the obtained apatites. Calcination process was conducted in a furnace at the stated temperature at a rate of 10 ^{o}C min^{-1} for 3 h.

3.2.3 Modification of hydroxyapatite

Coating of the HA surface was carried out by first dispersing the HA in absolute ethanol inside a beaker at a ratio of 1:10 (w/v) with continuous stirring at 60 ^{o}C. On the other hand, 2% (w/w) with respect to HA of the phosphate based modifier (Fabulase$^{(R)}$ 361) was dissolved in ethyl acetate 1:10 (w/v) inside another beaker and stirring was continued at 60 ^{o}C until total dissolution (Akindoyo et al., 2017). After total dissolution of the Fabulase$^{(R)}$ 361, content of the two beakers were mixed together and stirring was continued for another 1 h. After that, the mixture was filtered and total solvent removal was ensured by drying the modified HA overnight in a vacuum oven set at 105 ^{o}C.

3.3 Characterization of Hydroxyapatite

3.3.1 Thermogravimetric analysis

Thermogravimetric analysis was carried out in order to understand the effect of calcination temperature on thermal properties of the obtained HA using a TA analyser (TGA Q500 V6.4, Germany). Samples weighing about 5 ± 2 mg were placed in a platinum crucible and analysis was conducted under nitrogen atmosphere flowing at a rate of 40 mL min^{-1}. Heating was conducted at 10 ^{o}C min^{-1} from 25 ^{o}C to 1000^{o}C.

3.3.2 Fourier transform infrared (FTIR) spectroscopy

Functional group analysis of the produced HA was conducted using a Shimadzu FTIR spectrometer (Model-IR affinity-1S). Functional groups of Fabulase$^{(R)}$ 361 were also investigated and the possible change in FTIR spectra of the produced HA after modification was evaluated. The IR spectra were obtained over a wavelength range of 400-4000 cm^{-1} using the standard KBr technique.

3.3.3 Field emission scanning electron microscopy

Observation of the surface morphology of the obtained HA was made through FESEM analysis. This was used to get images of the samples surface as well as to obtain direct information about the typical shape and size of the obtained HA using a ZEISS, EVO 50 scanning electron microscope. Test samples were dried to make them moisture free and were then coated with platinum prior to FESEM observation in order to prevent any electrical discharge during observation.

3.3.4 Energy dispersive X-ray analysis

In order to verify the authenticity of the obtained HA, EDX analysis was conducted alongside FESEM. Stoichiometric molar ratio of calcium to phosphorus in the standard HA is 1.67 (Habraken et al., 2016). Therefore Ca/P ratio of the materials obtained from this study was investigated via elemental analysis with the help of EDX analyser.

3.3.5 X-ray fluorescence

Concentration of the elemental components especially the calcium and phosphorus concentration of the HA was determined through X-ray fluorescence spectroscopy. In addition to this, quantitative determination of CO_3^{2-} was carried out using a CHNS analyzer (vario MACRO cube Elementar, Germany), and the CO_3^{2-} content was determined as carbon.

3.3.6 Antimicrobial analysis of hydroxyapatite

Antimicrobial properties of the synthesized HA before and after surface modification were evaluated using gram positive and gram negative bacterial. The

Kirby-Bauer Test otherwise called the Zone of Inhibition Test was used to investigate the antimicrobial properties of the modified and unmodified HA. Generally, the size or diameter of the inhibition zone is related to the antimicrobial activities of the samples. A very large zone of inhibition is an indication of potent antimicrobial activity whereas a small or insignificant zone of inhibition is an indication that the tested sample has no or relatively low antimicrobial property (Nirmala et al., 2011).

3.4 Production of Composites

Composites were produced from PLA and unmodified HA at different wt% HA content (0-20 wt%). The different composite categories that were prepared are summarized in Table 3.2.

Table 3.2 Components of PLA-HA composites and their code names

Code	PLA (wt%)	HA (wt%)
PLA	100	0
5% HA	95	5
10% HA	90	10
15% HA	85	15
20% HA	80	20

Based on results from SEM observation and mechanical properties of the composites, further batches of composite containing 10 wt% surface modified HA was produced for comparison and further observation. The modified HA based composites was compared with unmodified HA based composites and both composite categories were evaluated with respect to pure PLA. The samples prepared for this category for investigation, and their code names are summarized in Table 3.3. For pure PLA, the code name PLA is given. The PLA-HA composite containing unmodified HA is herein referred to as PLA-unmodified HA and a code name PUHA is given. On the other hand, the PLA-HA composite containing the modified HA is herein referred to as PLA-modified HA composite with PMHA as its code name.

Table 3.3 Components of PLA-HA composites and their code names

Code	PLA (wt%)	HA (wt%)	Modifier (wt% with respect to HA)
PLA	100	0	-
PUHA	90	10	-
PMHA	90	10	2

Furthermore in order to specifically improve the impact properties of the PLA-HA composites, other categories of composites were prepared by incorporating different weight percent (0-15 wt%) of biostrong impact modifier. The biostong impact modifier is herein referred to as BS. The amount of HA in these categories of composite was fixed at 10 wt% of the surface modified HA. The different categories of composites produced and their code names are summarized in Table 3.4.

Table 3.4 Code names and composition of the composite categories

Code	**Sample composition (wt %)**		
	PLA	**HA**	**BS**
PLA	100	-	-
PHA	90	10	-
PHAB5	85	10	5
PHAB10	80	10	10
PHAB15	75	10	15

3.4.1 Mixing and compounding

Mixing and compounding of the composite was carried out using a twin screw extruder (Leistritz ZSE 18 HPE, *D* = 18 mm, *L/D* = 40). Prior to extrusion, the PLA was dried to moisture content < 0.1% using TR–Dry–Jet EASY 15 (TORO-systems) air drier. On the other hand, the HA was dried to moisture content <1% using a convectional laboratory oven. To ensure proper mixing and compounding, HA was side-fed into the compounder carrying the pre-melted PLA as illustrated in Figure 3.3, after which mixing and homogenisation occurred. After extrusion, the composite strand was cooled down with the help of a discharge conveyer after which it was cut to a length of 3 mm by a Scheer SGS 25-E strand pelletizer. The pellets were then dried to moisture content < 0.1% after which test samples were prepared using an injection molding machine (Arburg allrounder 320 C golden edition).

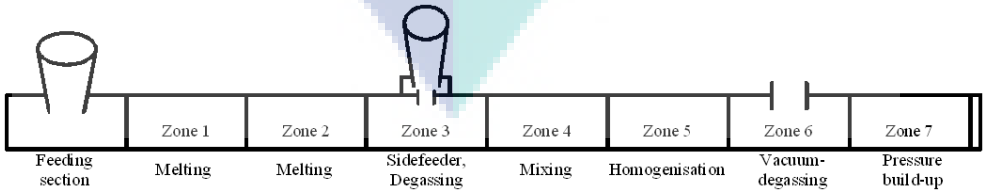

Figure 3.3 Pictorial illustration of extruder configuration during compounding of PLA, HA and BS

3.4.2 Modification of composite

Due to the inherent brittle nature of PLA and its composite with HA, impact modifier namely Biomax® Strong 120 (BS) was incorporated into the PLA-HA composite formulation in order to reduce its brittle tendency and improve its impact properties. Different wt% BS content was incorporated from 0-15 wt%.

3.4.3 Scanning electron microscopy

Morphology of the fractured surface of the composites was investigated through a Camscan Electron Optics scanning electron microscope (SEM) (Model-MV2300). After drying samples to make them moisture free, they were sputter coated with gold prior to SEM observation in order to make them conductive.

3.4.4 Fourier transform infrared spectroscopy (FTIR) of composite

Interactions between the HA, PLA and other composite additives were analysed through their functional groups using FTIR technique. Functional groups of the produced composites were analysed with the help of a Shimadzu FTIR spectrometer (Model-IR affinity-1S). This was used to investigate the chemical reactions which occurred during compounding and blending of the composite components. Changes in the functional groups of the individual components were also verified.

3.4.5 Tensile Test

Samples for tensile testing were prepared according to EN ISO 527. Testing was conducted using a Zwick/Roell Z010 testing machine. The crosshead speed was 5 mm min^{-1}, and the samples were dried and preconditioned at 50% relative humidity and at 23 ^{o}C, prior to tensile testing. Results of seven replicate samples were recorded to obtain the tensile strength (TS) and tensile modulus (TM).

3.4.6 Flexural Test

Flexural test samples were prepared according to EN ISO 178. Testing was carried out with the help of a Zwick/Roell Z010 testing machine which was operated at a cross head speed of 10 mm min^{-1}. Prior to flexural testing, the samples were dried and

conditioned at 23 ^{o}C, and 50% relative humidity. Results of seven replicate samples were recorded to obtain the flexural strength (FS) and flexural modulus (FM).

3.4.7 Charpy Impact Test

Charpy impact test was conducted according to EN ISO 179-1. Impact test was carried out using unotched samples, with the help of a Zwick charpy impact machine. The impact velocity was 2.93 ms^{-1}, and hammer of weight, 1 J, was used. Average of seven replicate samples was recorded to obtain the impact strength (IS).

3.4.8 Differential scanning calorimetry (DSC) analysis

Differential scanning calorimetry (DSC) analysis was carried out to determine the glass transition temperature (T_g), melting temperature (T_m) and crystallization temperature (T_c) of the composite material.

3.4.9 Thermogravimetric analysis (TGA)

Thermal properties of the PLA-HA composite were studied through TGA analysis. In addition, DTG analysis was used to support result of the TGA analysis. Thermogravimetric analysis (TGA) and differential thermal gravimetry (DTG) analysis were conducted using a TA analyzer (TGA Q500 V6.4, Germany). The sample was placed in a platinum crucible and analysis was performed under nitrogen atmosphere (flow rate: 40 mL min^{-1}) at 10 ^{o}C min^{-1} from room temperature to 800 ^{o}C.

3.4.10 Dynamic mechanical analysis (DMA)

Dynamic mechanical analysis (DMA) was used to obtain more information about the structure and viscoelastic properties of the PLA-HA composites. This was used to investigate the structure and damping of the composite as a function of time, stress, temperature and frequency. This analysis was conducted using a Dynamic Mechanical Analyzer (DMA Q800) instrument. Specimen analysis was performed from room temperature to 130 ^{o}C using a single cantilever mode (amplitude: 20 µm). The frequency was 1 Hz, and the heating rate was 3 ^{o}C min^{-1}. The cantilever has a length of 35 mm and the cross-section of the specimens was 10 mm x 4 mm.

3.4.11 Degradation studies

Controlled degradation of the composite was carried out through aging analysis. Tensile bar samples of PLA, and the PLA-HA composite were immersed in distilled water inside a beaker. The beaker and the content were then placed in a laboratory oven for a period of five weeks. The sample preparation was done in two parts, with both parts having similar content. The first part was placed in an oven set at 40 ^{o}C whereas the second part was placed in an oven set slightly above the T_g of PLA (65 ^{o}C). Samples were taken after 1, 3, and 5 weeks and dried after which tensile and flexural testing was conducted on them as described in previous section.

3.5 Antimicrobial Analysis

Antimicrobial properties of the PLA and selected categories of the PLA-HA composites were verified through exposure to two different bacterial. The bacterial strains investigated are *Escherichia coli* ATCC 8739 and *Staphylococcus aureus* ATCC 6838. These bacteria were collected from the culture store of the Central Laboratory of Universiti Malaysia Pahang after which they were kept in the chiller at 4 - 6 °C until the analysis was conducted.

3.6 Biocompatibility Studies

The biocompatibility of the PLA-HA composites was evaluated through cell culture assay.

3.6.1 Cell culture

Osteoblast cell lines were cultured in Dulbecco's modified Eagle's medium (DMEM) supplemented with 10% fetal bovine serum and 5% penicillin/ streptomycin. The cells were maintained at 37 ºC humidified 5% carbon dioxide (CO_2) atmosphere.

3.6.2 Cell proliferation test

The proliferation test was performed following the methods described in literature (Fauzi et al., 2011), with slight modification. Normally, at least 5 x 10^3 cells per well is necessary to perform proliferation assay for osteoblast cell lines. In this study, the cells were distributed in 12-well cell culture plates at a concentration of

approximately 1 x 10^4 cells prior to adding the materials in each different well in size of 10 mm x 10 mm. The cells were then allowed to adhere overnight and the culture medium was replaced with standard medium. The cell proliferation was viewed though images taken from inverted microscope after 1, 3, 5 and 7 days, using Trypan blue staining and also by MTS assay test.

3.6.3 Cell viability assay

The cell proliferation was quantified using MTS assay. The Cell Titer 96® Aqueous One Solution Reagent was thawed for about 10 min in a water bath at 37 °C, to completely thaw the 20 ml size. Cell Titer 96® Aqueous One Solution Reagent (20 µl) was pipetted into each well of the 96-well assay plate containing the samples in 100 µL of culture medium. The plate was then incubated at 37 °C for 3 h in a humidified, 5% CO2 atmosphere. The amount of soluble formazan produced by cellular reduction of MTS was measured by recording the absorbance at 490 nm using a 96-well plate reader. The absorbance recorded at 490 nm corresponds to the cell viability such that the cell viability can be calculated using Equation 3.8.

$$Cell\ viability = \frac{A_{sample}}{A_{control}} x\ 100 \qquad 3.8$$

Where, A_{sample} is the absorbance of the sample at 490 nm, $A_{control}$ is the absorbance of the positive control at 490 nm. Positive control means that the cells are incubated in the complete medium without the samples.

CHAPTER 4

RESULTS AND DISCUSSION

4.1 Properties of the Produced Hydroxyapatite (HA)

The properties of the produced HA are herein discussed based on the influence of calcination temperature. The HA produced after calcination at 950 ^{o}C was modified and the influence of surface modification on properties of the HA was further discussed in the subsections following this section.

4.1.1 General appearance of HA at different calcination temperature

Calcination of the raw bone powder at different temperature led to difference in colour of the apatite produced. The original colour of the cow bone powder was light yellow. The colour revealed by the produced apatite at different temperature is summarized in Table 4.1.

Table 4.1 Colour of obtained HA after calcination of cow bone powder at different temperature

Calcination temperature (^{o}C)	**Appearance**
650	Black
750	Dark grey
850	Light grey
950	White

The difference in colour of the samples with respect to calcination temperature can be related to the effect of organic matters (such as collagen and protein). The amount of organic matter removed from the starting material during calcination may be the reason for the different colours. Since the desired white colour of the hydroxyapatite was only obtained after calcination at 950 ^{o}C, it can be inferred that calcination at

950 ^{o}C was suitable for complete elimination of organic components from raw cow bone powder.

4.1.2 Thermo gravimetric analysis (TGA)

The TGA curves of raw cow bone powder (RAW) and the apatites obtained at different calcination temperature are illustrated in Figure 4.1. As can be seen from the spectra for raw cow bone powder, and the sample calcined at 650 ^{o}C, there was an early weight drop which occurred from 50-200 ^{o}C, which is attributed to the release of residual surface adsorbed moisture. This weight drop is not significantly obvious in the other samples, which suggests that the samples had insignificant amount of surface adsorbed moisture. Starting from 250 ^{o}C to around 500 ^{o}C, another stage of weight drop can be observed in the spectrum of RAW, and the sample calcined at 650 ^{o}C which is associated with the burning of organic components present in the samples. Presence of this stage of weight drop in the sample calcined at 650 ^{o}C can be ascribed to possible incomplete removal of organic components from the sample. Generally for all the samples, the other observable weight drop in temperature range from 600 ^{o}C to 800 ^{o}C may be attributed to endothermic dissociation of CO_3^{2-}. This suggests that the apatites obtained herein comprises reasonable amount of CO_3^{2-} ions.

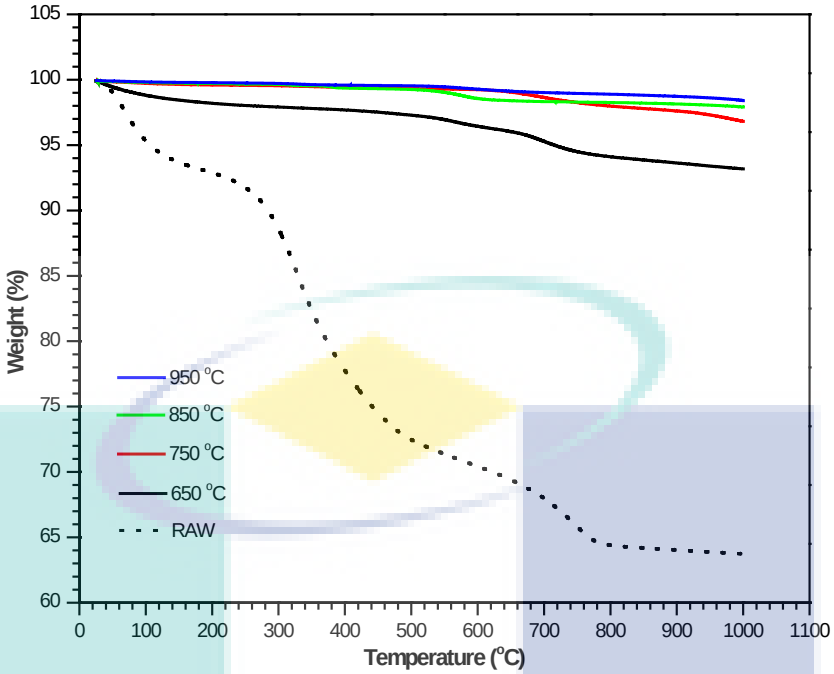

Figure 4.1 TGA spectra for raw cow bone powder (RAW) and HA obtained after calcination at 650 °C, 750 °C, 850 °C and 950 °C

4.1.3 Field emission scanning electron microscopy

The FESEM images of the raw cow bone powder (RAW) and samples calcined at different temperature are shown in Figure 4.2. As can be seen in Figure 4.2, the produced HA shows an almost uniform spherical shape with dispersion in the order RAW < 650 °C < 750 °C < 850 °C < 950 °C. Generally, HA can exhibit different morphological shape depending on the synthesis route and one of the reportedly possible shapes is spherical (Nirmala et al., 2011; Zhou et al., 2011), which aligns with what is obtained herein. It is noteworthy that after calcination at 950 °C, the HA produced, reveals good interconnectivity as is usually found in natural bone apatites. In addition, it shows greater increase in size compared with other samples which is attributed to the high tendency for HA particles to crystallize and therefore grow up under elevated temperature (Barakat et al., 2009; Quan et al., 2015). This observed size increase also conforms to results of the crystal size and crystallinity which was evaluated through XRD analysis.

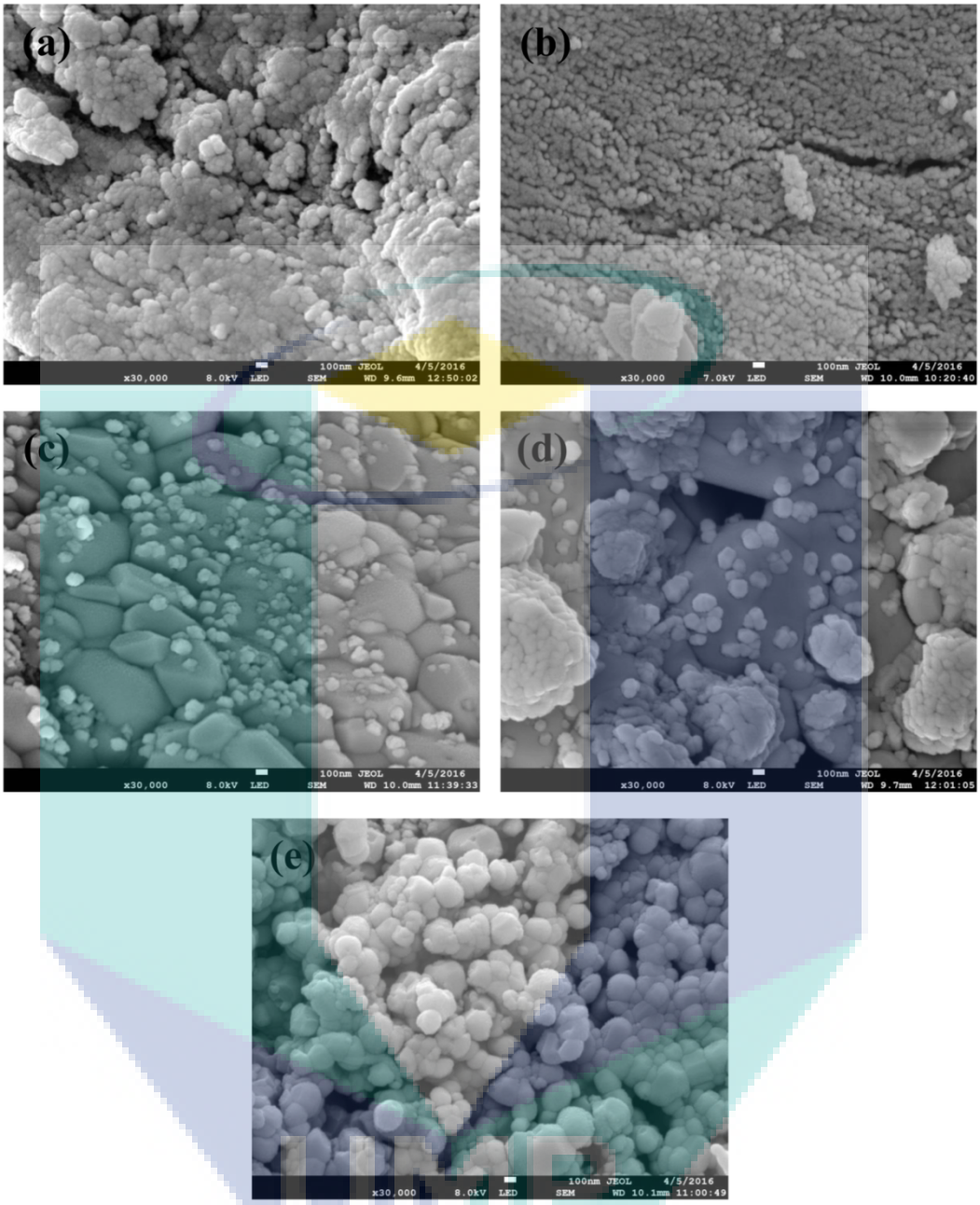

Figure 4.2 FESEM images for (a) raw cow bone powder (RAW), and samples calcined at (b) 650 ^{o}C, (c) 750 ^{o}C, (d) 850 ^{o}C and (e) 950 ^{o}C

4.1.4 Fourier transforms infrared (FTIR) spectroscopy analysis

Representative spectrum from the samples calcined at 950 ^{o}C is illustrated in Figure 4.3. For comparison purpose, FTIR spectrum for the raw cow bone powder (RAW) is also illustrated in Figure 4.3. The band which appeared at the higher wavelength from 3200-3500 cm^{-1} is an attribute of stretching vibrations of bonded –OH (Akindoyo, 2015). Representation of –OH groups also appeared at 1637 cm^{-1} in the spectrum of RAW which is attributed to presence of surface adsorbed moisture on the raw bone powder (Liuyun et al., 2012; Quan et al., 2015). This same observation was

also revealed through the TGA analysis. However, this peak may also be associated with the hydroxyl groups present in the HA structure (Jang et al., 2014). Around 2840-2930 cm^{-1} there is a low intense band which is a characteristic of C-H stretching vibrations (Akindoyo, 2015). This band which is conspicuous in the spectrum of RAW can be attributed to presence of organic components in the raw bone powder as confirmed through TGA analysis.

On the contrary, this band is not significant in the representative HA spectrum. This indicates that the organic components present in the starting materials has been removed after calcination at 950 ^{o}C thereby producing pure HA as reported in literature (Haberko et al., 2006). The double split peaks which can be seen at 1457 cm^{-1} and 1411 cm^{-1} are attributes of asymmetric CO_3^{2-} stretching which confirms that CO_3^{2-} really entered the HA lattice. This also aligns with the XRD and TGA results and it also conforms to report from previous study (Liuyun et al., 2012). The peaks at 1015 cm^{-1} and 960 cm^{-1}, are attributed to phosphate (PO_4^{3-}) stretching vibration, and the peak around 550-650 cm^{-1} is attributed to deformational vibration of (PO_4^{3-}) (Lü et al., 2007; Wu et al., 2015). The other peak at 872 cm^{-1} is a further confirmation of ionic CO_3^{2-} substitution into the HA lattice. This can however be attributed to type *A*- or type *B*-carbonate substitution, which indicates the presence of surface labile CO_3^{2-} (Quan et al., 2015). In general, these observations are consistent with TGA result and also align with what is reported in literature (Ooi et al., 2007).

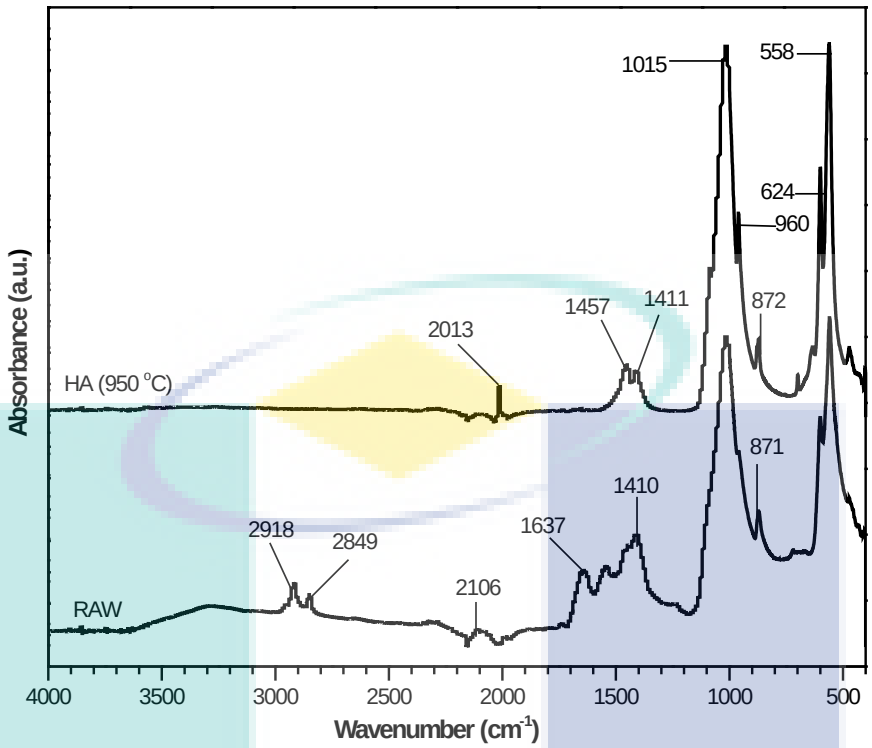

Figure 4.3 FTIR spectra for raw cow bone powder (RAW) and HA obtained at 950 °C

Considering the results obtained herein, it can be concluded that the produced HA has similar chemical features with the biominerals present in calcified bone and can therefore be exploited for fabricating bone replacement materials.

4.1.5 Elemental analysis

Based on the results obtained through TGA, XRD, FESEM and FTIR it can be inferred that pure HA was produced after calcination of the raw bone powder at 950 °C. Notwithstanding, further evaluation of the produced HA was conducted through analysis of its elemental composition. Firstly, energy dispersive X-ray (EDX) profile was taken for the FESEM image of the HA produced at calcination temperature of 950 °C (Figure 4.2e). The EDX profile of the material can be seen in Figure 4.4, which reveals highly pronounced Ca and P peaks. This is a good indication that the material exhibit similar elemental composition with standard HA (Jang et al., 2014). Based on the characteristic chemical structure of standard HA, it has been reported that the Ca/P stoichiometric ratio is approximately 1.67 (Habraken et al., 2016). Quantitative analysis of the EDX profile was used to obtain the Ca/P ratio of the produced HA. Likewise, X-ray photoelectron spectroscopy (XPS) was used to analyse the elemental composition of the HA and its Ca/P ratio was evaluated. The calcium and phosphorus content of the

HA produced, as analysed through EDX and XPS is summarized in Table 4.2. From quantitative analysis of these components, the Ca/P value was deduced and it is included in Table 4.2. As can be seen, the Ca/P value obtained for the HA is 1.70 (EDX) and 1.69 (XPS), and both of these values fall within the acceptable stable range (1.4 – 2.4) for atomic Ca/P ratio of HA (Ergun et al., 2011). It is noteworthy that the XPS Ca/P value corroborates the EDX data; therefore the Ca/P value obtained here is reasonably acceptable. In addition, these values are very close to stoichiometric ratio of normal apatite and can therefore be regarded as a bone-like apatite (Jiang et al., 2016). The little deviation in these values from the stoichiometric HA can be attributed to the presence of CO_3^{2-} ions which was confirmed through TGA and FTIR results. It can also be attributed to the compositional constituents of other minor elements which in addition to EDX and XPS, were further confirmed through CHNS and XRF. Be as it may, it is worthy of note that the presence of reasonable proportion of CO_3^{2-} as well as other minor elements are highly desirable to ensure good biological performance of HA, especially for bone replacement purposes.

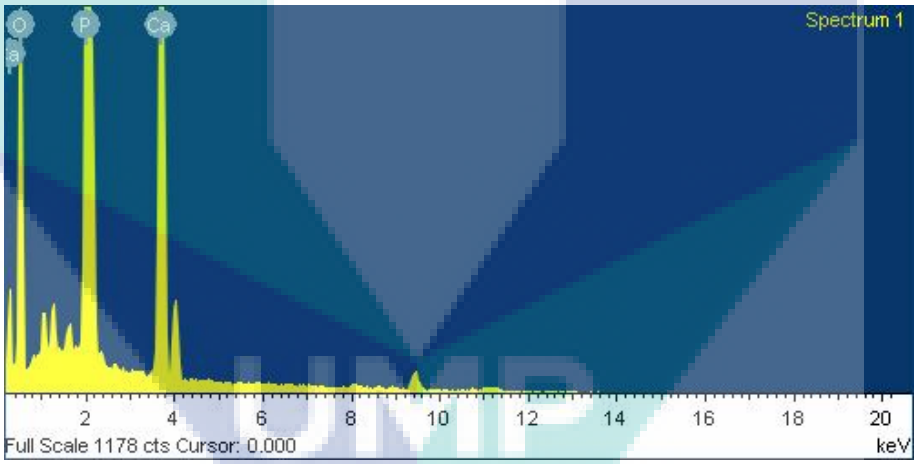

Figure 4.4 EDX profile of the HA produced at calcination temperature of 950 ^{o}C

Table 4.2 Composition and Ca/P value of major elements present in the HA, as obtained through EDX and XPS

EDX				XPS		
Element	**Weight %**	**Atomic %**	**Ca/P**	**Element**	**Atomic %**	**Ca/P**
Ca	30.21	23.08	1.70	Ca	10.63	1.69
P	21.24	13.57		P	6.29	
O	48.55	63.35		O	40.84	
				C	41.68	

4.2 Modification of HA Surface

In order to improve the compatibility of HA with PLA, and also to impart some antimicrobial properties onto the HA surface, modification of the produced HA was conducted. Surface of the HA obtained at calcination temperature of 950 ^{o}C was modified by incorporation of phosphate based modifier (Dicopper hydroxide phosphate) onto the HA surface. This particular surface modifier was selected based on its potentiality to offer dual effect to the modified HA. Firstly, it is expected that antimicrobial properties should be introduced onto the HA surface and secondly, dispersion and compatibility of HA with PLA is well envisaged.

4.2.1 Fourier transforms infrared spectroscopy (FTIR)

The FTIR spectra of the produced HA, phosphate based surface modifier, and surface modified HA are illustrated in Figure 4.5. Some of the important peaks include the bands at higher wavelength, above 3400 cm−1 and at 632 cm−1 which are characteristics of –OH stretching vibration (Liuyun et al., 2012). The band which can be seen around 2840-2930 cm^{-1} in modified HA is attributed to C-H stretching vibrations (Akindoyo et al., 2015b). This peak is not evident in the unmodified HA spectrum, which is associated with the elimination of organic components from the raw bone powder during HA production (Ruksudjarit et al., 2008). On the other hand, the appearance of this peak in the modified HA spectrum is an evidence of effective modification of HA surface by the surface modifier and it is interesting to note that this can influence the level of compatibility between HA and hydrophobic polymers such as PLA during composite production.

The double split peaks which is evident at 1457 cm^{-1} and 1413 cm^{-1} are attributes of the asymmetric stretching of CO_3^{2-} which is as a result of CO_3^{2-} substitution

into the lattice of the HA during production (Liuyun et al., 2012). Another peak which is associated with the ionic CO_3^{2-} substitution into the HA lattice can be seen at 876 cm^{-1} which is an attribute of either type *A*- or type *B*- CO_3^{2-} substitution. The peaks at 1009 cm^{-1} and 960 $cm^{-1}$are attributed to vibrational stretching of phosphate (PO_4^{3-}) and the peak around 550-650 cm^{-1} is due to vibrational deformation of phosphate (PO_4^{3-}) ions (Lü et al., 2007). It is noteworthy that the peak at 1009 cm^{-1} in spectrum of the unmodified HA had shifted upwards in the modified HA spectrum thereby appearing at 1016 cm^{-1}. This is a resultant effect of the surface modifier and this observable shift can be attributed to possible contractions emanating from increased intermolecular hydrogen bond owing to the increase number of –OH groups on the surface of the modified HA. Generally, it can be observed that after surface modification, the HA characteristic peaks are still retained with the inclusion of few other peaks which are believed to have been contributed by the surface modifier. This is an indication that the surface modifer did not convert the produced HA into another entire material but only modified its surface.

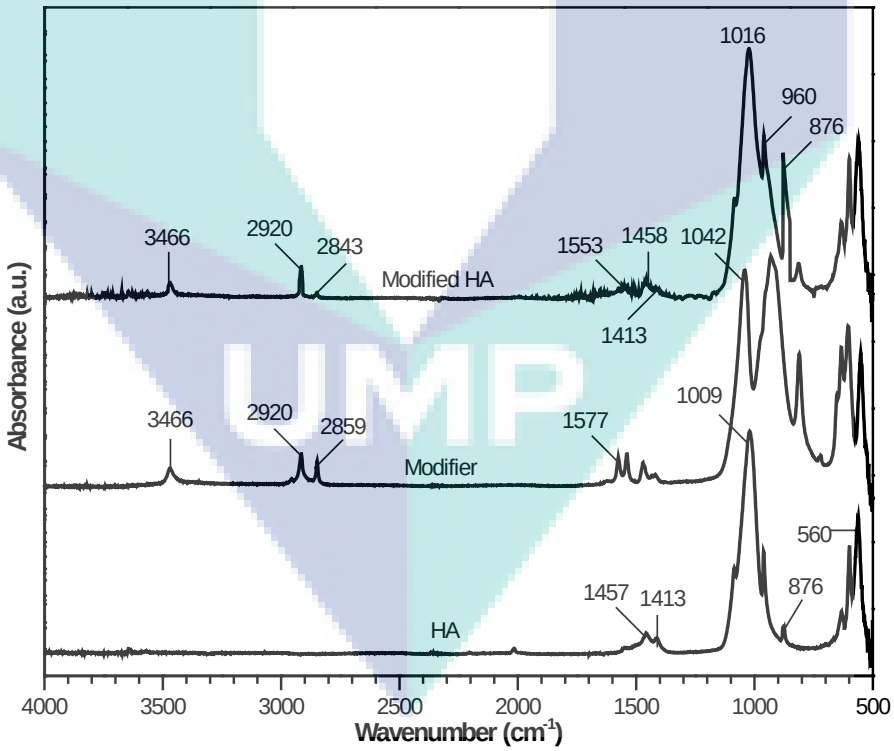

Figure 4.5 FTIR spectra of the produced HA, phosphate based surface modifier, and the modified HA

4.2.2 X-ray fluorescence

The results obtained from the XRF analysis of the modified HA is summarized in Table 4.3. Similar to what was obtained for the unmodified HA, large amount of calcium, and phosphorus were obtained whereas other minor elements were detected in lesser amounts (Table 4.3). The major difference in the data obtained for the unmodified HA and the modified HA is the amount of copper (Cu) detected. The modifying agent used for HA modification consists of copper ions which is needed to provide antibacterial properties to the HA. Therefore, the amount of copper (2.13 %) detected in the modified HA compared with the unmodified HA (36 ppm) is as a result of the presence of copper ions in the modifying agent.

Table 4.3 Elemental composition of the modified HA, as obtained through XRF and CHNS

Element	Quantity	Unit
Calcium (Ca)	30.89	%
Phosphorus (P)	10.52	%
Copper (Cu)	2.13	%
Carbon (C)	2.34	%
Magnesium (Mg)	0.28	%
Chlorine (Cl)	0.05	%
Potassium (K)	0.03	%
Strontium (Sr)	0.02	%
Sulphur (S)	0.02	%
Silicon (Si)	0.02	%
Aluminium (Al)	0.02	%
Iron (Fe)	86	Ppm
Zirconium (Zr)	3	Ppm

4.2.3 Antimicrobial properties

The inhibitory effect of modified and unmodified HA on different gram-negative and gram-positive bacteria, the list of the challenge microorganisms investigated, and the diameter of their inhibition zones are presented in Table 4.4. As can be seen in Table 4.4, the unmodified HA did not reveal significant zone of inhibition which indicates that the unmodified HA does not possess antibacterial properties.

On the other hand, the modified HA revealed significant inhibitory zones which are a confirmation of the antibacterial effect of the modified HA. Based on diameter of inhibition as can be seen in Table 4.4, the modified HA showed more potent antibacterial activity against Staphylococcus aureus which is gram (+) bacteria than other investigated bacteria which are gram (-) bacteria.

Generally, the cell wall of gram-positive bacteria consists of several layers of teichoic acids and peptidoglycan, which forms a thick and rigid structure. As for gram-negative bacteria, the cell wall is made up of a thin layer of peptidoglycan which is surrounded by another lipid membrane containing lipoproteins and lipopolysaccharides. This outer membrane layer present in the cell walls of gram-negative bacteria typically protects it from antibacterial agent which is usually the reason for reduced effect of antibiotics and antimicrobial agents on gram-negative bacteria compared with gram-positive bacteria (Nirmala et al., 2011). This phenomenon is very much consistent with the results obtained from this study. Therefore, the larger zone of inhibition observed for Staphylococcus aureus can be attributed to high susceptibility of gram-positive bacterial to antibacterial agents due to the lack of outer membrane protections which would normally protect gram-negative bacterial for antimicrobial agents (Nirmala et al., 2011).

Table 4.4 Challenge organisms and the zone of inhibition diameter formed with respect to modified and unmodified HA

Microorganisms	**Type**	**Diameter of inhibition zone (mm)**	
		HA	**Modified HA**
Escherichia coli	Gram (-)	0	34
Pseudomonas auruginosa	Gram (-)	0	34
Staphylococcus aureus	Gram (+)	0	45
Salmonella enterica	Gram (-)	0	32

4.3 Effects of HA Content on Properties of PLA-HA Composites

In order to obtain the optimum wt% content of HA to be incorporated into the PLA matrix for optimum performance, different wt% content of HA (5-20 wt%) was incorporated into the PLA matrix to produce PLA-HA composites. The HA content was selected based on preliminary studies. The effect of HA wt% on the properties of the PLA-HA composites was analysed.

4.3.1 Mechanical properties

The variation in tensile strength (TS), and tensile modulus (TM) of PLA and PLA-HA composites containing different wt% (5-20 wt%) HA content is illustrated in Figure 4.6. Likewise, the variation in flexural strength (FS) and flexural modulus (FM) of PLA and PLA-HA composites containing different wt% (5-20 wt%) HA content is illustrated in Figure 4.7. Looking at these two figures, the TS and FS can be seen to follow the same trend, showing observable decrease as the HA content increases. The TS and FS for PLA are 65.3 MPa and 106 MPa respectively. After incorporation of 5 wt% HA, the values reduced to 56.5 MPa (TS) and 98.5 MPa (FS). This decreased continues as the HA content increase and at 20 wt% HA content, the TS and FS had reduced to 47.4 MPa and 86.3 MPa respectively. This is a decrease of about 27% and 19% for TS and FS respectively. This observed decreases can be attributed to the low strength of HA as reported in literature (Cucuruz et al., 2016; Zhang et al., 2014), most probably due to elimination of the organic components from the raw bone powder during production of HA. In another vein, it has been previously reported that mechanical properties of PLA-HA composites can be influenced by the rate of HA dispersion within the PLA matrix (Liuyun et al., 2013). Thus dispersion issues might have influenced the observed reduction in TS and FS of the PLA-HA composites as the HA content increases which can be verified through SEM observation. Also, the reduction in TS as HA content increased may be attributed to possible premature failure at the PLA-HA interface.

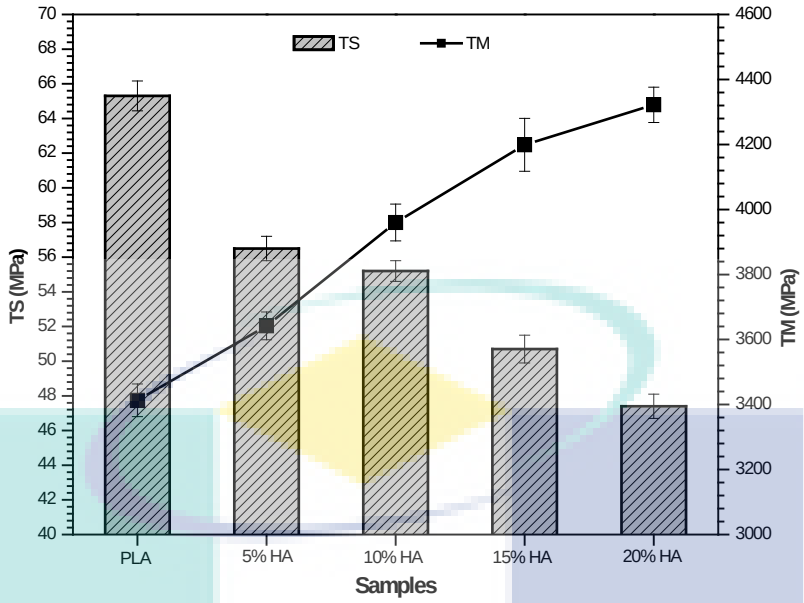

Figure 4.6 TS and TM of PLA-HA composites, containing different wt% HA content

On the other hand, TM (Figure 4.6) and FM (Figure 4.7) can be seen to exhibit similar trend of concurrent increases as the HA content increases. Specifically, the TM and FM of PLA are 3413 MPa and 3240 MPa respectively. There is an observable increase in these values as HA was incorporated into the PLA matrix and at 20 wt% HA content, the TM and FM of the PLA-HA composite are 4322 MPa and 4310 MPa respectively. The enhancement in TM and FM after inclusion of HA is attributed to the higher modulus of HA compared with PLA.

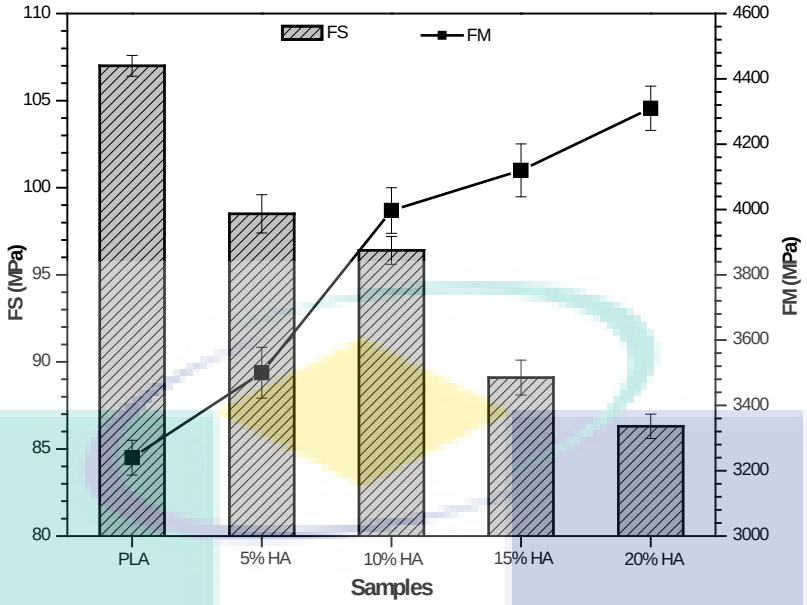

Figure 4.7 FS and FM of PLA-HA composites, containing different wt% HA content

4.3.2 Morphological properties

The images obtained from the SEM observation of the fractured surfaces of PLA and PLA-HA composites after mechanical test are shown in Figure 4.8. From this figure, it can be seen that the fractured surface of PLA is free without any observable presence of HA. On the other hand, the HA within the PLA-HA composite becomes more noticeable as the HA wt% content increases. Likewise, it can be seen that the dispersion of HA within the different categories of the PLA-HA composites is not uniform with observable agglomeration in the composites with higher HA content. Generally, the observable agglomeration in the PLA-HA composites with respect to HA content is in the order 5 wt%<10 wt%<15 wt%,20 wt%. It can therefore be inferred that as the amount of HA wt% content within the PLA-HA composite increases, there is an increasing tendency for agglomeration. Dispersion of HA within PLA matrix is one of the determinants of the mechanical performance of the resulting PLA-HA composite (Liuyun et al., 2013). From the SEM images in Figure 4.8, it can be seen that the dispersion of HA within the PLA-HA composites is poor leading to noticeable agglomeration, with the rate of agglomeration becoming worse for composites containing more than 10 wt% HA content. High degree of agglomeration can serve as stress concentration sites within the composite, thereby facilitating premature failure of the composite. Therefore, this can be the reason for the reduced TS, FS, and IS of PLA-HA composites as the HA content increases. At 5 wt%, the HA seem to be too low to be

noticed but at 10 wt%, the dispersion is more conspicuous. The improved dispersion may be attributed to the fact that at this wt% HA content, PLA was able to mitigate HA-HA agglomeration by coming between the HA particles. However, above this content, agglomeration becomes predominant.

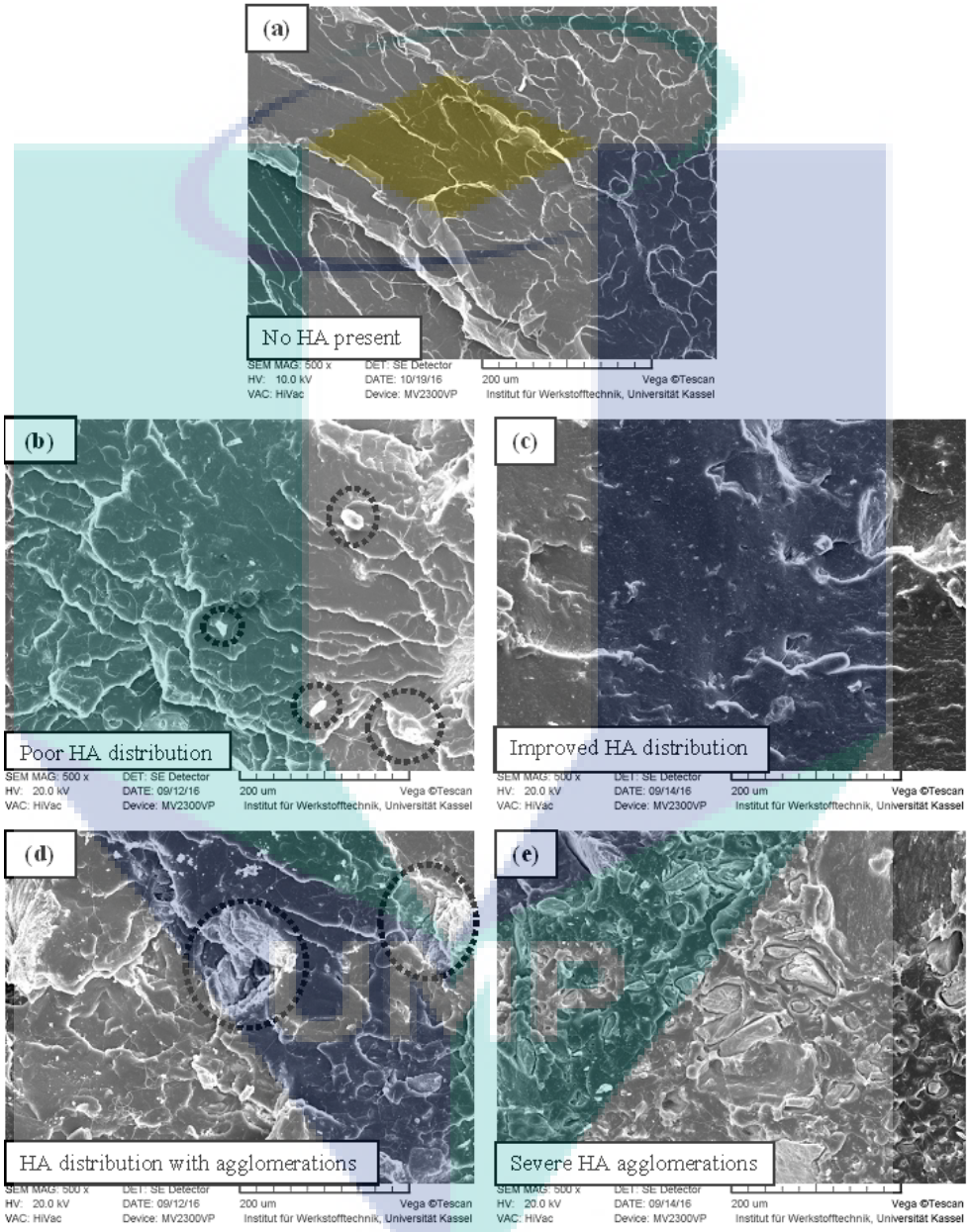

Figure 4.8 SEM images of fractures surface of (a) PLA and PLA-HA composites containing (b) 5% HA (c) 10% HA (d) 15% HA and (e) 20% HA

4.3.3 Fourier transforms infrared spectroscopy

The FTIR spectra of PLA, and PLA-HA composites containing different wt% HA content are illustrated in Figure 4.9. Generally, it can be seen that the spectra are

similar and with some conspicuous important peaks. Some of the important peaks include band around 2999-2850 cm^{-1} which represents symmetric and asymmetric C-H stretching (Akindoyo, 2015). The peak at 1750 cm^{-1} is attributed to C=O stretching vibration of carboxylic acid and ester groups of PLA. The characteristic stretching peak of $–CH_3$ appeared at 1455 cm^{-1}, whereas the C-H deformational peak can be seen at 1375 cm^{-1}. It is believed that as the amount of HA in the composite increases, the number of –OH groups to bond with the terminal –OH and –COOH groups of PLA would also increase. Thus the reduced intensity of the C=O stretching peak at 1750 cm^{-1} as the wt% HA content increases may be attributed to increased bonding within the composite (Akindoyo et al., 2015b). This is also an indication of esterification reaction between terminal carboxylic (–COOH) groups of PLA and –OH groups of the HA.

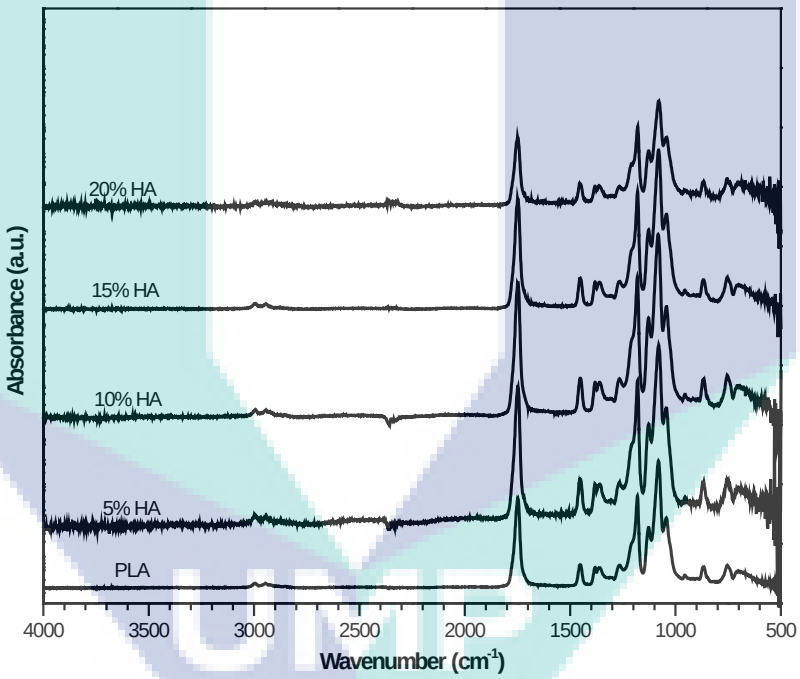

Figure 4.9 FTIR spectra of PLA and PLA-HA composites containing different wt% HA

4.3.4 Thermal properties

The TGA curves of PLA, and PLA-HA composites containing different wt% (5-20 wt%) HA content are illustrated in Figure 4.10. It can be seen from this figure that there is much similarity in pattern of the curves of all the samples. Generally, the temperature for onset of weight loss as a result of degradation of the sample begins around 240 ^oC and the weight drop continued until around 385 ^oC. In order to obtain the

degradation temperature otherwise called temperature of maximum degradation (T_d) of the samples, the DTG curves of the samples was used to support the TGA data.

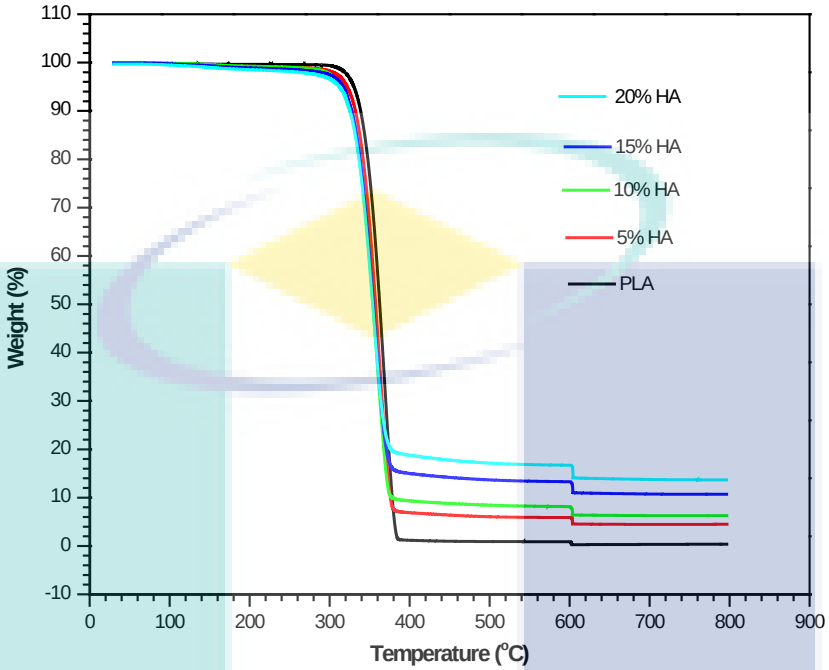

Figure 4.10 TGA curves of PLA and PLA-HA composites containing different wt% HA

The DTG curves of the samples are illustrated in Figure 4.11. It is customary to consider the temperature at which 50% of the sample weight was loss, as the indication of the maximum destabilization (Akindoyo et al., 2015b). Likewise, the degradation temperature (T_d) of the samples can be derived from the DTG curve in Figure 4.11. The TGA properties of the samples are summarized in Table 4.5. From Table 4.5, it can be seen that among the samples, PLA has the highest T_d, which is attributed to the closely parked and well-structured nature of semi crystalline PLA. However, considering the residue (%) at T≥700 ^{o}C of the samples in Table 4.5, it can be seen that the amount of residue obtained from each sample is closely related to the wt% content of HA within the sample. From literature, it was revealed that the extent of interfacial bonding between the matrix and filler is one of the main factors responsible for thermal stability in composites (Essabir et al., 2013b; Nair et al., 2001). Likewise, the extent of filler dispersion within a polymer matrix can influence the thermal stability of the resulting composite (Akindoyo, 2015; Essabir et al., 2013). Therefore as can be seen in Figure 4.11 and Table 4.5, the T_d of the PLA-HA composites decreases as the HA wt% content increases which might be attributed to poor dispersion of HA within the PLA at higher HA content as revealed through SEM observation.

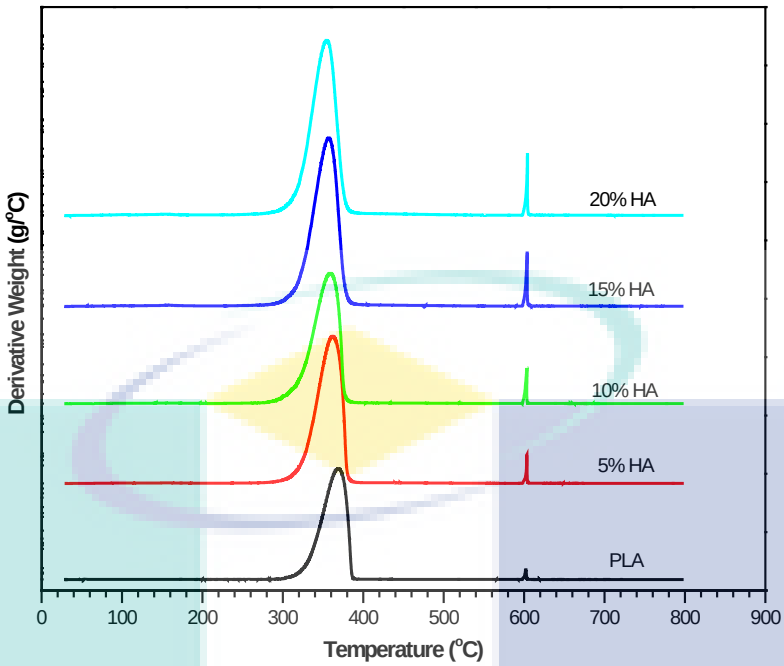

Figure 4.11 DTG curves of PLA and PLA-HA composites containing different wt% HA

Table 4.5 Thermal properties of PLA and PLA-HA composites containing different wt% HA

Samples	**T_{onset} (°C)**	**T_d (°C)**	**Residue (%) at ≥ 700 °C**
PLA	309	362	0.35
5% HA	240	360	3.22
10% HA	240	360	6.05
15% HA	240	358	13.97
20% HA	240	355	17.83

4.3.5 Differential scanning calorimetry

The DSC curves of PLA, and PLA-HA composites containing different wt% HA content are illustrated in Figure 4.12. From Figure 4.12, three distinct successive transitions can be seen from the DSC curves. The first endothermic peak represents the glass transition temperature, (T_g). The second peak is an exothermic transition which represents the crystallization temperature, T_c, whereas the third peak which is also an endothermic peak represents the melting temperature, T_m. As can be seen from Figure 4.12, there is an initial increase in T_g of PLA as the HA wt% content increases up till 10 wt% HA content. After 10 wt% HA content, the T_g of the composite dropped such that at 15 and 20 wt% HA content, the T_g is lower than for pure PLA.

Around the T_g of polymer matrices, the molecular chains become more flexible, as well as gain increased mobility (Jaszkiewicz et al., 2014). Therefore, the shift in T_g of the composites could either be as a result of increased mobility or delayed mobility as a result of increased stiffness (Jaszkiewicz et al., 2014). The initial right shift in T_g of PLA at 5 and 10 wt% HA content can be attributed to restriction imposed by the HA on molecular chain mobility of PLA due to higher stiffness of HA. However, above 10 wt% HA content, the dispersion of HA within the PLA matrix is poor as revealed by the SEM observation. Moreover, there is a high level of agglomeration within the composite which may lead to poor bonding between HA and PLA. These would lead to increased free volume within the composite such that molecular chains have higher tendency to move around. This could be the reason for the decrease in T_g of the composites containing 15 and 20 wt% HA.

The T_c of PLA can be seen to shift towards the lower temperature as the wt% HA content increases. This is an indication of faster crystallization which is believed to be caused by the presence of HA. This increase in the rate of crystallization can be attributed to the high tendency of HA to act as nucleation agents, thereby stimulating heterogeneous nucleation of the PLA matrix (Liuyun et al., 2013). Consequent upon this, a right shift of the endothermic T_m peak can be observed. Generally, whenever cold crystallization occurs, it often leads to the formation of imperfect crystals (Georgiopoulos et al., 2016) and this less perfect crystals would normally melt at temperatures higher than the temperature at which the more perfect crystals would melt. Therefore, the right shift in T_m of the composites can be associated with the presence of imperfect crystals within the composite due to the heterogeneous crystallization induced by HA, on the PLA matrix. This is because the T_m of the composites would be dependent on the fusion of imperfect crystals formed during cold crystallization, and the fusion of new spherulites formed during the process of recrystallization as reported elsewhere (Georgiopoulos et al., 2016).

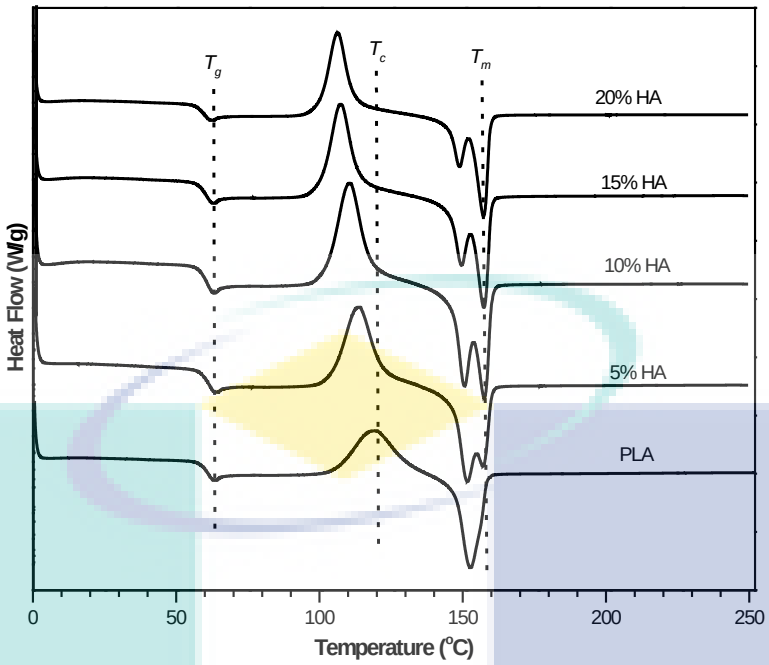

Figure 4.12 DSC thermograms of PLA and PLA-HA composites containing different wt% HA

4.3.6 Dynamic mechanical properties

The effect of temperature on the mechanical properties of PLA and PLA-HA composites was further evaluated through their dynamic mechanical properties. The variation of storage modulus (E′) of the samples with temperature is illustrated in Figure 4.13. It can be clearly seen from the figure that the E′ of all the samples remained almost constant at temperatures below the glass transition (T_g) region, but sharply falls at the glass transition region. Also, it is worthy of note that the E′ of pure PLA is lower compared with the composites. The increased modulus of PLA after the incorporation of HA can be associated with the stiffness imposed on the PLA matrix by HA, which can facilitate effective interfacial stress transfer within the composite. It can also be attributed to the higher modulus of HA compared with PLA (Ferri et al., 2016).

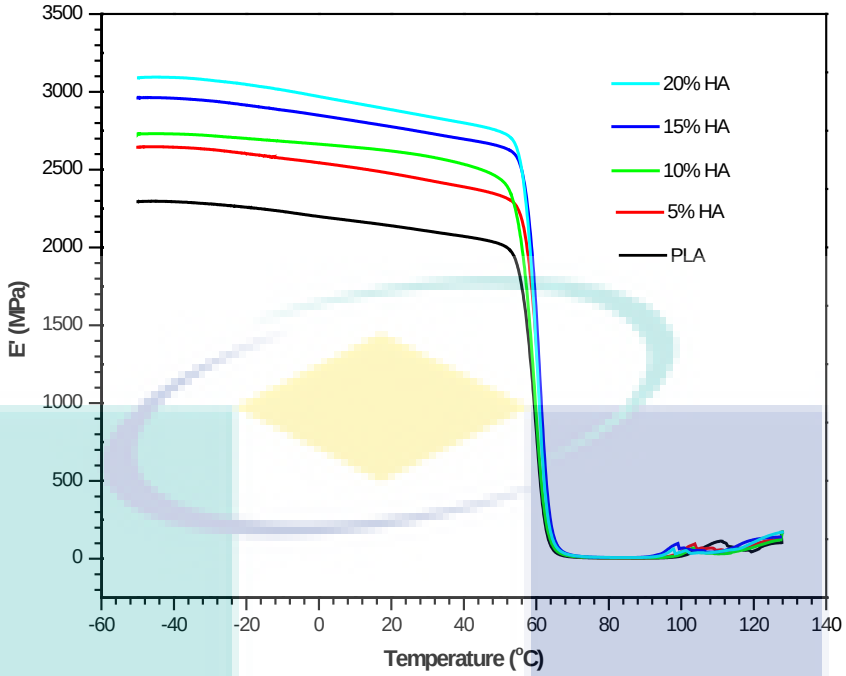

Figure 4.1 Storage modulus curves of PLA and PLA-HA composites containing different wt% HA

The loss modulus (E″) curves of PLA, and PLA-HA composites containing different wt% HA content are illustrated in Figure 4.14. As can be seen, there is a concurrent increase in E″ of all the samples, with increasing temperature. The E″ curves reached a maximum peak (maximum mechanical energy dissipation) at temperature around the glass transition region, before decreasing as the temperature was further increased. This is attributed to the possible increase in mobility of the PLA chains as temperature increased. Below and after the glass transition temperature (maximum peak value of E″ curve), the E″ of the composites is higher than pure PLA. The higher loss modulus peak revealed by the composites compared to PLA can be associated with increased chain segment within the fraction of PLA free volume after inclusion of HA. Based on this, the process of relaxation within the composite might have been inhibited (Romanzini et al., 2013). Furthermore, the observed higher peak of the composites suggests increased energy absorption which may be attributed to the increased energy dissipation sites formed as a result of larger interfacial area within the PLA-HA composites compared with pure PLA. Normally, lower energy dissipation indicates a strong interface such that there is an interrelationship between interfacial adhesion and loss modulus. As HA wt% content increases, the tendency for agglomeration also increases as revealed through SEM observation. This would lead to poor adhesion between HA and the PLA matrix. This could be the reason for the higher E″ peaks of

the composites compared with pure PLA. This can be further evaluated through the loss factor otherwise known as the damping parameter (tan δ) of the material (Etaati et al., 2014).

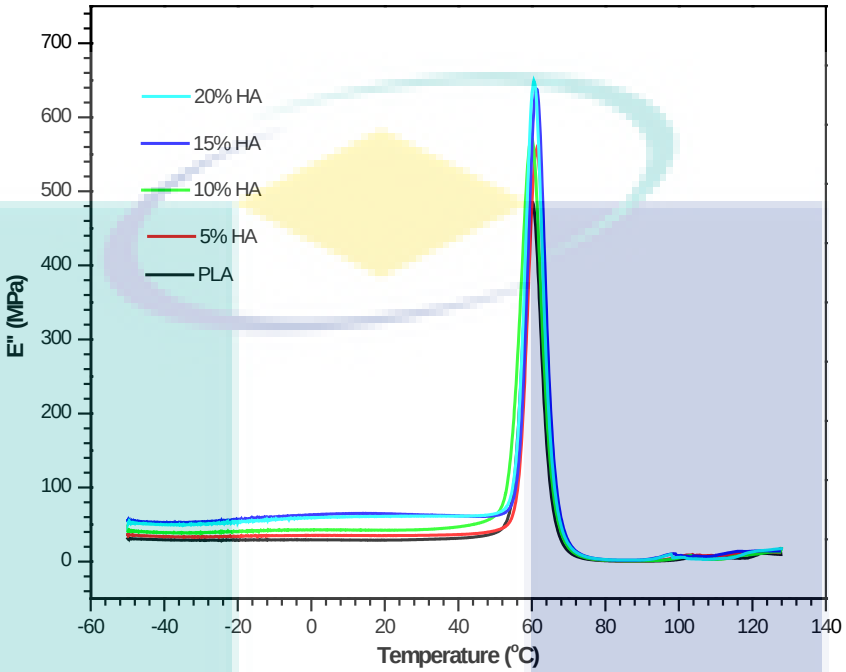

Figure 4.14 Loss modulus curves of PLA and PLA-HA composites containing different wt% HA

The damping parameter (tan δ) can be determined as the ratio of loss modulus E″ (energy dissipated) to the storage modulus E′ (energy stored). From literature, it was revealed that shear stress concentration, and viscoelastic energy dissipation within a composite may influence the damping parameter of the composite (Krishna et al., 2016). This implies that tan δ is largely dependent on the extent of interaction between the matrix and the filler. In essence, a good interaction would produce lower tan δ values whereas poor interaction would produce higher tan δ values due to increase in the polymer chain mobility (Krishna et al., 2016). The tan δ curves of PLA and PLA-HA composites are illustrated in Figure 4.15. It can be seen from the curves that the tan δ value of pure PLA is higher than the composites. This indicates increase in the load bearing capacity of the composites.

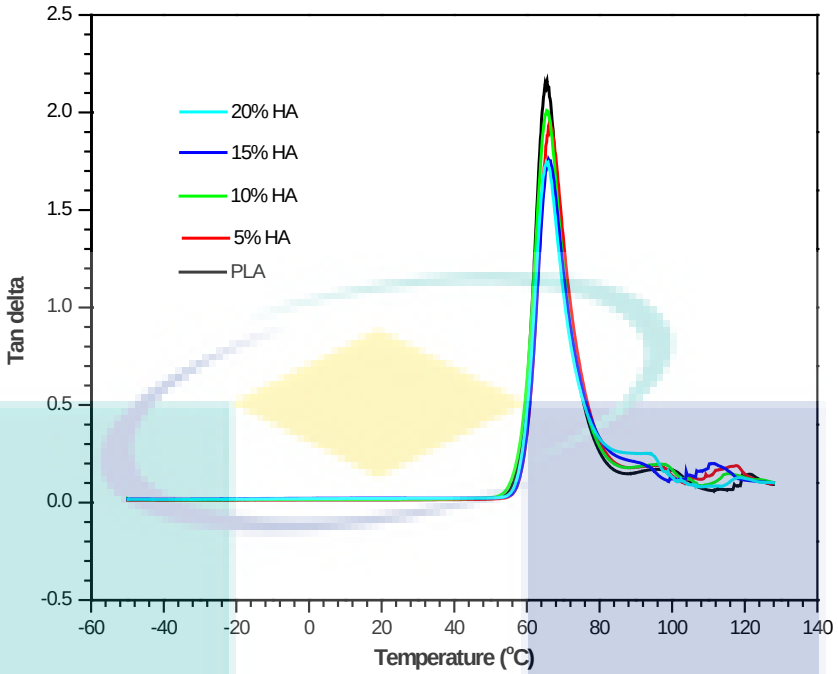

Figure 4.15 Tan delta curves of PLA and PLA-HA composites containing different wt% HA

4.4 Effects of HA Modification on Properties of PLA-HA Composites

Based on the results obtained from the effect of HA content on properties of PLA-HA composites, 10 wt% HA content was found to produce the best compromise between dispersion, mechanical, morphological, thermal and dynamic mechanical properties. Therefore, another composite category containing 10 wt% surface modified HA was produced for further investigation.

4.4.1 Morphological properties

The SEM images of the fractured surface of PLA-HA composites containing 10 wt% HA content before and after HA modification are shown on Figure 4.16. It is obvious from Figure 4.16 b that the dispersion of HA within the PLA matrix was highly improved after surface modification. In fact there is no observable agglomeration of HA within the composite. This is an indication of increased interaction at the PLA-HA interface during blending, which can be attributed to the increase in number of P-OH groups present on the HA surface after modification as illustrated in Figure 4.10. From the FTIR analysis of the produced HA, as discussed earlier, it was revealed that ionic substitution of CO_3^{2-} into the HA structure occurred during HA production. One consequence of this is the reduction in the number of available phosphate –OH groups on the HA surface to bond with PLA during blending. This will invariably decrease the

chemical interaction between PLA and HA within the composite. As illustrated in Figure 4.10, surface modification of HA, which led to increased number of –OH groups on the HA surface can increase the bonding of PLA with HA due to increased interaction of the available –OH groups on the HA surface with the PLA carboxyl groups. Notably, presence of more P-OH groups on the HA surface would enhance electrophoretic mobility of HA, and this accounts for the improved dispersion of HA within the composites (Figure 4.16 b).

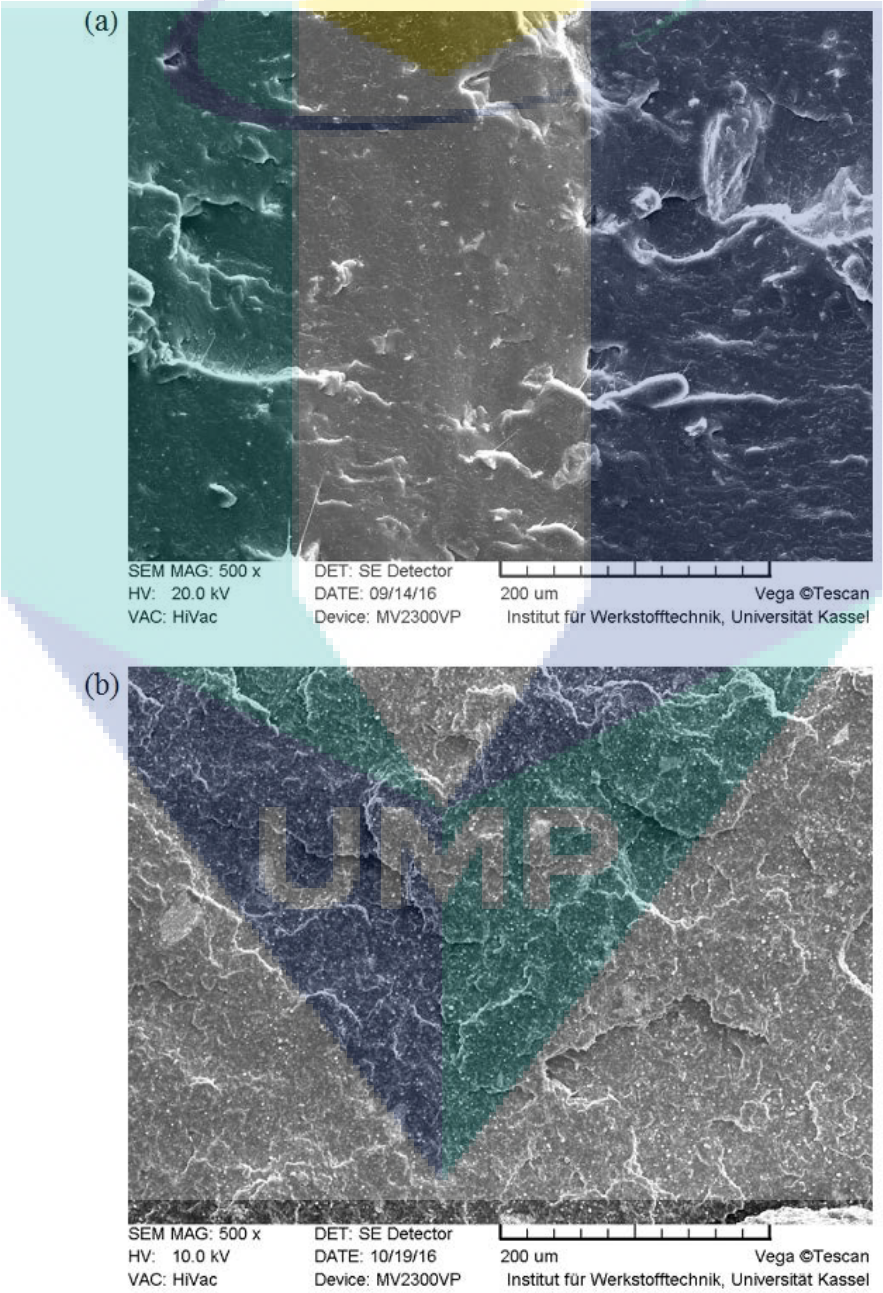

Figure 4.16 SEM images of PLA-HA composites containing 10 wt% (a) unmodified HA and (b) modified HA

4.4.2 Mechanical properties

The tensile strength (TS) and tensile modulus (TM) of PLA, and PLA-HA composites containing modified and unmodified HA, with a fixed HA wt% content of 10% is illustrated in Figure 4.17. Likewise, the flexural strength (TS), and flexural modulus (TM) of PLA, and PLA-HA composites containing modified and unmodified HA, with a fixed HA wt% content of 10% is illustrated in Figure 4.18. For easy nomenclature, the PLA-HA composite containing 10 wt% unmodified HA content is herein referred to as PUHA which stands for PLA-unmodified HA. On the other hand, the PLA-HA composite containing 10 wt% surface modified HA is herein referred to as PMHA which stands for PLA-modified HA.

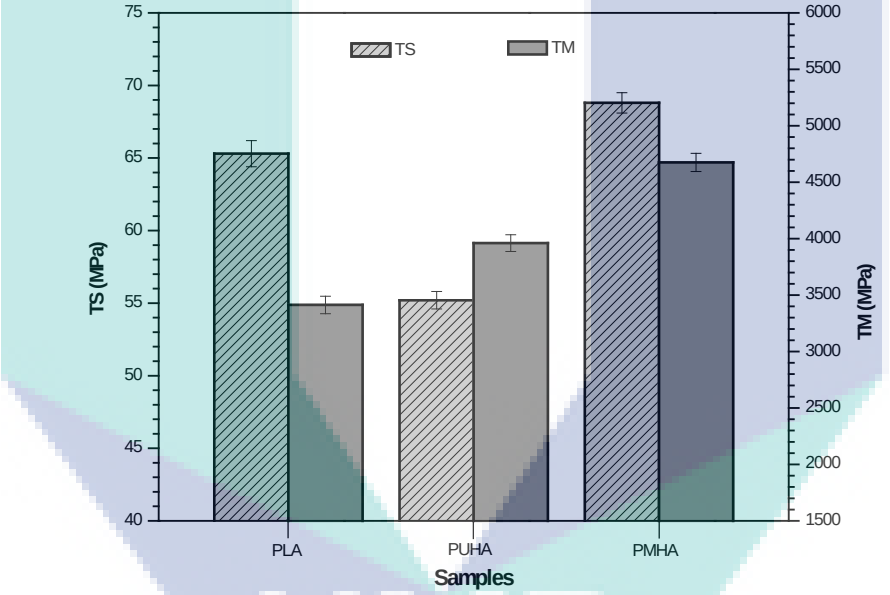

Figure 4.17 TS and TM of PLA, PLA-unmodified HA composite (PUHA), and PLA-modified HA composite (PMHA)

As can be seen from Figure 4.17, the TS of PUHA is lower compared with pure PLA and the reason for this is well explained in previous section. However, it can be seen in Figure 4.17 that TS and TM of the composite increased from 55.2 MPa and 3960 MPa respectively for PUHA, to 68.8 MPa (TS) and 4675 MPa (TM) after incorporation of the modified HA. The increase in TS and TM of PMHA compared with PUHA is about 25% and 18% respectively. In same manner, from Figure 4.18, the FS and FM can be seen to increase from 96.4 MPa and 3997 MPa respectively for PUHA to 115.2 MPa and 4798 MPa respectively for PMHA. This improvement in tensile and flexural properties can be attributed to the improved dispersion of HA within the modified PLA-HA composite as revealed by the SEM result. It also suggests improved

load transfer between the PLA and HA which may be attributed to increased hydrogen bond formation between –OH groups of the surface modified HA and carbonyl groups as well as carboxylic acid ends of PLA (Akindoyo et al., 2015; Alam et al., 2012), as illustrated in Figure 4.26. The FTIR results revealed that there was ionic substitution of CO_3^{2-} into the HA lattice. This would affect the number of active –OH groups available to form bonds with PLA during blending. Specifically, literature revealed that –OH content of HA obtained through heat treatment are most often lower than expected (Quan et al., 2015). Therefore, it can be inferred that the increase in the number of –OH groups on the surface of the modified HA is obviously one major factor that is responsible for the improved mechanical properties of PMHA composite compared with PUHA.

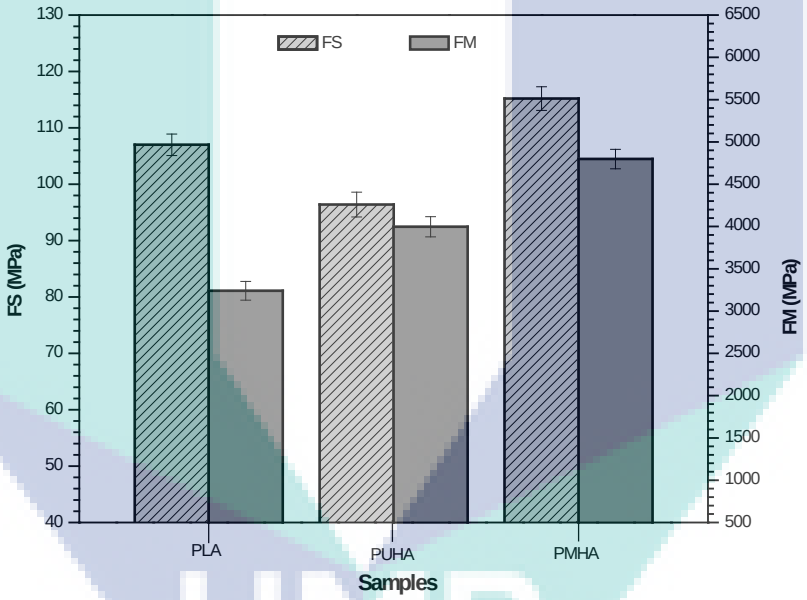

Figure 4.18 FS and FM of PLA, PLA-unmodified HA composite (PUHA), and PLA-modified HA composite (PMHA)

4.4.3 Fourier transforms infrared spectroscopy of composites

The FTIR spectra of PLA and PLA-HA composites containing modified (PMHA) and unmodified (PUHA) HA are illustrated in Figure 4.19. The main peak at the higher wavelength is –OH stretching vibration peak at 3455 cm^{-1}in the PMHA spectra. Another observable peak is the band at 2999-2850 cm^{-1} which is attributed to symmetric and asymmetric C-H stretching (Akindoyo et al., 2015b). Other peaks include C=O stretching vibration at 1750 cm^{-1}, the characteristic stretching peak of $–CH_3$ at 1455 cm^{-1}, and the C-H deformational peak at 1375 cm^{-1}. It is worthy of note that the peak at 3455 cm^{-1} in the PMHA spectra is not evident in the PUHA spectra.

This can be attributed to type *A* substitution of carbonates for –OH groups which is explained in the previous section on FTIR properties of HA. However, this peak which appeared at 3466 cm^{-1} in the modified HA spectra (see Figure 4.5), has shifted to a lower wavenumber (3455 cm^{-1}) in the PMHA spectra (Figure 4.19). This is an indication of hydrogen bonding between the –OH groups of the modified HA and carbonyl groups of PLA (Akindoyo et al., 2015; Alam et al., 2012). This same reason can be associated with the peak shift from 1750 cm^{-1} in the PLA spectra to lower wavenumber regions in the PLA-HA composites. However, it is worthy of note that the downward shift in this peak is further in the PMHA spectra than in PUHA. Increase in the number of –OH to participate in hydrogen bonding with PLA may have contributed to this observation, and it is an indication of better hydrogen bonding in the PMHA composite than in PUHA composite. Furthermore, it signifies esterification reaction between terminal carboxylic (–COOH) groups of PLA and –OH groups of the HA. This observation also explains the reason for the improved mechanical properties of PMHA composite compared with PUHA composite.

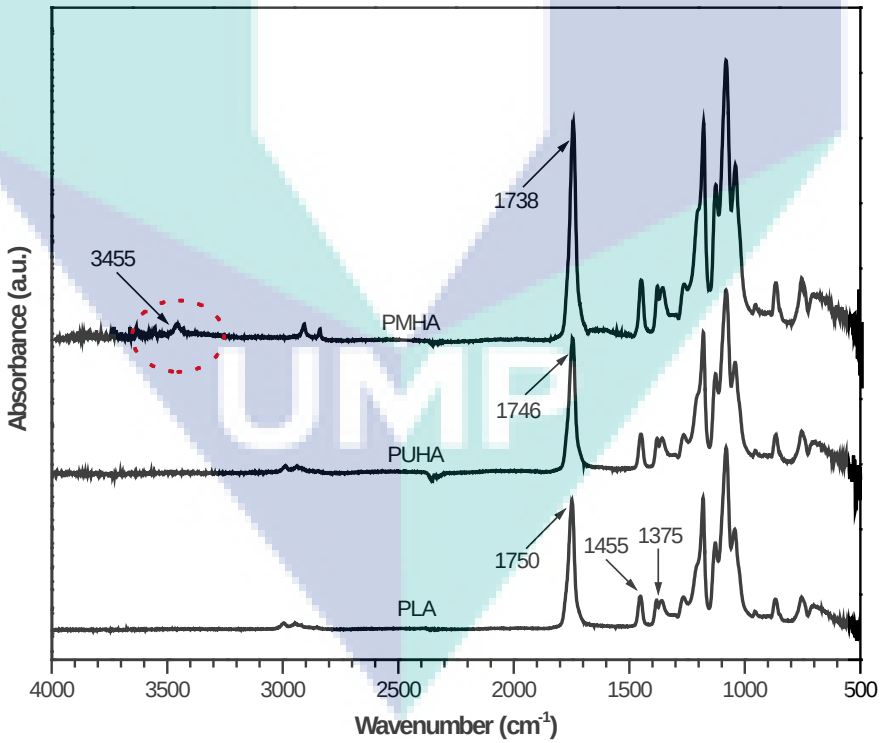

Figure 4.19 FTIR spectra of PLA, PLA-unmodified HA composite (PUHA), and PLA-modified HA composite (PMHA)

4.4.4 Thermogravimetric properties

The TGA curves of PLA, PUHA, and PMHA are illustrated in Figure 4.20. It can be seen from this figure that the curves of all the samples followed similar pattern. In general, the temperature for onset of weight loss as a result of degradation of the sample is around 240 ^{o}C and the weight drop continued until around 385 ^{o}C. In order to obtain the degradation temperature otherwise called temperature of maximum degradation (T_d) of the samples, the DTG curves of the samples was used to support the TGA information. The DTG curves of the samples are illustrated in Figure 4.21 and the degradation temperature (T_d) of the samples can be derived from the DTG curve in Figure 4.21. It is also customary to consider the temperature at which 50% of the sample weight was loss, as the indication of the maximum destabilization (Akindoyo, 2015). The TGA properties of the samples are summarized in Table 4.6 and it can be seen that among the samples, PLA has the highest T_d. This can be associated with the closely parked and well-structured nature of semi crystalline PLA.

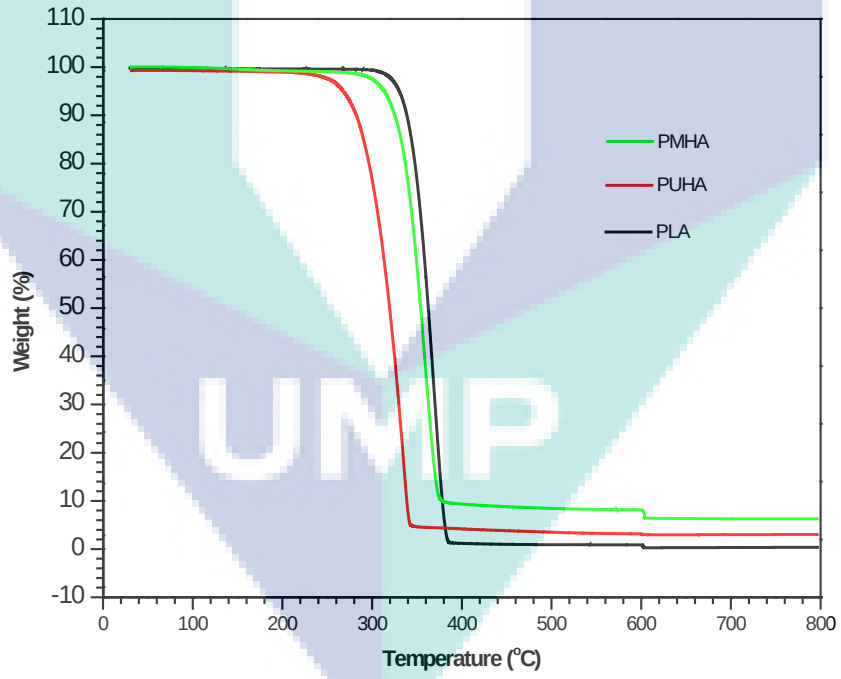

Figure 4.20 TGA curves and of PLA, PLA-unmodified HA composite (PUHA), and PLA-modified HA composite (PMHA)

However, considering the residue (%) at T≥750 ^{o}C of the samples in Table 4.6, it can be seen that the modified HA composite (PMHA) has the largest amount of residue which is an indication of higher thermal stability.

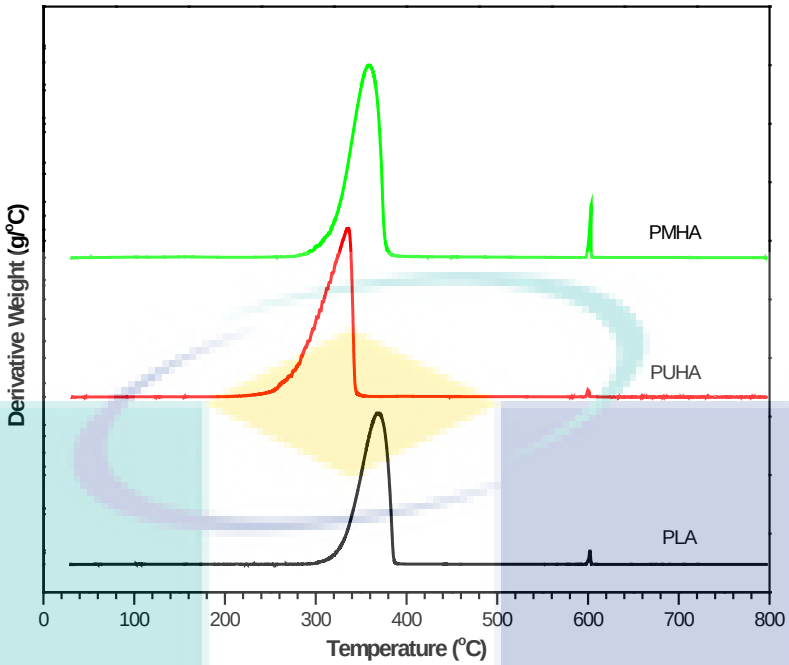

Figure 4.21 DTG curves of PLA, PLA-unmodified HA composite (PUHA), and PLA-modified HA composite (PMHA)

Table 4.6 Thermal properties of PLA and its composite with unmodified and modified HA

Samples	**T_{onset} (°C)**	**T_d (°C)**	**Residue (%) at $T \geq 750$ °C**
PLA	309	362	0.35
PUHA	240	321	6.17
PMHA	307	353	10.27

4.4.5 Differential scanning calorimetric properties

The DSC curves of PLA, PUHA, and PMHA are illustrated in Figure 4.22. It is obvious from this figure that the curve revealed three distinct successive transitions. The first one which represents the glass transition temperature, (T_g), is an endothermic transition. The second transition is an exothermic transition which represents the crystallization temperature, T_c. The third transition is an endothermic transition which represents the melting temperature, T_m. Through a close observation of the curves, it can be seen that there is a slight shift in the T_g of the composites to a higher temperature. It is well known that around the T_g of polymer matrices, the molecular chains gain more flexibility and mobility (Jaszkiewicz et al., 2014). Therefore, the shift in T_g of the composites indicates a delay in the free mobility of the polymer chains which can be accrued to restriction imposed by the HA on molecular chain mobility of

PLA. On the contrary, the T_c of the composites can be seen to shift towards the lower temperature compared to pure PLA. This is an indication of faster crystallization which is believed to be caused by the presence of HA. This increase in the rate of crystallization may be attributed to the high tendency of HA to act as nucleation agents, thereby stimulating heterogeneous nucleation of the PLA matrix (Liuyun et al., 2013).

Consequent upon this, a right shift of the endothermic T_m peak can be observed. Generally, whenever cold crystallization occurs, it often leads to the formation of imperfect crystals (Georgiopoulos et al., 2016) and this less perfect crystals would normally melt at temperatures higher than the temperature at which the more perfect crystals would melt. Thus the higher T_m of the composites can be associated with the presence of imperfect crystals within the composite due to the heterogeneous crystallization induced by HA, on the PLA matrix. When this happens, the T_m of the composites would rather be determined by the fusion of imperfect crystals formed during cold crystallization, and the fusion of new spherulites formed during the process of recrystallization (Georgiopoulos et al., 2016).

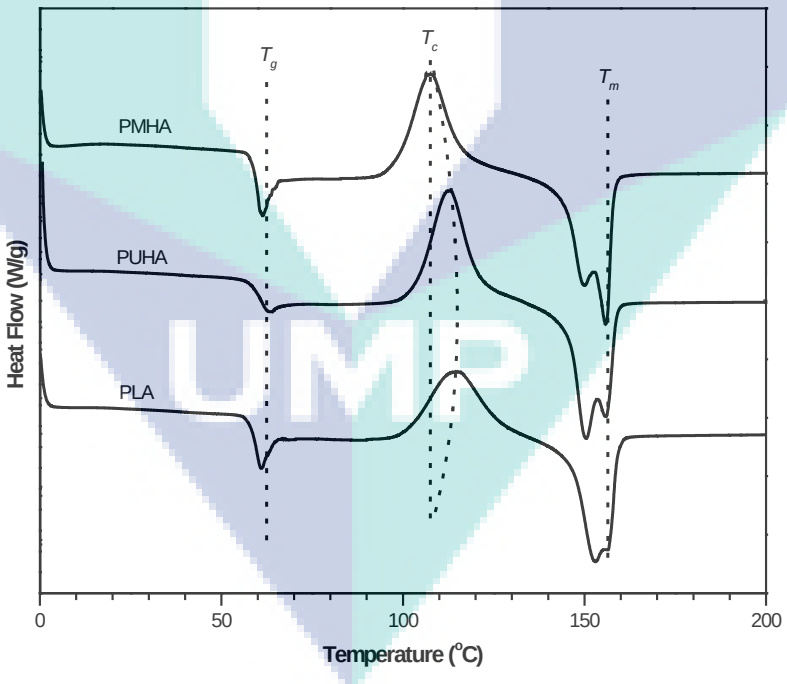

Figure 4.22 DSC spectra of PLA, PLA-unmodified HA composite (PUHA), and PLA-modified HA composite (PMHA)

4.4.6 Dynamic mechanical properties

The variation of storage modulus (E′) of PLA, PUHA, and PMHA composites with temperature is illustrated in Figure 4.23. It can be clearly seen from the figure that the E′ of all the samples remained almost constant at temperatures below the glass transition (T_g) region, but sharply falls at the glass transition region. Also, it is worthy of note that the E′ of pure PLA is lower compared with the composites. The increased modulus of PLA after the incorporation of HA can be associated with the stiffness imposed on the PLA matrix by HA, as this would ensure effective interfacial stress transfer within the composite. Be as it may, it is also noteworthy that the increase in E′ of PLA is higher in the modified HA based composite (PMHA), than the unmodified HA composite (PUHA).

It was gathered from literature that the E′ of composites can be influenced by different factors including filler dispersion, matrix type, type of reinforcing filler, interfacial adhesion, and so on (Essabir et al., 2013b; Nair et al., 2001). This implies that apart from the stiffness imposed on the PLA matrix by HA, the improved HA dispersion which was revealed through SEM observation, might also have contributed to the higher E′ of PMHA. Likewise, the improved interfacial adhesion between the modified HA and PLA must have influenced the improved modulus of the modified PLA-HA composite. This is because the improved HA dispersion and better interfacial adhesion between PLA and the modified HA would enhance the ability of PLA to withstand higher degree of mechanical constraints via recoverable viscoelastic deformation.

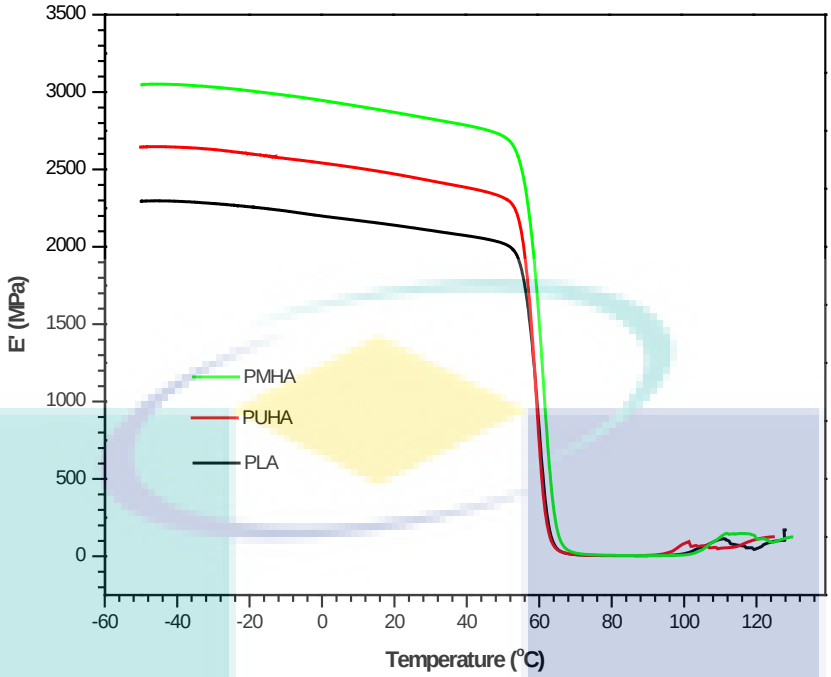

Figure 4.23 Storage modulus curves of PLA, PLA-unmodified HA composite (PUHA), and PLA-modified HA composite (PMHA)

The loss modulus (E″) curves of PLA, PUHA, and PMHA composites are illustrated in Figure 4.24. As can be seen, there is a concurrent increase in E″ of all the samples, with increasing temperature. The E″ curves reached a climax (maximum mechanical energy dissipation) at temperature around the glass transition region, before decreasing as temperature further increased. This is attributed to the possible increase in mobility of the PLA chains as temperature increased. The higher loss modulus peak revealed by the composites compared to PLA can be accrued to increase in chain segment within the fraction of PLA free volume after inclusion of HA. Based on this, the process of relaxation within the composite might have been inhibited (Romanzini et al., 2013).

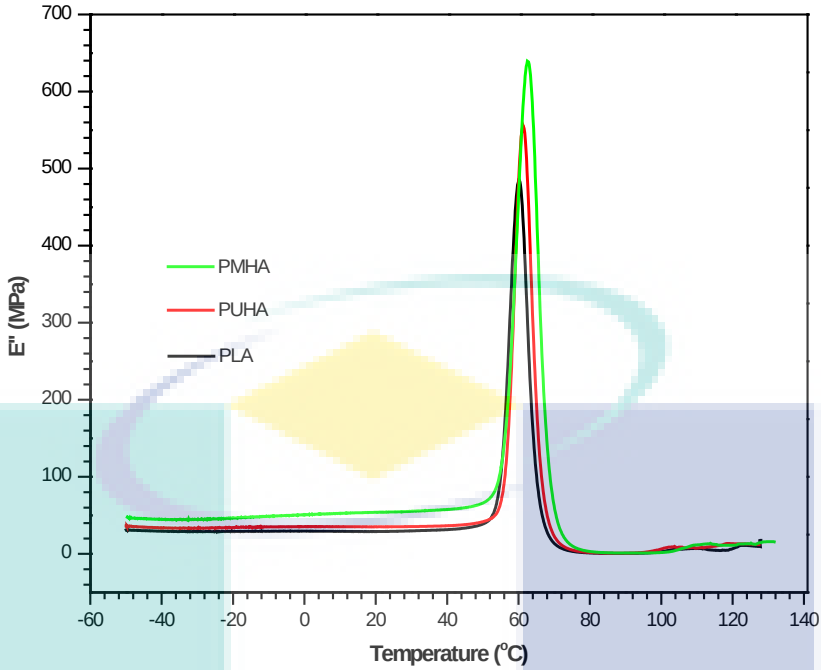

Figure 4.24 Loss modulus curves of PLA, PLA-unmodified HA composite (PUHA), and PLA-modified HA composite (PMHA)

The damping parameter (tan δ) can be determined as the ratio of loss modulus E″ (energy dissipated) to the storage modulus E′ (energy stored). The tan δ curves of PLA, PUHA and PMHA composites are illustrated in Figure 4.25. It can be seen from the curves that the tan δ value of pure PLA is higher than the composites which indicates increase in the load bearing capacity of the composites. Interestingly, the modified HA composite (PMHA) revealed the lowest tan δ peak value which is an indication of improved adhesion between the modified HA and PLA compared with the unmodified HA composite (PUHA). The improved interfacial adhesion in the PLA-HA composite would invariably lead to improvement in load transfer efficiency within the composite. This accounts for the increased mechanical performance of the modified HA composite as discussed in previous section.

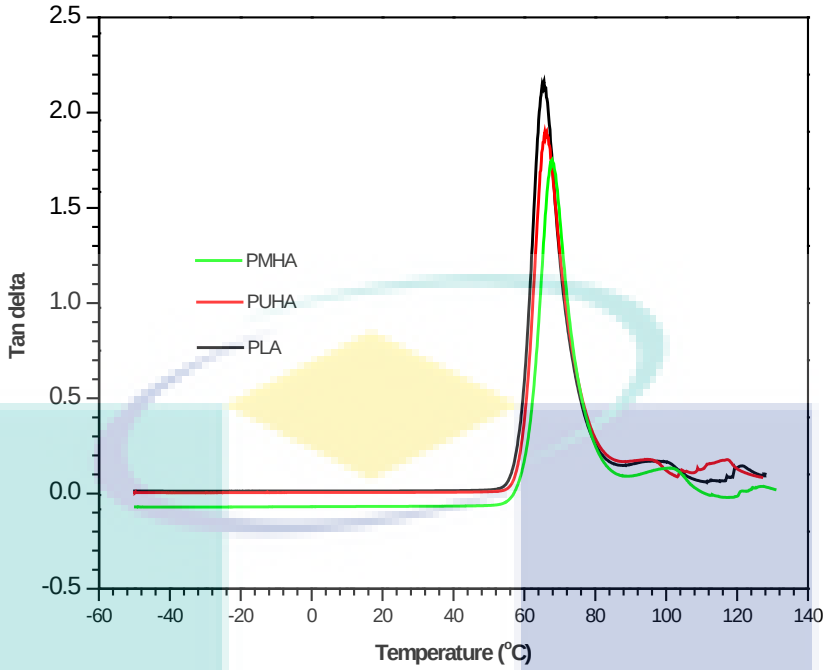

Figure 4.25 Tan delta curves of PLA, PLA-unmodified HA composite (PUHA), and PLA-modified HA composite (PMHA)

4.5 Effects of Impact Modification on Properties of PLA-HA Composites

In order to improve the impact properties of the PLA-HA composite, biostrong impact modifier was incorporated into the formulation at different (0-15 wt%) biostrong (BS) content. The samples prepared for investigation include pure PLA, (denoted by code name PLA), PLA-HA composite containing 10 wt% surface modified HA (denoted by PHA), and impact modified PLA-HA composites containing PLA+10 wt% surface modified HA+biostrong (BS). The impact modified composites are coded as PHAB, followed by 5, 10 or 15 which indicate the wt% BS incorporated into the PLA-HA composites. For example, PHAB5 represents PLA-HA composite containing 5 wt% BS.

4.5.1 Mechanical properties

The tensile strength (TS), tensile modulus (TM) of PLA, PHA, and the PLA-HA composites containing different wt% BS content is illustrated in Figure 4.26. Likewise, the flexural strength (FS), and flexural modulus (FM) of PLA, PHA and PLA-HA composites containing different wt% BS content is illustrated in Figure 4.27. From these two figures, it can be seen that tensile and flexural properties of the impact modified composites are dependent on the BS content.

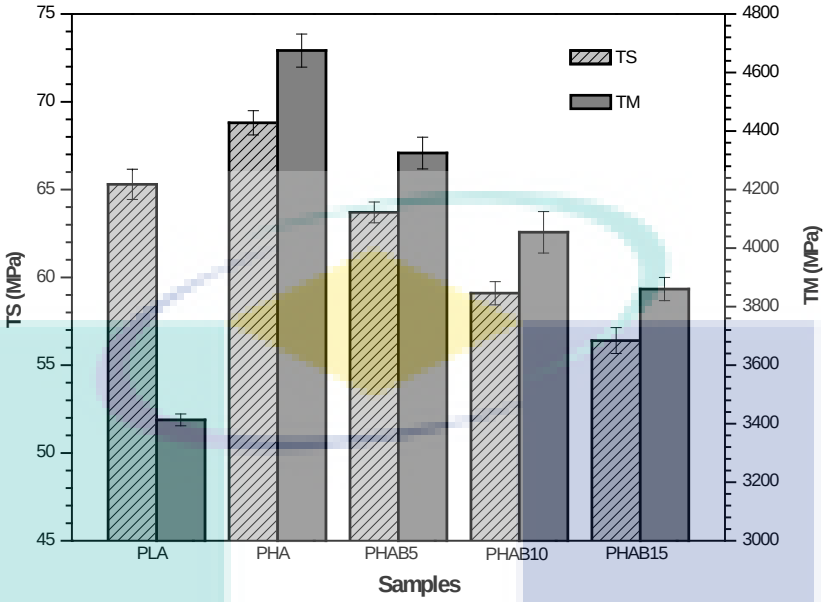

Figure 4.26 Tensile strength (TS) and tensile modulus (TM) of PLA, PLA-modified HA composite (PHA), and PLA-modified HA composites containing 5 wt% (PHAB5), 10 wt% (PHAB10), and 15 wt% (PHAB15) HA content

In Figure 4.26, a reduction in the TS and TM of the impact modified composites can be observed. Similarly, the FS and FM in Figure 4.27 can be seen to follow the same trend. The increase (%) or decrease (%) in mechanical properties of the composites with respect to pure PLA is summarized in Table 4.7. As can be seen from Table 4.7, the largest amount of reduction in TS, TM, FS, and FM was observed for PHAB15, which is the composite with the largest amount (15 wt%) of BS. Compared with the composite without impact modifier (PHA), PHAB15 was found to reveal a reduction of 22%, 21%, 32%, and 21% in TS, TM, FS, and FM respectively. However, it is not unusual to observe a decrease in tensile and flexural properties of polymer based materials when softer components are incorporated into them.

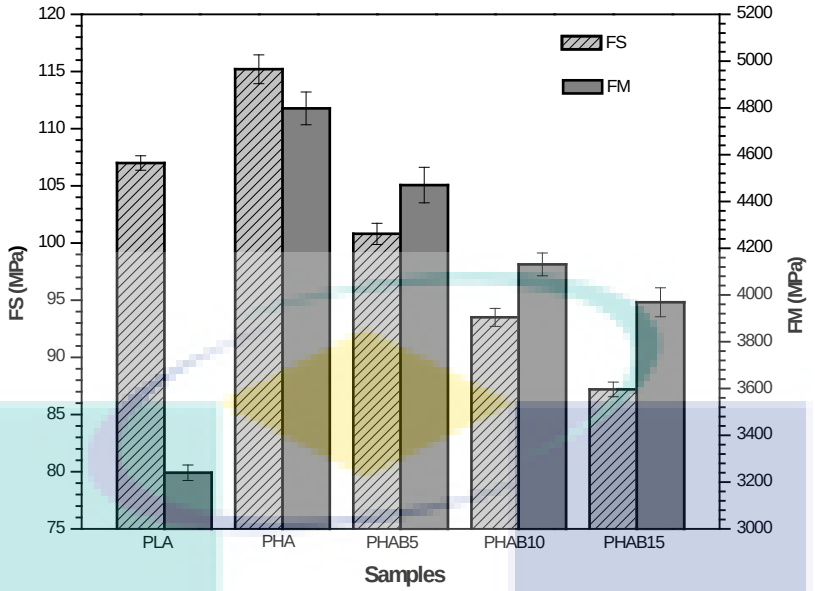

Figure 4.27 Flexural strength (FS) and flexural modulus (FM) of PLA, PLA-modified HA composite (PHA), and PLA-modified HA composites containing 5 wt% (PHAB5), 10 wt% (PHAB10), and 15 wt% (PHAB15) HA content

Generally, it is expected that for semicrystalline materials such as PLA, the inherent bulk crystallinity would normally enhance the tensile and flexural properties of its composites (Pongtanayut et al., 2013). Based on this, it can be inferred that the decrease in tensile and flexural properties of the composites containing BS is due to possible suppression of the inherent crystallinity of PLA within the composites (Pongtanayut et al., 2013).

Be as it may, tensile and flexural properties alone are not sufficient on their own to provide an overall assessment of the suitability of materials for load bearing applications. Indeed, very good energy absorption ability during deformation process is highly desirable (Notta-Cuvier et al., 2016). Specifically, due to the possibility for fracture, very good energy absorption capacity is a very important property which is necessary for determining the suitability of materials to be used as fixations (Ferri et al., 2016).

Table 4.7 Percentage decrease or increase in TS, TM, FS, FM and IS of PLA with respect to HA and BS addition

Sample code	TS (MPa)	TM (MPa)	FS (MPa)	FM (MPa)	IS (KJ m^{-2})
PLA	-	-	-	-	-
PHA	5.09	27.00	7.12	32.47	-10.61
PHAB5	-2.51	21.09	-6.15	27.52	22.13
PHAB10	-10.49	15.81	-14.44	21.57	25.99
PHAB15	-15.78	11.58	-22.71	18.37	37.87

The impact strength (IS) of PLA, PHA and PLA-HA composites containing different wt% BS content is illustrated in Figure 4.28. It is obvious from this figure that the incorporation of BS strongly influences the IS of the impact modified composites. Generally, impact modifiers often act as lubricants to lubricate polymer chain molecules. In the case of PLA, the impact modifier would help to lubricate the PLA molecules, thereby increasing its flexibility and reducing its inherent brittle nature. From Figure 4.28, it can be seen that the IS of PLA-HA composite increases after the incorporation of BS impact modifier which indicates improved toughness. Compared to pure PLA, the IS of the PLA-HA composite containing 15 wt% BS (PHAB15), increased by about 38% (see Table 4.7). More interestingly, compared with the PLA-HA composite without impact modifier (PHA), an increase of about 44% was observed in PHAB15.

The increase in IS of the PLA-HA composites after the incorporation of BS suggests that the BS particles (further confirmed through SEM observation) might possibly have acted as stress concentrators. This can influence the energy absorption of the impact modified composites during fracture, which might have led to the observed increase in IS as can be seen in Table 4.7 and Figure 4.28. From the results of the mechanical properties, it can be inferred that the composite with the smallest amount of BS (PHAB5), presents the most desirable compromise between tensile, flexural and impact properties. Notably, the IS of the PLA-HA composite was reasonably improved without an adverse reduction in tensile and flexural properties.

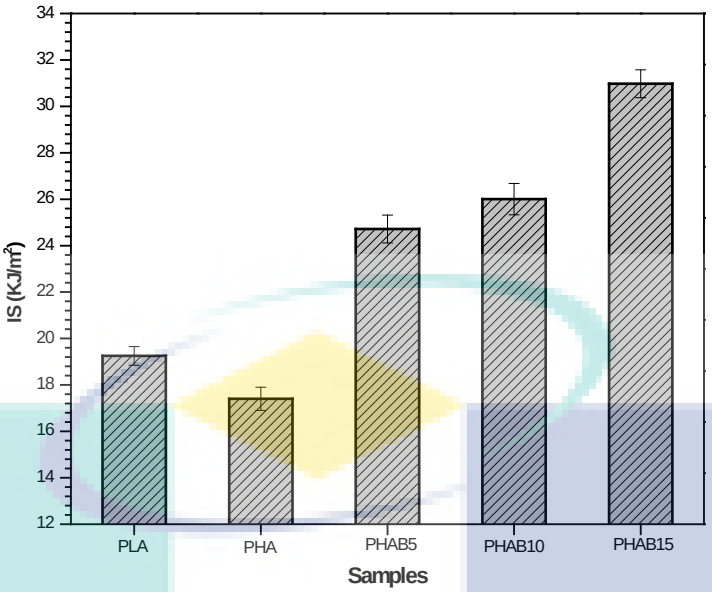

Figure 4.28 Impact strength (IS) of PLA, PLA-modified HA composite (PHA), and PLA-modified HA composites containing 5 wt% (PHAB5), 10 wt% (PHAB10), and 15 wt% (PHAB15) HA content

4.5.2 Morphological properties

In order to obtain more information on the bonding properties of PLA and its composites with HA and BS, SEM images of the fractured surfaces of the composites were analysed. The SEM images of the fractured surfaces of PLA, PHA, PHAB5, PHAB10 and PHAB15 are shown in Figure 4.29. From Figure 4.29a, it can be seen that the pure PLA exhibits a smooth morphology which is a characteristic of brittle materials. Likewise, the SEM image of PHA (PLA-HA composite without impact modifier) revealed fairly smooth morphology (Figure 4.29b) which indicates very little contribution of plastic deformation from the PLA matrix which is inherently brittle, as reported elsewhere (Pluta et al., 2012).

On the other hand, morphology of the composites containing BS can be seen to reveal well dispersed BS droplets, which become more evident and increases in size as the BS content increases (Figure 4.29c-e). Similar observation was also reported in literature (Bouzouita et al., 2016). Obvious domains of BS which are present in the impact modified composites are indications of the immiscibility of BS into the PLA-HA-BS system, which would further be evaluated through DSC analysis. It is believed that during the process of extrusion, BS was dispersed into the PLA matrix in the form of micro domains, which then forms thin layer that encapsulates the HA such that the interfacial boundary of PLA and HA is modified. Interestingly, this could be

responsible for the observed increase in IS of the impact modified composites (see Figure 4.28), which may be attributed to possible energy absorption, crack bridging, and matrix shear yielding as reported in literature (Pluta et al., 2012). However, this also might be the reason for the decreased tensile and flexural properties of the impact modified composites as compared with composite without impact modifier (PHA) (Figure 4.26 and Figure 4.27). This is attributed to possible disruption of the interfacial adhesion between PLA and HA as a result of the thin layer

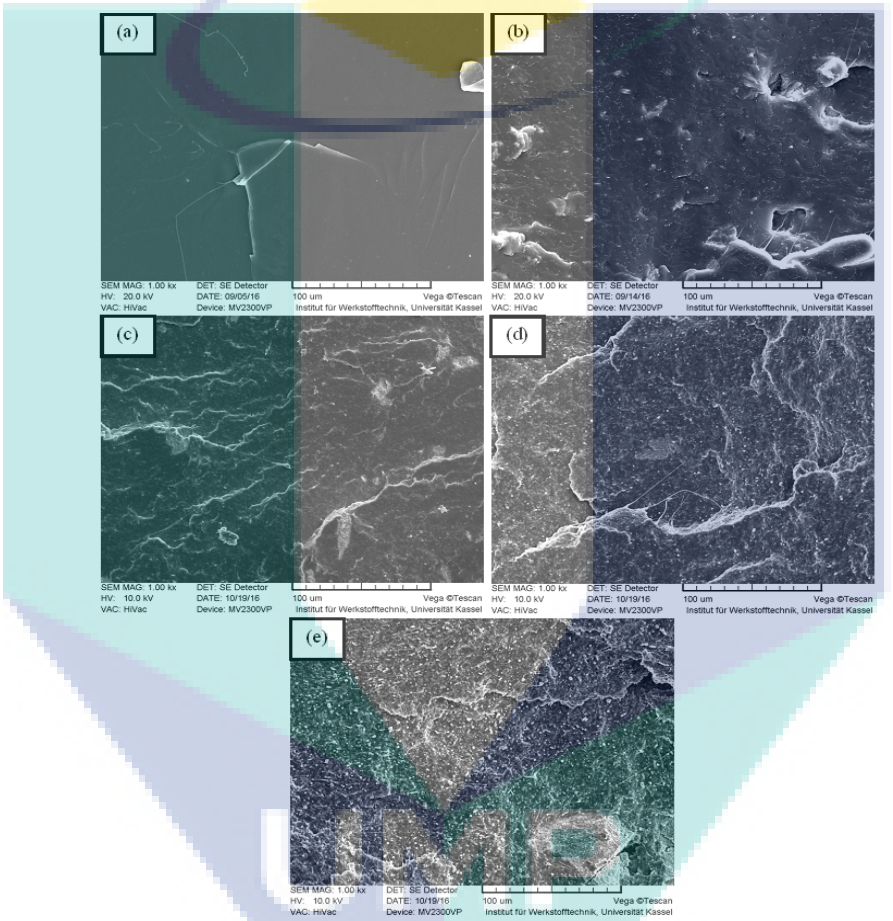

Figure 4.29 SEM images of fractured surfaces of (a) PLA, (b) PLA-modified HA composite (PHA), PLA-modified HA composites containing (c) 5 wt% HA (PHAB5), (d) 10 wt% HA (PHAB10), and (e) 15 wt% HA (PHAB15)

4.5.3 Fourier transforms infrared (FTIR) spectroscopy

In order to obtain viable information about the possible reactions during the composite production, functional groups analysis of the individual components (PLA, HA, and BS) was conducted prior to blending. Chemical changes to these components after blending was also investigated through analysis of FTIR spectra of the composites. The FTIR spectra of the individual components such as PLA, HA, and BS are illustrated

in Figure 4.30a, whereas the possible reaction scheme for this components is illustrated in Figure 4.30b.

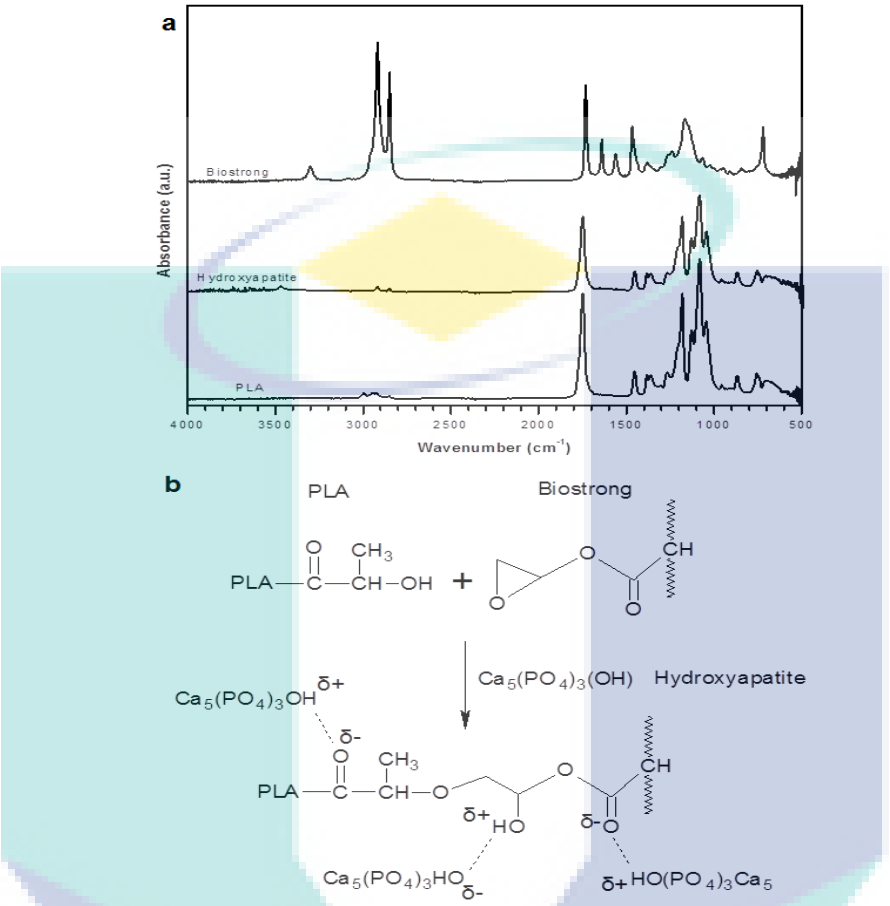

Figure 4.30 FTIR spectra of PLA, hydroxyapatite, and biostrong

As can be seen from Figure 4.30a, the main observable peaks include –OH stretching vibration of bonded hydroxyl groups at the higher wavelength around 3300-3200 cm^{-1} in the BS spectra and around 3500-3400 cm^{-1} in the HA spectra. Another obvious peak is the C-H characteristic stretching band at 3050-2830 cm^{-1} which is attributed to asymmetric and symmetric C-H stretching of ethyl and ethylene moieties. It is noteworthy that the intensity of this peak is intense in the BS spectra, which is associated with the fact that BS is an ethylene-acrylate copolymer, and therefore contains a reasonably high amount of ethylene components. Other notable peaks include the C=O intense peak at 1750 cm^{-1} which represents the stretching vibration of carboxylic, acetyl and ester groups (Akindoyo, 2015). The peak at 1452 cm^{-1} is attributed to CH_3 stretching whereas the small band around 1365 cm^{-1} is attributed to C-H deformation. The peak at 1083 cm^{-1} is an attribute of C-O stretching band (Choi et al., 2013). By observing the individual spectra in Figure 4.12a, the BS spectra can be seen

to reveal some peculiar peaks. This includes the C=C characteristic peaks at 1641 cm^{-1} and at 1555 cm^{-1} which are attributed to the acrylic moieties present in the BS.

The FTIR spectra of the PLA-HA composites with and without impact modifier are illustrated in Figure 4.31. The sites for possible reaction (Figure 4.30b) through bond formation between the composite components includes the HA –OH groups, the BS epoxy groups (Taib et al., 2012), and functional hydroxyl groups and carboxylic end groups of PLA (Akindoyo et al., 2015b). From Figure 4.31, it is obvious that all the composite categories revealed similar spectra. However, by comparing the composites spectra with the spectra obtained for the individual components there are some notable observations. Firstly, it can be seen that as the BS wt% content increases, the peak intensity of the band around 3050-2830 cm^{-1} becomes more intense. This suggests the increasing amount of ethylene components within the composite, which is attributed to the increasing wt% BS content (BS is an ethylene-acrylate copolymer) (Bouzouita et al., 2017; Pluta et al., 2012). From the PHA spectra, it can be seen that the –OH peak which appeared around 3450 cm^{-1} in the HA spectra (see Figure 4.30a) was not detected which indicates the formation of hydrogen bond between HA and functional groups of PLA.

Similarly, the peaks at 1641 cm^{-1} and 1555 cm^{-1} in the BS spectra (see Figure 4.30a) are not evident in the spectra of the impact modified composites (PHAB5, PHAB10, and PHAB15). The high tendency for chemical reaction between PLA and BS has been reported in literature (Taib et al., 2012). Therefore the disappearance of these peaks from the PLA-HA composites containing BS is a strong indication for the occurrence of chemical reactions at the molecular level between PLA, HA, and BS. In addition, the peaks at 1750 cm^{-1} and 1083 cm^{-1} in the PHA spectra can be seen to slightly shift towards a lower wavelength in the spectra of the impact modified composites. This downward tilt becomes farther (PHAB5<PHAB10<PHAB15) as the BS content increases. This gives good evidence for intermolecular interaction as well as good compatibility between BS and PLA.

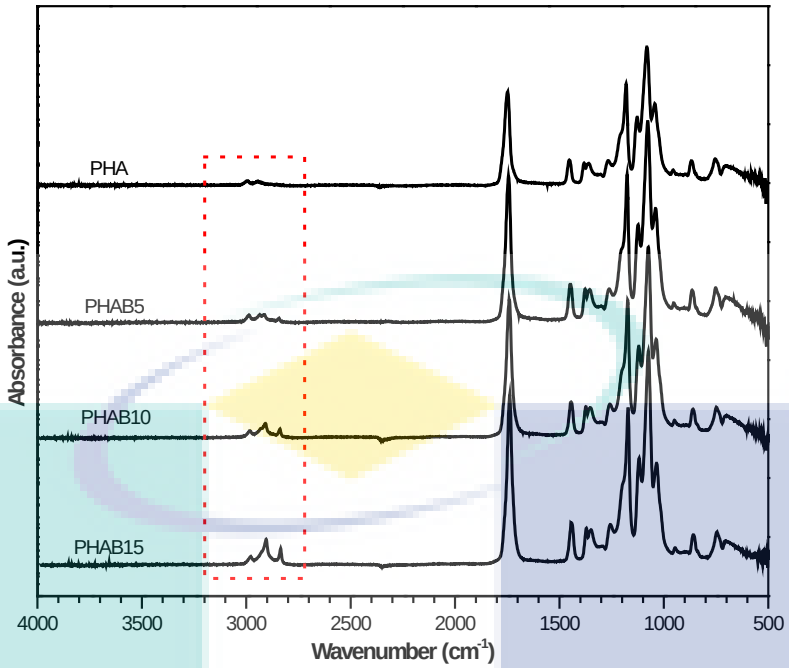

Figure 4.31 FTIR spectra of PLA-modified HA composite (PHA), PLA-modified HA composites containing 5 wt% HA (PHAB5), 10 wt% HA (PHAB10), and 15 wt% HA (PHAB15)

4.5.4 Thermal properties

The TGA curves of PLA and PLA-HA composites with and without impact modifier are illustrated in Figure 4.32. It can be seen from this figure that the onset of weight reduction as a result of thermal degradation of the samples started around 270 ^{o}C and continued till around 390 ^{o}C. The DTG curve of the samples was also used to analyse their thermal properties and the DTG curves are illustrated in Figure 4.33.

From the TGA and DTG curves, thermal properties of the samples were analysed and a summary of the thermal degradation properties obtained for the samples is presented in Table 4.8. By comparing the degradation properties of the PLA-HA composites with pure PLA, it is evident that the temperature for the onset of thermal degradation of the composites (T_{onset}) is lower. Likewise, the temperature of maximum degradation (T_d) of the composites, are lesser than pure PLA (Table 4.8). This can be associated with higher level of destabilization of the PLA structural framework within the composites. Among the category of composites presented in Figure 4.32 and Figure 4.33, the PLA-HA composite without impact modifier (PHA) can be seen to exhibit the highest thermal stability.

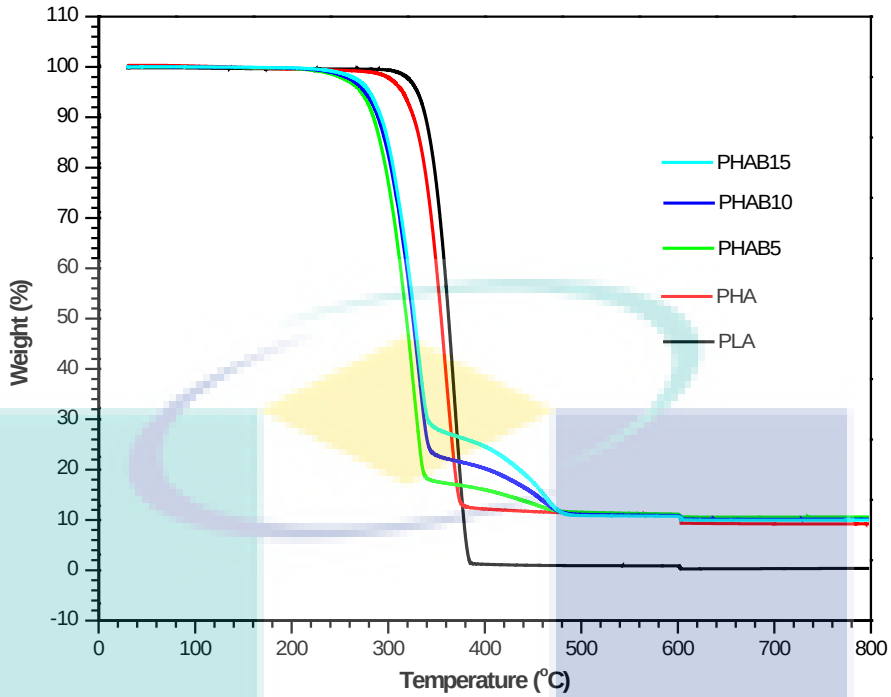

Figure 4.32 TGA thermograms of PLA, PLA-modified HA composite (PHA), PLA-modified HA composites containing 5 wt% HA (PHAB5), 10 wt% HA (PHAB10), and 15 wt% HA (PHAB15)

On the other hand, among the impact modified composites, the composite containing the least wt% BS content (PHAB5) can be seen to reveal the least thermal stability. It is well known that the strength of interfacial bond within a composite can influence the thermal stability of the composite. Also, electrostatic attraction between the carboxylate groups of polymers and the Ca^{2+} ions of HA has been reported to have a great influence on the degree of interfacial interaction in polymeric HA composites (Cucuruz et al., 2016). Therefore, as the BS wt% content increases there is much possibility for interference with the electrostatic interaction between PLA and HA. This may be attributed to the fact that BS formed thin layer over HA during compounding as highlighted through SEM result, and this might be responsible for the lower stability of the impact modified composites compared with the composite without impact modifier.

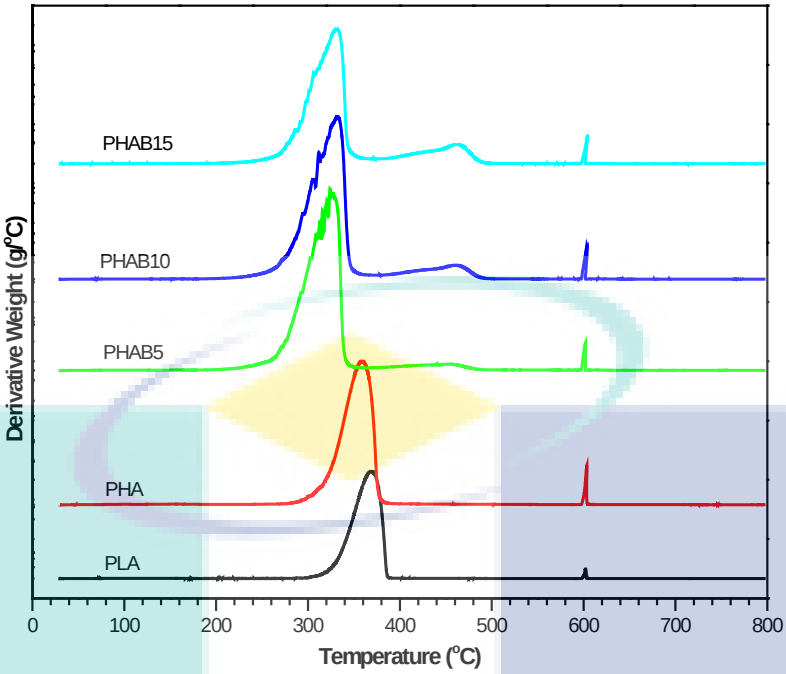

Figure 4.33 DTG thermograms of PLA, PLA-modified HA composite (PHA), PLA-modified HA composites containing 5 wt% HA (PHAB5), 10 wt% HA (PHAB10), and 15 wt% HA (PHAB15)

As the BS wt% content increases, the tendency for molecular interaction also increases which accounts for the higher thermal stability of PHAB15 compared with PHAB10 and PHAB5. Increased thermal resistance of impact modified composites was also reported previously (Notta-Cuvier et al., 2016). From the TGA data, the residue of the samples at T≥700 ^{o}C was calculated and the result is included in Table 4.8. It can be seen that the residue content of pure PLA is very low compared with the composites which may be accrued to the presence of HA in the composites.

Table 4.8 Thermal properties of PLA and the different composite categories

Sample code	**T_{onset} (^{o}C)**	**T_d (^{o}C)**	**Residue (%) at T≥700 ^{o}C**
PLA	330	369	0.33
PHA	314	360	10.29
PHAB5	272	324	10.17
PHAB10	276	332	10.14
PHAB15	280	334	9.95

4.5.5 Differential scanning calorimetry (DSC) analysis

The DSC thermograms of PLA, PHA, PHAB5, PHAB10, and PHAB15 for the first scanning section are illustrated in Figure 4.33. Similarly, the DSC thermograms of PLA, PHA, PHAB5, PHAB10, and PHAB15 for the second scanning section are

illustrated in Figure 4.34. From the DSC thermograms, the three transition stages such as the endothermic glass transition temperature (T_g), the exothermic crystallization temperature (T_c), and the endothermic melting temperature (T_m) were analysed. As can be seen from the first scan in Figure 4.34 and the second scan in Figure 4.35, the T_g of PHA slightly shifts towards the higher temperature region compared with pure PLA. On the contrary, the T_g of the impact modified composites shifted to a lower temperature region compared with pure PLA. Reason for the right shift in T_g of PHA is attributed to the restriction imposed on the molecular chain mobility of PLA due to the presence of HA as discussed earlier. Knowing fully well that around the T_g of polymers, the molecular chains of the polymer becomes more flexible and also gain an increased mobility. Thus, one main reason for the incorporation of impact modifiers into semi crystalline polymers such as PLA is in order for the impact modifier to lubricate the polymer chains, thereby making them more flexible and able to move more freely. Therefore, the downward shift in T_g of the PLA-HA composites containing BS suggests an increase in the polymer chain mobility. Summary of the DSC parameter of PLA, PHA, PHAB5, PHAB10, and PHAB15 is presented in Table 4.9.

On the other hand, the T_c of PHA can be seen to slightly move towards the lower temperature region compared with PLA whereas the T_c of the impact modified composites can be seen to move to the higher temperature region. The right shift in T_c of the impact composites becomes further as the wt% BS content increases. The left shift in T_c of PHA is an indication of faster rate of crystallization which is attributed to the heterogeneous crystallization effect of HA on PLA (Liuyun et al., 2013). From Figure 4.26, the exothermic crystallization peak of the impact modified composites can be seen to become broader with an observable decrease in magnitude as the BS wt% content increases. It has been reported that incorporation of other entities into semi crystalline materials would either lead to an easier or a bit more difficult crystallization process within the material (Ren et al., 2006). Therefore, it can be inferred that the crystallization activities at the interface of PLA-HA composites was reduced after the incorporation of BS. The SEM results revealed that HA was encapsulated by a thin layer of BS which might have disrupted the heterogeneous nucleation activities at the PLA-HA interface. This would decrease the rate of crystallization, and invariably the degree of PLA crystallinity within the impact modified PLA-HA composites.

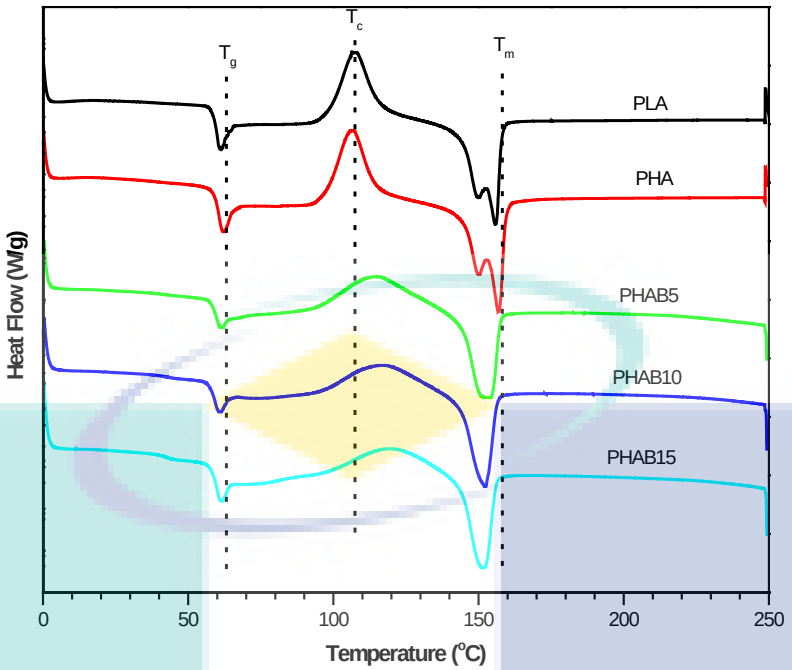

Figure 4.2 DSC thermograms during first heating scan of PLA, PLA-modified HA composite (PHA), PLA-modified HA composites containing 5 wt% HA (PHAB5), 10 wt% HA (PHAB10), and 15 wt% HA (PHAB15)

It is interesting to note that the crystallization peak was not evident in the second scan thermograms of the PLAB5, PLAB10, and PLAB15. Notably, the crystallization behaviour of semi crystalline polymers such as PLA in a partially miscible blend is often influenced by the nucleation activities at the interfacial boundaries of the two components (Pongtanayut et al., 2013). Indeed, due to the rubbery nature of BS, increase in the wt% BS content could lead to the formation of larger droplets (see Figure 4.29), which could interfere with the interfacial contact area between HA and PLA. This would reduce the interfacial activities at the interface which could be the reason for slow crystallization during the first scan, as well as total disappearance of the T_c peak from the second scan thermograms of the impact modified composites. This is an indication that incorporation of BS influenced the crystallization kinetics of the PLA-HA composite as illustrated in Figure 4.34, Figure 4.35, and Table 4.9.

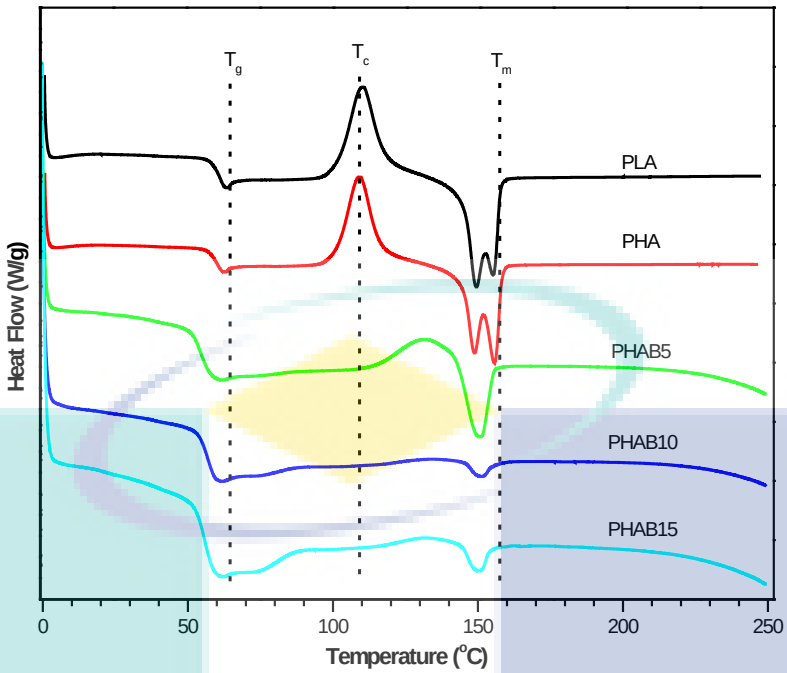

Figure 4.35 DSC thermograms during the second heating scan of PLA, PLA-modified HA composite (PHA), PLA-modified HA composites containing 5 wt% HA (PHAB5), 10 wt% HA (PHAB10), and 15 wt% HA (PHAB15)

Figure 4.34 and Figure 4.35 reveals close similarity in the endothermic melting peak (split peaks) of PLA and PHA in the first and second scan sections. This may be accrued to the different crystalline nature of the beta- and alpha- forms of semi crystalline PLA (Pongtanayut et al., 2013). On the other hand, the PHAB5, PHAB10, and PHAB15 all revealed single and reduced T_m peaks. This is a resultant effect of the reduced crystallization activities at the PLA-HA interface owing to restrictions imposed on PLA crystallization within the composites. Similar observation was also reported in literature for composites containing PLA and epoxidized natural rubber (Pongtanayut et al., 2013).

The degree of PLA crystallization in the composites was calculated as described in the methods section, and the result is included in Table 4.9. It can be seen from Table 4.9 that the crystallinity of PLA in the PHA becomes reduced after the incorporation of BS. The reduction in PLA crystallinity becomes larger as the BS wt% content in the PLA-HA composite increases. This observable reduction in PLA crystallinity within the composite suggests higher free volume content within the composite, which indicates an increase in the amorphous content (Taib et al., 2012). Increased amorphous nature of the PLA-HA composites as the BS wt% content increases would facilitate a reduction in stiffness of the composite, which might be responsible for the reduced tensile and

flexural properties of the impact modified composites as illustrated in Figure 4.26 and Figure 4.35. Notwithstanding, reduction in PLA crystallinity could be an advantage from medical point. This would enhance the degradation of the materials, thereby making the active components readily available at the implant site within a short period of time following implantation (Ferri et al., 2016).

Table 4.9 DSC properties of thermograms of PLA, PLA-modified HA composite (PHA), PLA-modified HA composites containing 5 wt% HA (PHAB5), 10 wt% HA (PHAB10), and 15 wt% HA (PHAB15)

Sample code	1st Scan					2nd Scan				
	T_g (°C)	T_c (°C)	T_{m1} (°C)	T_{m2} (°C)	X_c (%)	T_g (°C)	T_c (°C)	T_{m1} (°C)	T_{m2} (°C)	X_c (%)
PLA	61.77	109.78	148.34	155.91	27.89	62.21	111.34	148.23	155.35	28.48
PHA	63.36	106.34	149.50	158.74	36.56	63.64	108.37	150.09	158.44	34.43
PHAB5	61.42	115.22	153.74	-	24.57	60.91	132.35	149.58	-	5.66
PHAB10	61.13	117.89	152.28	-	22.16	60.91	-	149.44	-	2.63
PHAB15	61.11	119.18	151.01	-	19.16	60.91	-	148.19	-	1.55

4.5.6 Dynamic mechanical properties

The storage modulus (E′) curves of PLA, PHA, PHAB5, PHAB10, and PHAB15 are illustrated in Figure 4.35. It can be seen from this figure that PHA revealed higher E′ compared with PLA which is accrued to the high modulus of HA compared with PLA. However, incorporation of BS into the PLA-HA composite led to decreased E′ and the observed decreases becomes larger as the BS wt% content increases. For Example, after incorporation of 5wt% BS (PHAB5), the reduction in E′ of the composite compared with PHA is <1%, from 3065 MPa to 3048 MPa. After incorporation of 15 wt% BS (PHAB15), the initial E′ of the PLA-HA composite was reduced from 3065 MPa (PHA) to 1923 MPa (PHAB15), which is a reduction of about 37%.

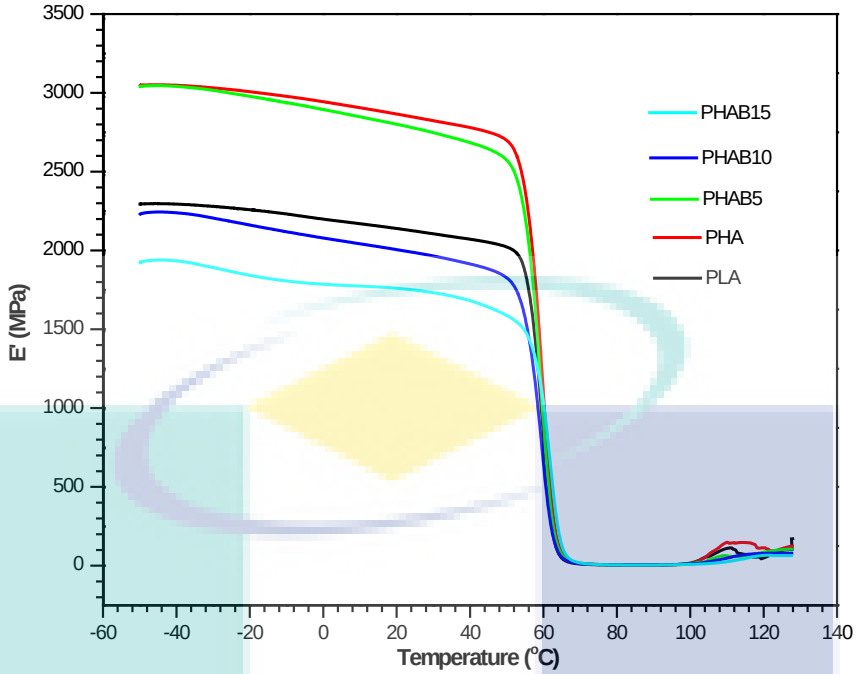

Figure 4.36 Storage modulus, E′, curves of of PLA, PLA-modified HA composite (PHA), PLA-modified HA composites containing 5 wt% HA (PHAB5), 10 wt% HA (PHAB10), and 15 wt% HA (PHAB15)

The reduction in E′ of the PLA-HA composites as BS wt% content increases can be attributed to possible reduction in stiffness of the composite as concluded based on the DSC results. This observation is also similar to what was previously reported for impact modified PLA blends elsewhere (Taib et al., 2012). Generally, from Figure 4.18, the E′ of all the samples can be seen to decrease gradually as temperature increases and then sharply drops around 57-63 ^{o}C. This temperature region signifies the glass transition region of the material and the sudden drop in E′ of the composites at this region is associated with the chain mobility. The chain mobility is as a result of softening and segmental movement of PLA molecules within the composite (Taib et al., 2012). At temperature above 100 ^{o}C, a slight increase in E′ of pure PLA and PHA can be observed which indicates the cold crystallization of PLA during the heat scanning process. It is worthy of note that this small peak is not evident in the impact modified composites which is in agreement with the DSC results that after incorporation of BS into the PLA-HA composite, the PLA crystallization process was suppressed.

In order to further investigate the effects of BS on the PLA-HA composite, the damping behaviour of the samples were evaluated through the damping coefficient, tan δ. The tan δ curves of PLA, PHA, PHAB5, PHAB10, and PHAB15 are illustrated in Figure 4.37. One salient characteristic of tan δ is that it can provide a more precise

measurement of the glass transition temperature, T_g. The T_g can be determined from the tan δ curve as the temperature at which the tan δ attained its maximum peak height. As can be seen in Figure 4.37, the tan δ peak height of the composites decreases as the BS wt% content increases, with a slight left shift in the T_g. This observation agrees with the DSC result and also aligns with what was reported in previous research (Taib et al., 2012). The reason for this can be attributed to partial miscibility of BS and PLA and it is also an indication of molecular interaction between PLA and BS as illustrated in Figure 4.16.

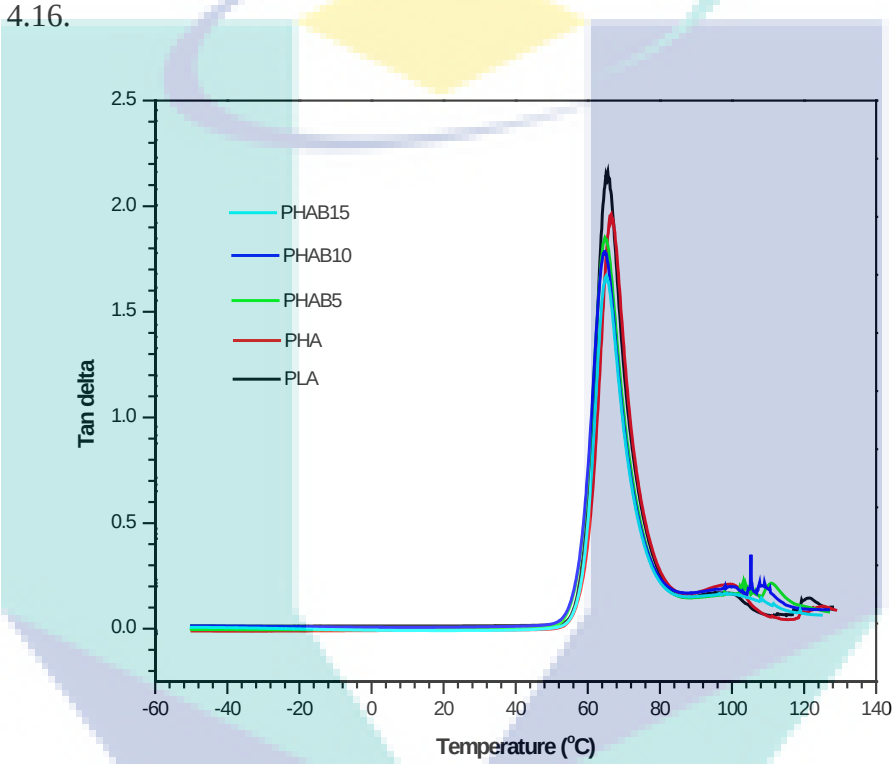

Figure 4.37 Tan delta curves of PLA, PLA-modified HA composite (PHA), PLA-modified HA composites containing 5 wt% HA (PHAB5), 10 wt% HA (PHAB10), and 15 wt% HA (PHAB15)

For comparison purposes, one composite type which revealed the best compromise in tensile, flexural and thermal properties was selected among the various groups of PLA-HA composite investigated thus far in this study. These composites were further compared with each other and their properties were compared with pure PLA. Comparative properties of the samples are further discussed in the following sections. These samples include pure PLA (PLA), PLA-unmodified HA composite (PUHA), PLA-modified HA composite (PMHA), PLA-modified HA composites containing 5 wt% HA (PHAB5). All of the PLA-HA composite type discussed in the subsequent sections contains 10 wt% HA.

4.6 Antimicrobial Properties of PLA-HA Composites

The antimicrobial properties of PLA and different categories of PLA-HA composites were investigated by viewing the growth of two different bacteria on the individual samples. The bacteria investigated are Escherichia coli (gram-negative bacteria), and Staphylococcus aureus (gram-positive bacteria). Fluorescence images of the growth behaviour of Escherichia coli on PLA, PUHA, PMHA, and PHAB5 is shown in Figure 4.38. Likewise, the growth behaviour of Staphylococcus aureus on PLA, PUHA, PMHA, and PHAB5 is shown in Figure 4.39. From these two figures, it can be seen that for PLA and PUHA samples, the growth of bacteria is highly pronounced and the entire surface area of the samples are well covered by the bacteria. On the other hand, the samples containing the modified HA (PMHA and PHAB5) tend to inhibit the overall spread of bacterial on their surfaces. This is particularly obvious in Figure 4.38 where the bacteria were restricted to grouped colonies rather than spreading in large numbers on the entire sample surface. This observation further confirms the antibacterial activity of the modified HA as discussed earlier.

Generally, the cell wall of gram-positive bacteria consists of several layers of teichoic acids and peptidoglycan, which forms a thick and rigid structure. As for gram-negative bacteria, the cell wall is made up of a thin layer of peptidoglycan which is surrounded by another lipid membrane containing lipoproteins and lipopolysaccharides. This outer membrane layer present in the cell walls of gram-negative bacteria typically protects it from antibacterial agent which is usually the reason for reduced effect of antibiotics and antimicrobial agents on gram-negative bacteria compared with gram-positive bacteria (Nirmala et al., 2011). This phenomenon is very much consistent with the results obtained from this study. Therefore, the larger zone of inhibition observed for Staphylococcus aureus can be attributed to high susceptibility of gram-positive bacterial to antibacterial agents due to the lack of outer membrane protections which would normally protect gram-negative bacterial for antimicrobial agents (Nirmala et al., 2011).

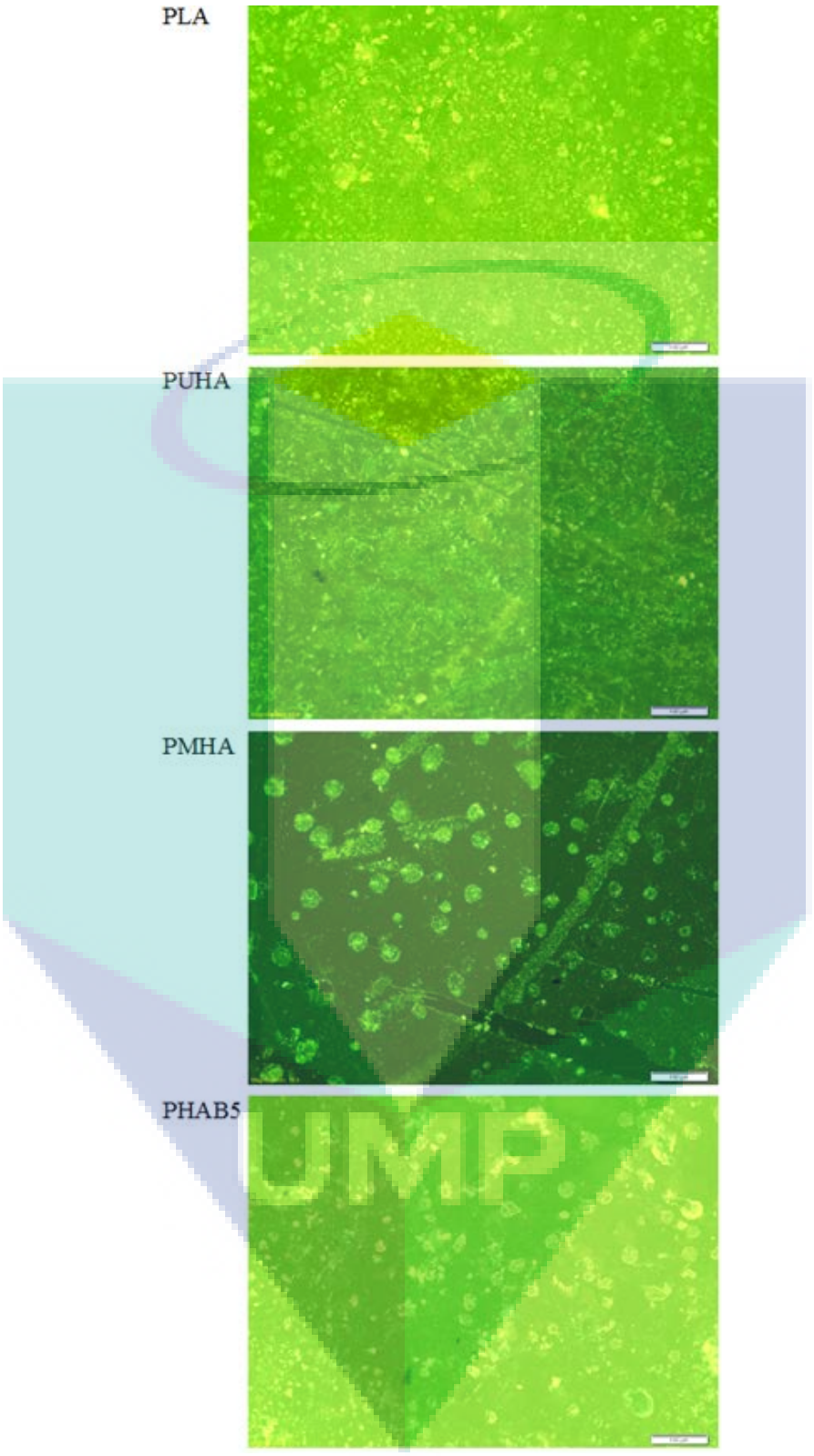

Figure 4.38 Inhibition effect of PLA, PLA-unmodified HA composite (PUHA), PLA-modified HA composite (PMHA), PLA-modified HA composites containing 5 wt% HA (PHAB5) on Escherichia coli

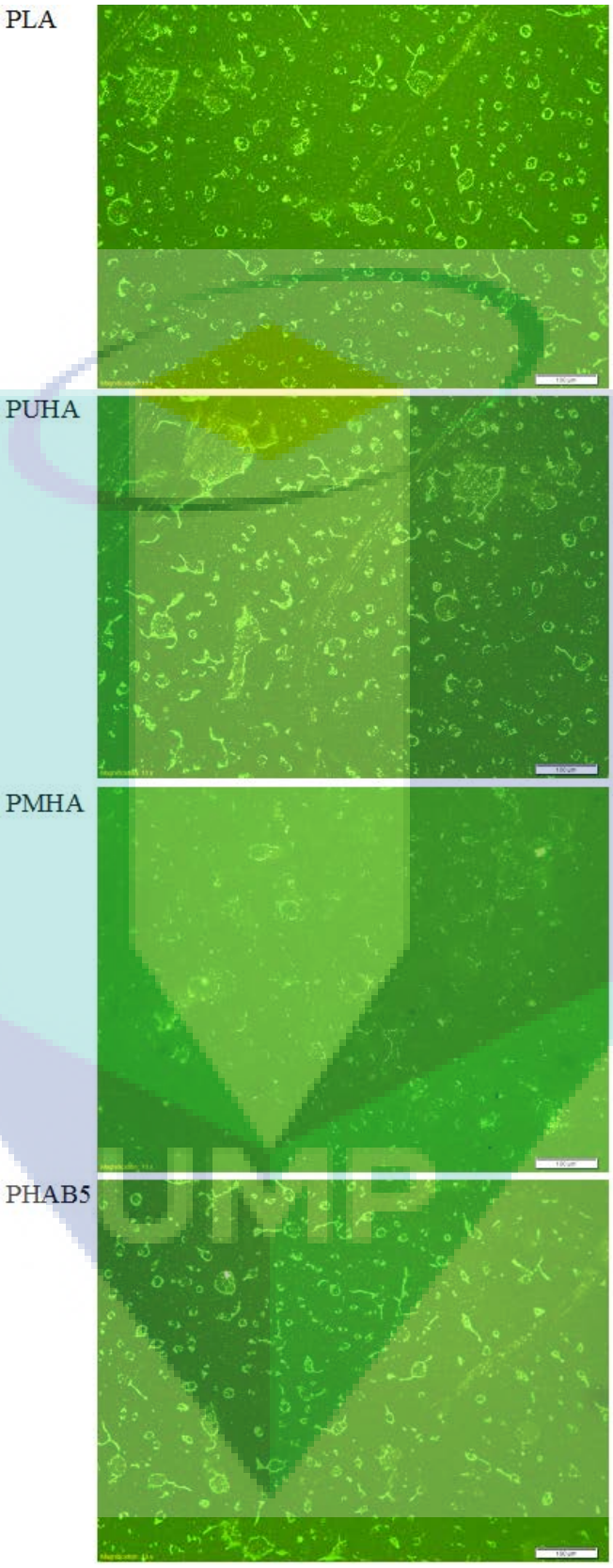

Figure 4.39 Inhibition effect of PLA, PLA-unmodified HA composite (PUHA), PLA-modified HA composite (PMHA), PLA-modified HA composites containing 5 wt% HA (PHAB5) on Staphylococcus aureus

4.7 In vitro Biocompatibility Study

Biocompatibity of PLA and PLA-HA composites was assessed through in vitro biocompatibility analysis.

4.7.1 Composite degradation pH

The change in pH value of the complete osteoblast cell media after the different samples have been submerged for different number of days is illustrated in Figure 4.40.

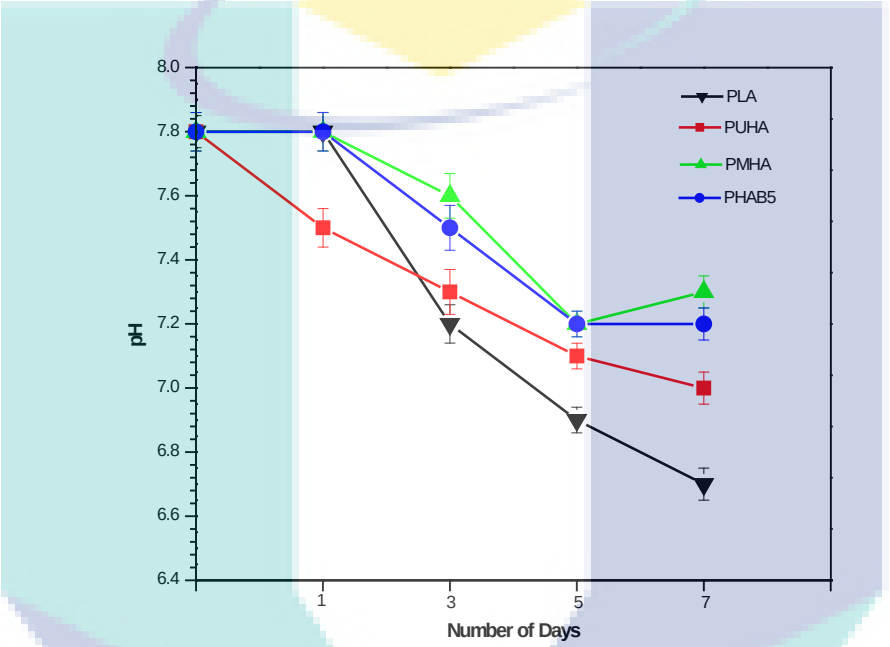

Figure 4.40 The effect of PLA, PLA-unmodified HA composite (PUHA), PLA-modified HA composite (PMHA), PLA-modified HA composites containing 5 wt% HA (PHAB5) on pH of complete osteoblast cell media

Generally, it can be seen that the pH values of the media decreases as the number of days increases which is attributed to acidic degradation products released following PLA degradation. However, it is worthy of note that the pH values of the media into which the composites were submerged are higher than for pure PLA which is as a result of the neutralization effects of HA within the composites.

It was reported that the change in pH values of PLA-HA composites after immersion in cell media is closely related to the sample composition, degradation of PLA, neutralization effect of HA, and possible detachment of HA from the PLA matrix (Hong et al., 2010). The higher media pH values of the composites suggests that the acidic products derived from the autocatalytic degradation of PLA was restrained through the neutralization effect of HA. Notwithstanding, comparing the different

composite categories, it can be seen that the unmodified HA based composite (PUHA) tend to reveal larger pH decrease compared with the modified HA based composites (PMHA and PHAB5). This could be as a result of poor interfacial bonding between the unmodified HA and PLA as discussed in previous sections. The poor adhesion might have created more cavities in the PUHA composite, thereby accelerating the rate of PLA hydrolysis such that the PLA degradation becomes more dominant over neutralization effect of HA.

On the other hand the modified HA composites reveals moderate decrease in media pH which indicates that the undesirable detachment of HA from the PLA matrix was inhibited by the improved interfacial adhesion between the modified HA and PLA (Jiang et al., 2016). In order to investigate the degradation of the samples in aqueous medium, the aging analysis was conducted.

4.7.2 Cell attachment and proliferation

The images obtained for the samples with the help of an inverted microscope after 1, 3, 5, and 7 days cell culture is shown in Figure 4.41. As can be seen the osteoblast cells adhered to all the samples throughout the culture period, and the number of adhered cells seem to increase as the culture day increases. This is an indication that the samples are biocompatible (Jiang et al., 2016). However, the rate of cell proliferation on the sample surfaces can be seen to be different from each other. Significantly, Figure 4.41 shows that the PLA-HA composites revealed improved cell adhesion compared with pure PLA. Reason for this can be accrued to the lack of surface epitopes on PLA which could support the cell proliferation (Nakagawa et al., 2006; Woo et al., 2007). Thus the higher proliferation of the PLA-HA composites indicates that presence of HA in the composites was able to enhance the interaction between osteoblast cells and the PLA-HA composites as reported in similar research (Hickey et al., 2015). In essence, presence of HA in dense PLA-HA composites as prepared in this study can promote cell attachment and growth, thereby ensuring good biological performance of the PLA-HA composites (Jiang et al., 2016; Matesanz et al., 2015).

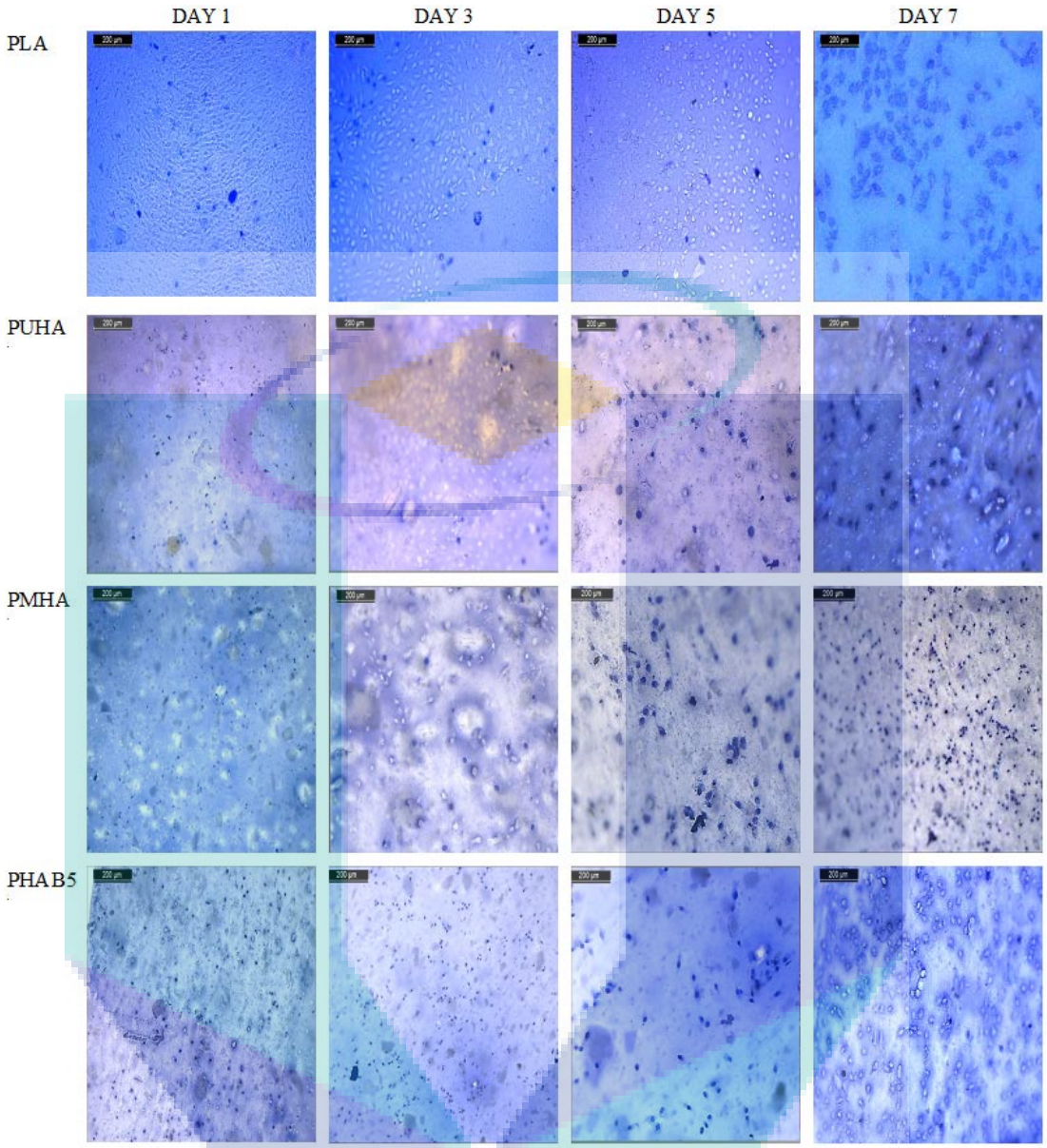

Figure 4.41 Growth of osteoblast cells on the surface of PLA, PLA-unmodified HA composite (PUHA), PLA-modified HA composite (PMHA), PLA-modified HA composites containing 5 wt% HA (PHAB5) cultured for different number of days

4.7.3 Cell viability

In order to quantify the cell proliferation on the samples surfaces, viability of the cells was assessed as described in the methodology section. The trend of the cell viability on the sample surfaces at 1, 3, 5, and 7 days of cell culture on the samples is illustrated in Figure 4.42. It can be seen from this figure that viability (%) of the PLA-HA composites are higher than for pure PLA which aligns to the images presented in Figure 4.24. Significantly, after day 5, there seem not to be much observable increase in viability (%) of the composites whereas PLA revealed a decrease in viability after day

5. This suggests that the osteoblast cells attained confluence on day 5 as supported by the microscopic images presented in Figure 4.42.

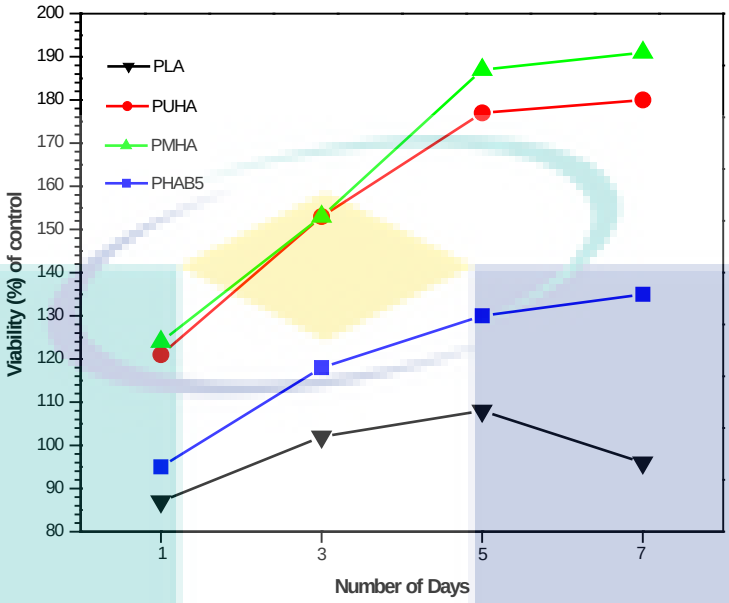

Figure 4.42 Viability of osteoblast cells on the surface of PLA, PLA-unmodified HA composite (PUHA), PLA-modified HA composite (PMHA), PLA-modified HA composites containing 5 wt% HA (PHAB5) cultured for different number of days

For comparison, the viability of the osteoblast cell on the individual sample surface after the 7 days culture period is illustrated in Figure 4.43. As can be seen, and as stated earlier, the PLA-HA composites revealed higher viability than PLA. In fact, whereas the viability (%) of the composites is higher than the control, PLA revealed a lower viability compared with the control, similar to what was reported for PLGA based composites in a previous study (Jiang et al., 2016). This indicates that the incorporated HA was not cytotoxic and its presence in the composite was able to favourably improve the biological performance of PLA (Hou et al., 2013).

Based on the cell response of PLA and the PLA-HA composites, it can be seen that incorporation of HA into PLA was able to offer better cell attachment and proliferation to the PLA matrix. It is interesting to note that modification of HA did not present obvious cytotoxicity to the PLA-HA composite. However, incorporation of impact modifier can be seen to slow down the rate of cell proliferation on the PLA-HA composite surface as evident from Figure 4.41 and Figure 4.43. This could be associated with possible reduction in the degree of contact between the osteoblast cells and the HA within the composites. This is as a result of encapsulation of HA by the BS impact modifier during blending as explained in previous sections. Be as it may, BS did

not present cytotoxicity to the PLA-HA composite as can be seen from Figure 4.43 that the viability (%) of the impact modified composites (PHAB5) is higher than the control.

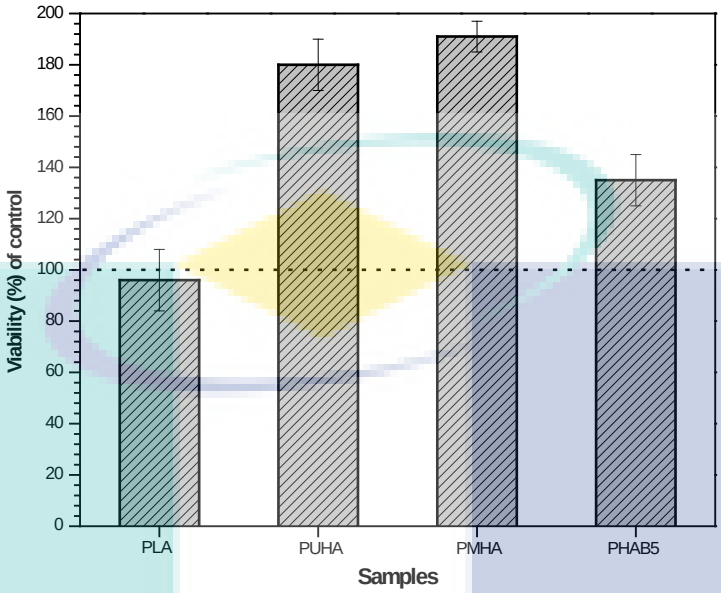

Figure 4.43 Viability of osteoblast cells on the surface of PLA, PLA-unmodified HA composite (PUHA), PLA-modified HA composite (PMHA), PLA-modified HA composites containing 5 wt% HA (PHAB5) after 7 days culture period

CHAPTER 5

CONCLUSION AND RECOMMENDATION

5.1 Conclusion

Natural hydroxyapatite (HA) was extracted from cow bone through ultrasound treatment of the raw bone followed by calcination at different temperatures from 650-950 ^{o}C. Ultrasound treatment in ordinary water medium is found to be suitable for cleaning the bone. The HA produced after calcination at 950 ^{o}C was found to exhibit desirable properties similar to stoichiometric HA. Results of XRD and FTIR indicated that chemical features of the extracted HA are consistent with the standard HA. in general, the main phase of the produced HA is consistent with standard HA through all the characterization techniques such as TGA, FTIR, XRD, FESEM, EDX, and XPS.

Surface modification of HA was achieved through the help of phosphate based modifier (Fabulase$^{(R)}$ 361). The modifier was able to impart antimicrobial properties onto the HA surface. It is interesting to note that surface modification of HA did not convert the HA into an entire new material. Specifically, the results indicated that the HA still retained its characteristic biomineral similarity with calcified tissues and it would be of immense benefit if it is employed for application in bone tissue engineering.

Composites were prepared from poly(lactic acid) (PLA) and the produced HA at different (0-20 wt%) HA content. Based on the morphological study and mechanical properties, 10 wt% HA content was selected for further analysis. Another batch of PLA-HA composite was prepared by incorporating surface modified HA at 10 wt% HA loading into the PLA matrix. It was however observed that the impact properties of the PLA-HA composite is inferior to PLA even after modification of the HA. An impact

modifier, biostrong (BS), was incorporated into the composite for possible enhancement of impact properties.

Surface modification of HA led to better dispersion of HA in the PLA matrix. This resulted into remarkable improvement in properties, which is necessary for load bearing applications. On the other hand, incorporation of impact modifier led to sacrifice of some mechanical properties of the composites. However, up to 5 wt% impact modifier content, the reduction is minimal and it came alongside a remarkable improvement in impact properties which is needed for load bearing applications. Antimicrobial analysis and in vitro biocompatibility studies of PLA and selected composite categories revealed that the composite containing modified HA presents reasonable inhibitory features to both gram positive and gram negative bacteria. Likewise, the cell response of the samples revealed that incorporation of HA into PLA offered better cell attachment and proliferation to the PLA matrix. Interestingly, modification of HA did not present obvious cytotoxicity to the composite. However, incorporation of impact modifier was found to slow down the rate of cell proliferation on the composite. This was accrued to possible reduction in the degree of contact between the osteoblast cells and the HA within the composites.

5.2 Recommendation

Based on the results obtained herein, it can be inferred that Fabulase$^{(R)}$ 361 is effective for overcoming agglomeration issues associated with PLA-HA composites. Also, due to the versatility of the extrusion and injection moulding processes, PLA-HA bone replacement composites can be fabricated even at possible large scale. It is however recommended that further research should focus on altering the modifier content in order to investigate the possible influence it might have on the mechanical, thermal, dynamic mechanical properties and biological performance of the PLA-HA composite.

In addition, it is recommended that other natural sources should be exploited for the production of HA in order to reduce the environmental pollution issues associated with chemical synthesis routes. Moreover, in vivo biocompatibility test should be performed on dense PLA-HA composites. Furthermore, other impact modifiers should be exploited in order to investigate the similarity or possible difference between them

and the well-established biostrong impact modifier. It is also recommended that medical grade PLA and impact modifiers should be used for further studies.

.

REFERENCES

Agarwal, R., & García, A. J. (2015). Biomaterial strategies for engineering implants for enhanced osseointegration and bone repair. *Advanced drug delivery reviews, 94*, 53-62.

Agrawal, & Athanasiou, K. A. (1997). Technique to control pH in vicinity of biodegrading PLA-PGA implants. *Journal of biomedical materials research, 38*(2), 105-114.

Akindoyo. (2015). *Oil Palm Empty Fruit Bunch (EFB) Fiber Reinforced Poly (lactic) Acid Composites: Effects of Fiber Treatment and Impact Modifier*. UMP.

Akindoyo, Beg, M., Ghazali, S., Heim, H., & Feldmann, M. (2017). Effects of surface modification on dispersion, mechanical, thermal and dynamic mechanical properties of injection molded PLA-hydroxyapatite composites. *Composites Part A: Applied Science and Manufacturing, 103*, 96-105.

Akindoyo, Beg, M. D. H., Ghazali, S., & Islam, M. R. (2015). Effects of poly (dimethyl siloxane) on the water absorption and natural degradation of poly (lactic acid)/oil-palm empty-fruit-bunch fiber biocomposites. *Journal of Applied Polymer Science, 132*(45).

Akindoyo, Beg, M. D. H., Ghazali, S. B., Islam, M. R., & Mamun, A. A. (2015b). Preparation and Characterization of Poly (lactic acid)-Based Composites Reinforced with Poly Dimethyl Siloxane/Ultrasound-Treated Oil Palm Empty Fruit Bunch. *Polymer-Plastics Technology and Engineering, 54*(13), 1321-1333.

Akindoyo, J., Beg, M., Ghazali, S., Akindoyo, E., & Jeyaratnam, N. (2017b). *Synthesis of Hydroxyapatite through Ultrasound and Calcination Techniques.* Paper presented at the IOP Conference Series: Materials Science and Engineering.

Alam, A. M., Beg, M., Prasad, D. R., Khan, M., & Mina, M. (2012). Structures and performances of simultaneous ultrasound and alkali treated oil palm empty fruit bunch fiber reinforced poly (lactic acid) composites. *Composites Part A: Applied Science and Manufacturing, 43*(11), 1921-1929.

Antonakos, A., Liarokapis, E., & Leventouri, T. (2007). Micro-Raman and FTIR studies of synthetic and natural apatites. *Biomaterials, 28*(19), 3043-3054.

Armentano, I., Dottori, M., Fortunati, E., Mattioli, S., & Kenny, J. (2010). Biodegradable polymer matrix nanocomposites for tissue engineering: a review. *Polymer degradation and stability, 95*(11), 2126-2146.

Barakat, N. A., Khil, M. S., Omran, A., Sheikh, F. A., & Kim, H. Y. (2009). Extraction of pure natural hydroxyapatite from the bovine bones bio waste by three different methods. *Journal of materials processing technology, 209*(7), 3408-3415.

Bordjih, K., Jouzeau, J.-Y., Mainard, D., Payan, E., Delagoutte, J.-P., & Netter, P. (1996). Evaluation of the effect of three surface treatments on the biocompatibility of 316L stainless steel using human differentiated cells. *Biomaterials, 17*(5), 491-500.

Borum-Nicholas, L., & Wilson, O. (2003). Surface modification of hydroxyapatite. Part I. Dodecyl alcohol. *Biomaterials, 24*(21), 3671-3679.

Borum, L., & Wilson, O. (2003). Surface modification of hydroxyapatite. Part II. Silica. *Biomaterials, 24*(21), 3681-3688.

Bos, R. R. (2005). Treatment of pediatric facial fractures: the case for metallic fixation. *Journal of oral and maxillofacial surgery, 63*(3), 382-384.

Bose, S., Roy, M., & Bandyopadhyay, A. (2012). Recent advances in bone tissue engineering scaffolds. *Trends in biotechnology, 30*(10), 546-554.

Böstman, & Pihlajamäki, H. (2000). Clinical biocompatibility of biodegradable orthopaedic implants for internal fixation: a review. *Biomaterials, 21*(24), 2615-2621.

Bouzouita, Notta-Cuvier, D., Delille, R., Lauro, F., Raquez, J.-M., & Dubois, P. (2017). Design of toughened PLA based material for application in structures subjected to severe loading conditions. Part 2. Quasi-static tensile tests and dynamic mechanical analysis at ambient and moderately high temperature. *Polymer Testing, 57*, 235-244.

Bouzouita, Samuel, C., Notta-Cuvier, D., Odent, J., Lauro, F., Dubois, P., & Raquez, J. M. (2016). Design of highly tough poly (l-lactide)-based ternary blends for automotive applications. *Journal of Applied Polymer Science, 133*(19).

Chae, T., Yang, H., Ko, F., & Troczynski, T. (2014). Bio-inspired dicalcium phosphate anhydrate/poly (lactic acid) nanocomposite fibrous scaffolds for hard tissue regeneration: In situ synthesis and electrospinning. *Journal of Biomedical Materials Research Part A*, *102*(2), 514-522.

Champion, E. (2013). Sintering of calcium phosphate bioceramics. *Acta biomaterialia*, *9*(4), 5855-5875.

Cheng, Y., Deng, S., Chen, P., & Ruan, R. (2009). Polylactic acid (PLA) synthesis and modifications: a review. *Frontiers of chemistry in China*, *4*(3), 259-264.

Choi, Choi, M.-C., Han, D.-H., Park, T.-S., & Ha, C.-S. (2013). Plasticization of poly (lactic acid)(PLA) through chemical grafting of poly (ethylene glycol)(PEG) via in situ reactive blending. *European Polymer Journal*, *49*(8), 2356-2364.

Choi, Lee, H. J., Kim, K. J., Kim, H.-M., & Lee, S. C. (2006). Surface modification of hydroxyapatite nanocrystals by grafting polymers containing phosphonic acid groups. *Journal of colloid and interface science*, *304*(1), 277-281.

Choy, M. T., Tang, C. Y., Chen, L., Wong, C. T., & Tsui, C. P. (2014). In vitro and in vivo performance of bioactive Ti6Al4V/TiC/HA implants fabricated by a rapid microwave sintering technique. *Materials Science and Engineering: C*, *42*, 746-756.

Cucuruz, A. T., Andronescu, E., Ficai, A., Ilie, A., & Iordache, F. (2016). Synthesis and characterization of new composite materials based on poly (methacrylic acid) and hydroxyapatite with applications in dentistry. *International journal of pharmaceutics*.

Deng, G Kumbar, S., W-H Lo, K., D Ulery, B., & T Laurencin, C. (2011). Novel polymer-ceramics for bone repair and regeneration. *Recent Patents on Biomedical Engineering*, *4*(3), 168-184.

Dong, G.-C., Sun, J.-S., Yao, C.-H., Jiang, G. J., Huang, C.-W., & Lin, F.-H. (2001). A study on grafting and characterization of HMDI-modified calcium hydrogenphosphate. *Biomaterials*, *22*(23), 3179-3189.

Dorozhkin, S. V. (2013). Calcium orthophosphate-based bioceramics. *Materials*, *6*(9), 3840-3942.

Dorozhkin, S. V. (2015a). Calcium orthophosphate-containing biocomposites and hybrid biomaterials for biomedical applications. *Journal of functional biomaterials*, *6*(3), 708-832.

Dorozhkin, S. V. (2015b). Calcium orthophosphate deposits: preparation, properties and biomedical applications. *Materials Science and Engineering: C*, *55*, 272-326.

Ergun, C., Evis, Z., Webster, T. J., & Sahin, F. C. (2011). Synthesis and microstructural characterization of nano-size calcium phosphates with different stoichiometry. *Ceramics international*, *37*(3), 971-977.

Essabir, Elkhaoulani, A., Benmoussa, K., Bouhfid, R., Arrakhiz, F., & Qaiss, A. (2013b). Dynamic mechanical thermal behavior analysis of doum fibers reinforced polypropylene composites. *Materials & Design*, *51*, 780-788.

Essabir, Hilali, E., Elgharad, A., El Minor, H., Imad, A., Elamraoui, A., & Al Gaoudi, O. (2013). Mechanical and thermal properties of bio-composites based on polypropylene reinforced with Nut-shells of Argan particles. *Materials & Design*, *49*, 442-448.

Etaati, A., Pather, S., Fang, Z., & Wang, H. (2014). The study of fibre/matrix bond strength in short hemp polypropylene composites from dynamic mechanical analysis. *Composites Part B: Engineering*, *62*, 19-28.

Fauzi, A. N., Norazmi, M. N., & Yaacob, N. S. (2011). Tualang honey induces apoptosis and disrupts the mitochondrial membrane potential of human breast and cervical cancer cell lines. *Food and Chemical Toxicology*, *49*(4), 871-878.

Ferri, J., Gisbert, I., García-Sanoguera, D., Reig, M., & Balart, R. (2016). The effect of beta-tricalcium phosphate on mechanical and thermal performances of poly (lactic acid). *Journal of Composite Materials*, *50*(30), 4189-4198.

Ficai, A., Andronescu, E., Voicu, G., Albu, M. G., & Ilie, A. (2010). Biomimetically synthesis of collagen/hydroxyapatite composite materials. *Mat Plast*, *47*, 205-208.

Friedman, R. J., Bauer, T. W., Garg, K., Jiang, M., An, Y. H., & Draughn, R. A. (1995). Histological and mechanical comparison of hydroxyapatite-coated cobalt-chrome and titanium implants in the rabbit femur. *Journal of Applied Biomaterials, 6*(4), 231-235.

Fu, C., Zhang, X., Savino, K., Gabrys, P., Gao, Y., Chaimayo, W., . . . Yates, M. Z. (2016). Antimicrobial silver-hydroxyapatite composite coatings through two-stage electrochemical synthesis. *Surface and Coatings Technology*.

Geetha, M., Singh, A., Asokamani, R., & Gogia, A. (2009). Ti based biomaterials, the ultimate choice for orthopaedic implants–a review. *Progress in materials science, 54*(3), 397-425.

Georgiopoulos, P., Christopoulos, A., Koutsoumpis, S., & Kontou, E. (2016). The effect of surface treatment on the performance of flax/biodegradable composites. *Composites Part B: Engineering, 106*, 88-98.

Gokcekaya, O., Ueda, K., Narushima, T., & Ergun, C. (2015). Synthesis and characterization of Ag-containing calcium phosphates with various Ca/P ratios. *Materials Science and Engineering: C, 53*, 111-119.

Gültekin, N., Tıhmınlıoğlu, F., Çiftçioğlu, R., Çiftçioğlu, M., & Harsa, Ş. (2004). *Preparation and characterization of polylactide-hydroxyapatite biocomposites.* Paper presented at the Key Engineering Materials.

Guo, G., Sun, Y., Wang, Z., & Guo, H. (2005). Preparation of hydroxyapatite nanoparticles by reverse microemulsion. *Ceramics international, 31*(6), 869-872.

Gupta, B., Revagade, N., & Hilborn, J. (2007). Poly (lactic acid) fiber: an overview. *Progress in polymer science, 32*(4), 455-482.

Haberko, K., Bućko, M. M., Brzezińska-Miecznik, J., Haberko, M., Mozgawa, W., Panz, T., . . . Zarębski, J. (2006). Natural hydroxyapatite—its behaviour during heat treatment. *Journal of the European Ceramic Society, 26*(4), 537-542.

Habraken, W., Habibovic, P., Epple, M., & Bohner, M. (2016). Calcium phosphates in biomedical applications: materials for the future? *Materials Today, 19*(2), 69-87.

He, L.-H., Standard, O. C., Huang, T. T., Latella, B. A., & Swain, M. V. (2008). Mechanical behaviour of porous hydroxyapatite. *Acta biomaterialia, 4*(3), 577-586.

Hickey, D. J., Ercan, B., Sun, L., & Webster, T. J. (2015). Adding MgO nanoparticles to hydroxyapatite–PLLA nanocomposites for improved bone tissue engineering applications. *Acta biomaterialia, 14*, 175-184.

Hong, S., Hu, X., Yang, F., Bei, J., & Wang, S. (2010). An injectable scaffold: rhBMP-2-loaded poly (lactide-co-glycolide)/hydroxyapatite composite microspheres. *Acta biomaterialia, 6*(2), 455-465.

Hou, R., Zhang, G., Du, G., Zhan, D., Cong, Y., Cheng, Y., & Fu, J. (2013). Magnetic nanohydroxyapatite/PVA composite hydrogels for promoted osteoblast adhesion and proliferation. *Colloids and Surfaces B: Biointerfaces, 103*, 318-325.

Hutmacher, D., Goh, J., & Teoh, S. (2001). An introduction to biodegradable materials for tissue engineering applications. *ANNALS-ACADEMY OF MEDICINE SINGAPORE, 30*(2), 183-191.

Ignjatovic, N., Suljovrujic, E., Budinski-Simendic, J., Krakovsky, I., & Uskokovic, D. (2004). Evaluation of hot-pressed hydroxyapatite/poly-L-lactide composite biomaterial characteristics. *Journal of Biomedical Materials Research Part B: Applied Biomaterials, 71*(2), 284-294.

Ignjatović, N., Tomić, S., Dakić, M., Miljković, M., Plavšić, M., & Uskoković, D. (1999). Synthesis and properties of hydroxyapatite/poly-L-lactide composite biomaterials. *Biomaterials, 20*(9), 809-816.

Ilie, A., Andronescu, E., Ficai, D., Voicu, G., Ficai, M., Maganu, M., & Ficai, A. (2011). New approaches in layer by layer synthesis of collagen/hydroxyapatite composite materials. *Central European Journal of Chemistry, 9*(2), 283-289.

Isobe, T., Nakamura, S., Nemoto, R., Senna, M., & Sfihi, H. (2002). Solid-state double nuclear magnetic resonance study of the local structure of calcium phosphate nanoparticles synthesized by a wet-mechanochemical reaction. *The Journal of Physical Chemistry B, 106*(20), 5169-5176.

Jang, D.-W., Franco, R. A., Sarkar, S. K., & Lee, B.-T. (2014). Fabrication of porous hydroxyapatite scaffolds as artificial bone preform and its biocompatibility evaluation. *Asaio Journal*, *60*(2), 216.

Jarudilokkul, S., Tanthapanichakoon, W., & Boonamnuayvittaya, V. (2007). Synthesis of hydroxyapatite nanoparticles using an emulsion liquid membrane system. *Colloids and Surfaces A: Physicochemical and Engineering Aspects*, *296*(1), 149-153.

Jaszkiewicz, A., Bledzki, A., van der Meer, R., Franciszczak, P., & Meljon, A. (2014). How does a chain-extended polylactide behave?: a comprehensive analysis of the material, structural and mechanical properties. *Polymer Bulletin*, *71*(7), 1675-1690.

Jeon, B. J., Jeong, Y. G., Min, B. G., Lyoo, W. S., & Lee, S. C. (2011). Lead ion removal characteristics of poly (lactic acid)/hydroxyapatite composite foams prepared by supercritical CO2 process. *Polymer Composites*, *32*(9), 1408-1415.

Jiang, L., Jiang, L., Xiong, C., & Su, S. (2016). Improving the degradation behavior and in vitro biological property of nano-hydroxyapatite surface-grafted with the assist of citric acid. *Colloids and Surfaces B: Biointerfaces*.

Joschek, S., Nies, B., Krotz, R., & Göpferich, A. (2000). Chemical and physicochemical characterization of porous hydroxyapatite ceramics made of natural bone. *Biomaterials*, *21*(16), 1645-1658.

Kangping, Z., Jianwen, Z., & Henglei, Q. (2012). Development and Application of Biomedical Ti Alloys Abroad [J]. *Rare Metal Materials and Engineering*, *11*, 039.

Kasuga, T., Ota, Y., Nogami, M., & Abe, Y. (2000). Preparation and mechanical properties of polylactic acid composites containing hydroxyapatite fibers. *Biomaterials*, *22*(1), 19-23.

Keogh, M. B., O'Brien, F. J., & Daly, J. S. (2010). A novel collagen scaffold supports human osteogenesis—applications for bone tissue engineering. *Cell and tissue research*, *340*(1), 169-177.

Krishna, K. V., & Kanny, K. (2016). The effect of treatment on kenaf fiber using green approach and their reinforced epoxy composites. *Composites Part B: Engineering*, *104*, 111-117.

Laurencin, Khan, Y., & El-Amin, S. F. (2006). Bone graft substitutes. *Expert review of medical devices*, *3*(1), 49-57.

Lee, K., & Goodman, S. B. (2008). Current state and future of joint replacements in the hip and knee. *Expert review of medical devices*, *5*(3), 383-393.

Li, Lu, X., & Zheng, Y. (2008). Effect of surface modified hydroxyapatite on the tensile property improvement of HA/PLA composite. *Applied Surface Science*, *255*(2), 494-497.

Li, Yang, C., Zhao, H., Qu, S., Li, X., & Li, Y. (2014). New developments of Ti-based alloys for biomedical applications. *Materials*, *7*(3), 1709-1800.

Lichte, P., Pape, H., Pufe, T., Kobbe, P., & Fischer, H. (2011). Scaffolds for bone healing: concepts, materials and evidence. *Injury*, *42*(6), 569-573.

Lim, Auras, R., & Rubino, M. (2008). Processing technologies for poly (lactic acid). *Progress in polymer science*, *33*(8), 820-852.

Liu, Troczynski, T., & Tseng, W. J. (2001). Water-based sol–gel synthesis of hydroxyapatite: process development. *Biomaterials*, *22*(13), 1721-1730.

Liuyun, Chengdong, X., Dongliang, C., & Lixin, J. (2012). Effect of n-HA with different surface-modified on the properties of n-HA/PLGA composite. *Applied Surface Science*, *259*, 72-78.

Liuyun, Chengdong, X., Lixin, J., Dongliang, C., & Qing, L. (2013). Effect of n-HA content on the isothermal crystallization, morphology and mechanical property of n-HA/PLGA composites. *Materials Research Bulletin*, *48*(3), 1233-1238.

Liuyun, J., Chengdong, X., Lixin, J., & Lijuan, X. (2013b). Effect of different precipitation procedures on the properties of nano-hydroxyapatite/poly-lactic-co-glycolic acid composite. *Polymer Composites*, *34*(7), 1158-1162.

López-Álvarez, M., Rodríguez-Valencia, C., Serra, J., & González, P. (2013). Bio-inspired ceramics: promising scaffolds for bone tissue engineering. *Procedia Engineering*, *59*, 51-58.

Lü, X. Y., Fan, Y. B., Gu, D., & Cui, W. (2007). *Preparation and characterization of natural hydroxyapatite from animal hard tissues.* Paper presented at the Key Engineering Materials.

Malinin, T. I., Levitt, R. L., Bashore, C., Temple, H. T., & Mnaymneh, W. (2002). A study of retrieved allografts used to replace anterior cruciate ligaments. *Arthroscopy: The Journal of Arthroscopic & Related Surgery, 18*(2), 163-170.

Matesanz, M. C., Linares, J., Onaderra, M., Feito, M. J., Martínez-Vázquez, F. J., Sánchez-Salcedo, S., . . . Vallet-Regí, M. (2015). Response of osteoblasts and preosteoblasts to calcium deficient and Si substituted hydroxyapatites treated at different temperatures. *Colloids and Surfaces B: Biointerfaces, 133*, 304-313.

Meng, D., James, R., Laurencin, C. T., & Kumbar, S. G. (2012). Nanostructured polymeric scaffolds for orthopaedic regenerative engineering. *IEEE transactions on nanobioscience, 11*(1), 3-14.

Metikoš-Huković, M., Tkalčec, E., Kwokal, A., & Piljac, J. (2003). An in vitro study of Ti and Ti-alloys coated with sol–gel derived hydroxyapatite coatings. *Surface and Coatings Technology, 165*(1), 40-50.

Misra, D. (1985). Adsorption of zirconyl salts and their acids on hydroxyapatite: use of the salts as coupling agents to dental polymer composites. *Journal of dental research, 64*(12), 1405-1408.

Murariu, M., & Dubois, P. (2016). PLA composites: From production to properties. *Advanced drug delivery reviews, 107*, 17-46.

Murugan, R., Ramakrishna, S., & Rao, K. P. (2006). Nanoporous hydroxy-carbonate apatite scaffold made of natural bone. *Materials letters, 60*(23), 2844-2847.

Nair, Thomas, S., & Groeninckx, G. (2001). Thermal and dynamic mechanical analysis of polystyrene composites reinforced with short sisal fibres. *Composites Science and Technology, 61*(16), 2519-2529.

Nakagawa, M., Teraoka, F., Fujimoto, S., Hamada, Y., Kibayashi, H., & Takahashi, J. (2006). Improvement of cell adhesion on poly (L-lactide) by atmospheric plasma treatment. *Journal of Biomedical Materials Research Part A, 77*(1), 112-118.

Narayanan, Vernekar, V. N., Kuyinu, E. L., & Laurencin, C. T. (2016). Poly (lactic acid)-based biomaterials for orthopaedic regenerative engineering. *Advanced drug delivery reviews*.

Nirmala, R., Sheikh, F. A., Kanjwal, M. A., Lee, J. H., Park, S.-J., Navamathavan, R., & Kim, H. Y. (2011). Synthesis and characterization of bovine femur bone hydroxyapatite containing silver nanoparticles for the biomedical applications. *Journal of Nanoparticle Research, 13*(5), 1917-1927.

Notta-Cuvier, D., Bouzouita, A., Delille, R., Haugou, G., Raquez, J.-M., Lauro, F., & Dubois, P. (2016). Design of toughened PLA based material for application in structures subjected to severe loading conditions. Part 1. Quasi-static and dynamic tensile tests at ambient temperature. *Polymer Testing, 54*, 233-243.

Ojijo, V., & Ray, S. S. (2013). Processing strategies in bionanocomposites. *Progress in polymer science, 38*(10), 1543-1589.

Olszta, M. J., Cheng, X., Jee, S. S., Kumar, R., Kim, Y.-Y., Kaufman, M. J., . . . Gower, L. B. (2007). Bone structure and formation: a new perspective. *Materials Science and Engineering: R: Reports, 58*(3), 77-116.

Ooi, C., Hamdi, M., & Ramesh, S. (2007). Properties of hydroxyapatite produced by annealing of bovine bone. *Ceramics international, 33*(7), 1171-1177.

Panchbhavi, V. K. (2010). Synthetic bone grafting in foot and ankle surgery. *Foot and ankle clinics, 15*(4), 559-576.

Pang, Y., & Bao, X. (2003). Influence of temperature, ripening time and calcination on the morphology and crystallinity of hydroxyapatite nanoparticles. *Journal of the European Ceramic Society, 23*(10), 1697-1704.

Parhi, P., Ramanan, A., & Ray, A. R. (2004). A convenient route for the synthesis of hydroxyapatite through a novel microwave-mediated metathesis reaction. *Materials letters, 58*(27), 3610-3612.

Pluta, M., Murariu, M., Dechief, A. L., Bonnaud, L., Galeski, A., & Dubois, P. (2012). Impact-modified polylactide–calcium sulfate composites: Structure and properties. *Journal of Applied Polymer Science*, *125*(6), 4302-4315.

Pongtanayut, K., Thongpin, C., & Santawitee, O. (2013). The effect of rubber on morphology, thermal properties and mechanical properties of PLA/NR and PLA/ENR blends. *Energy Procedia*, *34*, 888-897.

Quan, L., Matinlinna, J. P., Chen, Z., Ning, C., Ni, G., Pan, H., & Darvell, B. W. (2015). Effect of thermal treatment on carbonated hydroxyapatite: Morphology, composition, crystal characteristics and solubility. *Ceramics international*, *41*(5), 6149-6157.

Rakmae, S., Ruksakulpiwat, Y., Sutapun, W., & Suppakarn, N. (2012). Effect of silane coupling agent treated bovine bone based carbonated hydroxyapatite on in vitro degradation behavior and bioactivity of PLA composites. *Materials Science and Engineering: C*, *32*(6), 1428-1436.

Raquez, J.-M., Habibi, Y., Murariu, M., & Dubois, P. (2013). Polylactide (PLA)-based nanocomposites. *Progress in polymer science*, *38*(10), 1504-1542.

Ren, Z., Dong, L., & Yang, Y. (2006). Dynamic mechanical and thermal properties of plasticized poly (lactic acid). *Journal of Applied Polymer Science*, *101*(3), 1583-1590.

Rezwan, K., Chen, Q., Blaker, J., & Boccaccini, A. R. (2006). Biodegradable and bioactive porous polymer/inorganic composite scaffolds for bone tissue engineering. *Biomaterials*, *27*(18), 3413-3431.

Romanzini, D., Lavoratti, A., Ornaghi, H. L., Amico, S. C., & Zattera, A. J. (2013). Influence of fiber content on the mechanical and dynamic mechanical properties of glass/ramie polymer composites. *Materials & Design*, *47*, 9-15.

Ruksudjarit, A., Pengpat, K., Rujijanagul, G., & Tunkasiri, T. (2008). Synthesis and characterization of nanocrystalline hydroxyapatite from natural bovine bone. *Current applied physics*, *8*(3), 270-272.

Sadat-Shojai, M., Khorasani, M.-T., Dinpanah-Khoshdargi, E., & Jamshidi, A. (2013). Synthesis methods for nanosized hydroxyapatite with diverse structures. *Acta biomaterialia*, *9*(8), 7591-7621.

Sarig, S., & Kahana, F. (2002). Rapid formation of nanocrystalline apatite. *Journal of Crystal Growth*, *237*, 55-59.

Shelton, W. R., Papendick, L., & Dukes, A. D. (1997). Autograft versus allograft anterior cruciate ligament reconstruction. *Arthroscopy: The Journal of Arthroscopic & Related Surgery*, *13*(4), 446-449.

Shen, Yang, H., Ying, J., Qiao, F., & Peng, M. (2009). Preparation and mechanical properties of carbon fiber reinforced hydroxyapatite/polylactide biocomposites. *Journal of Materials Science: Materials in Medicine*, *20*(11), 2259-2265.

Shih, W.-J., Chen, Y.-F., Wang, M.-C., & Hon, M.-H. (2004). Crystal growth and morphology of the nano-sized hydroxyapatite powders synthesized from CaHPO 4· 2H 2 O and CaCO 3 by hydrolysis method. *Journal of Crystal Growth*, *270*(1), 211-218.

Sun, F., Zhou, H., & Lee, J. (2011). Various preparation methods of highly porous hydroxyapatite/polymer nanoscale biocomposites for bone regeneration. *Acta biomaterialia*, *7*(11), 3813-3828.

Taib, R., Ghaleb, Z., & Mohd Ishak, Z. (2012). Thermal, mechanical, and morphological properties of polylactic acid toughened with an impact modifier. *Journal of Applied Polymer Science*, *123*(5), 2715-2725.

Tayton, E., Purcell, M., Aarvold, A., Smith, J., Briscoe, A., Kanczler, J., . . . Oreffo, R. (2014). A comparison of polymer and polymer–hydroxyapatite composite tissue engineered scaffolds for use in bone regeneration. An in vitro and in vivo study. *Journal of Biomedical Materials Research Part A*, *102*(8), 2613-2624.

Thanh, D. T. M., Trang, P. T. T., Huong, H. T., Nam, P. T., Phuong, N. T., Trang, N. T. T., . . . Seo–Park, J. (2015). Fabrication of poly (lactic acid)/hydroxyapatite (PLA/HAp) porous nanocomposite for bone regeneration. *International Journal of Nanotechnology*, *12*(5-7), 391-404.

Vila, O. F., Bago, J. R., Navarro, M., Alieva, M., Aguilar, E., Engel, E., . . . Blanco, J. (2013). Calcium phosphate glass improves angiogenesis capacity of poly (lactic acid) scaffolds and stimulates differentiation of adipose tissue-derived mesenchymal stromal cells to the endothelial lineage. *Journal of Biomedical Materials Research Part A, 101*(4), 932-941.

Wahit, M. U., Akos, N. I., & Laftah, W. A. (2012). Influence of natural fibers on the mechanical properties and biodegradation of poly (lactic acid) and poly (ε-caprolactone) composites: A review. *Polymer Composites, 33*(7), 1045-1053.

Wang, De Boer, J., & De Groot, K. (2004). Preparation and characterization of electrodeposited calcium phosphate/chitosan coating on Ti6Al4V plates. *Journal of dental research, 83*(4), 296-301.

Wang, Li, Y., Wei, J., & De Groot, K. (2002). Development of biomimetic nano-hydroxyapatite/poly (hexamethylene adipamide) composites. *Biomaterials, 23*(24), 4787-4791.

Wang, & Nancollas, G. H. (2008). Calcium orthophosphates: crystallization and dissolution. *Chemical reviews, 108*(11), 4628-4669.

Webster, T. J., & Ejiofor, J. U. (2004). Increased osteoblast adhesion on nanophase metals: Ti, Ti6Al4V, and CoCrMo. *Biomaterials, 25*(19), 4731-4739.

Williams, D. F. (2008). On the mechanisms of biocompatibility. *Biomaterials, 29*(20), 2941-2953.

Witte, F., Feyerabend, F., Maier, P., Fischer, J., Störmer, M., Blawert, C., . . . Hort, N. (2007). Biodegradable magnesium–hydroxyapatite metal matrix composites. *Biomaterials, 28*(13), 2163-2174.

Woo, K. M., Seo, J., Zhang, R., & Ma, P. X. (2007). Suppression of apoptosis by enhanced protein adsorption on polymer/hydroxyapatite composite scaffolds. *Biomaterials, 28*(16), 2622-2630.

Wu, S.-C., Hsu, H.-C., Hsu, S.-K., Lin, F.-W., & Ho, W.-F. (2015). Preparation and characterization of porous calcium-phosphate microspheres. *Ceramics international, 41*(6), 7596-7604.

Yanoso-Scholl, L., Jacobson, J. A., Bradica, G., Lerner, A. L., O'Keefe, R. J., Schwarz, E. M., . . . Awad, H. A. (2010). Evaluation of dense polylactic acid/beta-tricalcium phosphate scaffolds for bone tissue engineering. *Journal of Biomedical Materials Research Part A, 95*(3), 717-726.

Yeong, K., Wang, J., & Ng, S. (2001). Mechanochemical synthesis of nanocrystalline hydroxyapatite from CaO and CaHPO 4. *Biomaterials, 22*(20), 2705-2712.

Yu, T., Wang, Y.-Y., Yang, M., Schneider, C., Zhong, W., Pulicare, S., . . . Lai, S. K. (2012). Biodegradable mucus-penetrating nanoparticles composed of diblock copolymers of polyethylene glycol and poly (lactic-co-glycolic acid). *Drug delivery and translational research, 2*(2), 124-128.

Zhang, Liu, J., Zhou, W., Cheng, L., & Guo, X. (2005). Interfacial fabrication and property of hydroxyapatite/polylactide resorbable bone fixation composites. *Current applied physics, 5*(5), 516-518.

Zhang, Liu, W., Schnitzler, V., Tancret, F., & Bouler, J.-M. (2014). Calcium phosphate cements for bone substitution: chemistry, handling and mechanical properties. *Acta biomaterialia, 10*(3), 1035-1049.

Zhou, & Lee, J. (2011). Nanoscale hydroxyapatite particles for bone tissue engineering. *Acta biomaterialia, 7*(7), 2769-2781.